USGS
science for a changing world

Trace Elements and Major-Element Oxides in the Phosphoria Formation at Enoch Valley, Idaho—Permian Sources and Current Reactivities[1]

By D. Z. Piper[2]

Open-File Report 99-163

1999

U.S. DEPARTMENT OF THE INTERIOR
U.S. GEOLOGICAL SURVEY

[1] Prepared as part of the Western U.S. Phosphate Project and in cooperation with U.S. Bureau of Land Management, U.S. Forest Service, Agrium U.S. Inc., FMC Corporation, J.R. Simplot Company, Rhodia Inc., Solutia Inc.

[2] U. S. Geological Survey (M/S 902), 345 Middlefield Road, Menlo Park, CA 94025

CONTENTS

FIGURE TITLES

TABLE TITLES

TRACE ELEMENTS AND MAJOR-ELEMENT OXIDES IN THE PHOSPHORIA FORMATION AT ENOCH VALLEY, IDAHO: PERMIAN SOURCES AND CURRENT REACTIVITIES

David Z. Piper

ABSTRACT

Major-element-oxides in the Phosphoria Formation at Enoch Valley, Idaho are partitioned into normative-mineral components in order to determine the marine and detrital fractions of the rocks. The components are apatite, dolomite, calcite, organic matter, and biogenic silica (not determined in this study)—the marine-derived fraction of the samples; and an aluminosilicate/detrital quartz component—the detrital fraction of the samples. Proportionality constants of major-element oxides used in the calculation of each component (for example, apatite = P_2O_5 x 2.5; detrital terrigenous debris = Al_2O_3 x 6) represent values previously determined for five other sections of the Phosphoria Formation (Medrano and Piper, 1995). The coherence of the normative scheme was checked for the Enoch Valley samples by comparing total CO_2, measured by combustion and a thermal conductivity detector, to CO_2 calculated from stoichiometries of the marine components and their concentrations in each sample. The correlation coefficient was 0.99. As SiO_2 was not measured and, thus biogenic silica not calculated, a further check of coherence by summing components to 100% could not be done. However, the sums exclusive of biogenic silica closely approach 100%, requiring biogenic silica to be absent, or nearly so, in several of the samples.

Plots of Al_2O_3 x 6 versus K_2O, TiO_2, Fe_2O_3, Ba, and Li, show strong positive correlations, demonstrating the relatively constant trace-element and major-element-oxide composition of the detrital fraction. The composition closely approaches the composition of the world shale average, or WSA (Wedepohl, 1969-1978). Factor analysis further confirms the partitioning of these oxides and elements into the detrital fraction. For trace elements that fail to show such correlations or factor loadings, the trace-element contribution of the detrital fraction (Al_2O_3 x 6) is determined from minima of plots of trace elements versus the detrital fraction. These minima too suggest a trace-element composition for the detrital fraction that approximates the trace-element composition of WSA.

The marine fraction of trace elements in each sample then represents the difference between the bulk trace-element content of a sample and its detrital contribution of trace elements. For those trace elements whose marine contribution dominates the detrital contribution, strong positive factor loadings with one or more of the marine components—apatite, calcite, dolomite, and organic matter—validate the normative calculation of partitioning elements between the two source fractions—detrital (terrigenous debris) and marine (seawater-derived matter). These elements include Ag, Cr, Cu, Mo, Se. Several trace elements—Cd, Ni, V, Zn—do not show a strong correlation with any of the marine components, but are also strongly enriched above a detrital contribution. Some fraction of this group may be present as a sulfide, or incorporated in a sulfide. Pyrite can be seen in several hand specimens, but its low concentration has precluded determination of its abundance, quantitatively, by the normative calculation and significantly limits its contribution to the marine, trace-element inventory.

The interelement relations of the trace elements within the marine fraction alone identify the redox conditions of bottom water and primary productivity of the photic zone, or surface water. Relations between Cu, Zn, and Mo suggest a biogenic source, that define primary productivity and further preclude the occurrence of sulfate reduction in the bottom water at the time of deposition. By contrast, the relations between Cr, U, V, and, less so, Se require that bottom water was, nonetheless, oxygen depleted, to the point of denitrifying, throughout most of the depositional history of this deposit.

Of equal, if not greater, importance to this study, the partitioning of elements such as selenium between the different host components—terrigenous aluminosilicates, apatite, organic matter, pyrite, calcite, dolomite, and biogenic silica—contributes to the

behavior of trace elements under current subaerial, oxidizing conditions of weathering. Very simply stated, interelement relations between trace elements identify where the trace elements came from and trace-element partitioning between mineral components determines where they are going.

INTRODUCTION

The U. S. Geological Survey (USGS) has studied the Phosphoria Formation, a Permian sedimentary deposit in southeast Idaho (fig. 1), and related rock units in the Western U.S. Phosphate Field throughout much of the twentieth century. The purposes of the early work were, largely, to evaluate the economic resources of this deposit and to define its origin, in order to enhance exploration for similar deposits of the agricultural commodity phosphate (Mansfield, 1916; Condit, 1924; McKelvey and others, 1959; Sheldon, 1963; Gulbrandsen, 1966; Murata and others, 1972; Maughan, 1976; Piper and Medrano, 1994). In response to a request by the Bureau of Land Management (BLM), a new series of resource and geoenvironmental studies was undertaken by the Survey in 1998. To carry out these studies, the Survey has formed cooperative research relationships with two Federal agencies, BLM and the U. S. Forest Service, which are responsible for land management and resource conservation on public lands; and with five private companies currently leasing or developing phosphate resources in southeastern Idaho. They are Agrium U.S. Inc. (Rasmussen Ridge mine), FMC Corporation (Dry Valley mine), J. R. Simplot Company (Smokey Canyon mine), Rhodia Inc. (Wooley Valley mine, now inactive), and Solutia Inc. (Enoch Valley mine).

Present studies consist of (1) integrated, multidisciplinary research directed toward resource and reserve estimations of phosphate in selected 7.5-minute quadrangles; (2) elemental residence, mineralogical, and petrochemical characteristics; (3) reaction pathways, transport, and fate of potentially toxic trace elements associated with the occurrence, development, and societal use of phosphate; (4) geophysical signatures; and (5) improving the understanding of depositional origin. The results of this work will be released in open-file reports for prompt availability to other workers. The open-file reports associated with this series of studies also will be submitted to each of the Federal and industry cooperators for technical review. However, the USGS is solely responsible for the data contained in these reports.

In this study I address issues three and five. The distribution of trace elements and their host phases in the Phosphoria Formation are calculated from analyses of rock samples from the Solutia Mine in Enoch Valley, using a normative scheme described by Medrano and Piper (1992, 1995) and specific to this formation. The deposit is strongly enriched in a number of trace elements. Their absolute concentrations have been enhanced by a low sedimentation rate of terrigenous debris that was similar to the depositional rate currently in the central Pacific Ocean, resulting in a large seawater-derived fraction that is hosted mainly by chert, carbonate fluorapatite, calcite or/and dolomite, organic matter, and possibly sulfide minerals.

Interpretations of the distribution of trace elements in this deposit have been made possible through research over the past several decades by oceanographers who have examined the behavior of trace elements in seawater and sediment from different environments of the modern ocean (Elderfield, 1970; Bertine and Turekian, 1973; Bruland, 1983; Landing and Bruland, 1987; Jacobs and others, 1987; Piper, 1988; Piper and others, 1988; Francois, 1988; Anderson and others, 1989a; Shaw and others, 1990; Emerson and Huested, 1991; Bruland and others, 1991; Crusius and others, 1996). Results of their research have led to the identification in ancient sedimentary deposits of those trace elements whose accumulation from seawater characterized the levels of primary productivity in the photic zone and redox conditions of the bottom water at the time of deposition (Coveney and Glascock, 1989; Piper, 1991; Piper and Isaacs, 1995, 1996; Dean and others, 1995, 1998; Heltz and others, 1996). I show here that (1) interelement relations of trace elements in the marine components alone identify their sources as phytoplanktonic debris and/or material derived inorganically from a seawater depleted in O_2, and (2) the partitioning of trace elements into their host mineral components contributes to trace-element reactivities under current conditions of subaerial weathering. Thus, the high concentration of trace elements gives a clear view of the environment of deposition in Permian time. On the down side, the high concentration of several elements that can be quite toxic (for example, selenium) and their association with labile components of the sediment are

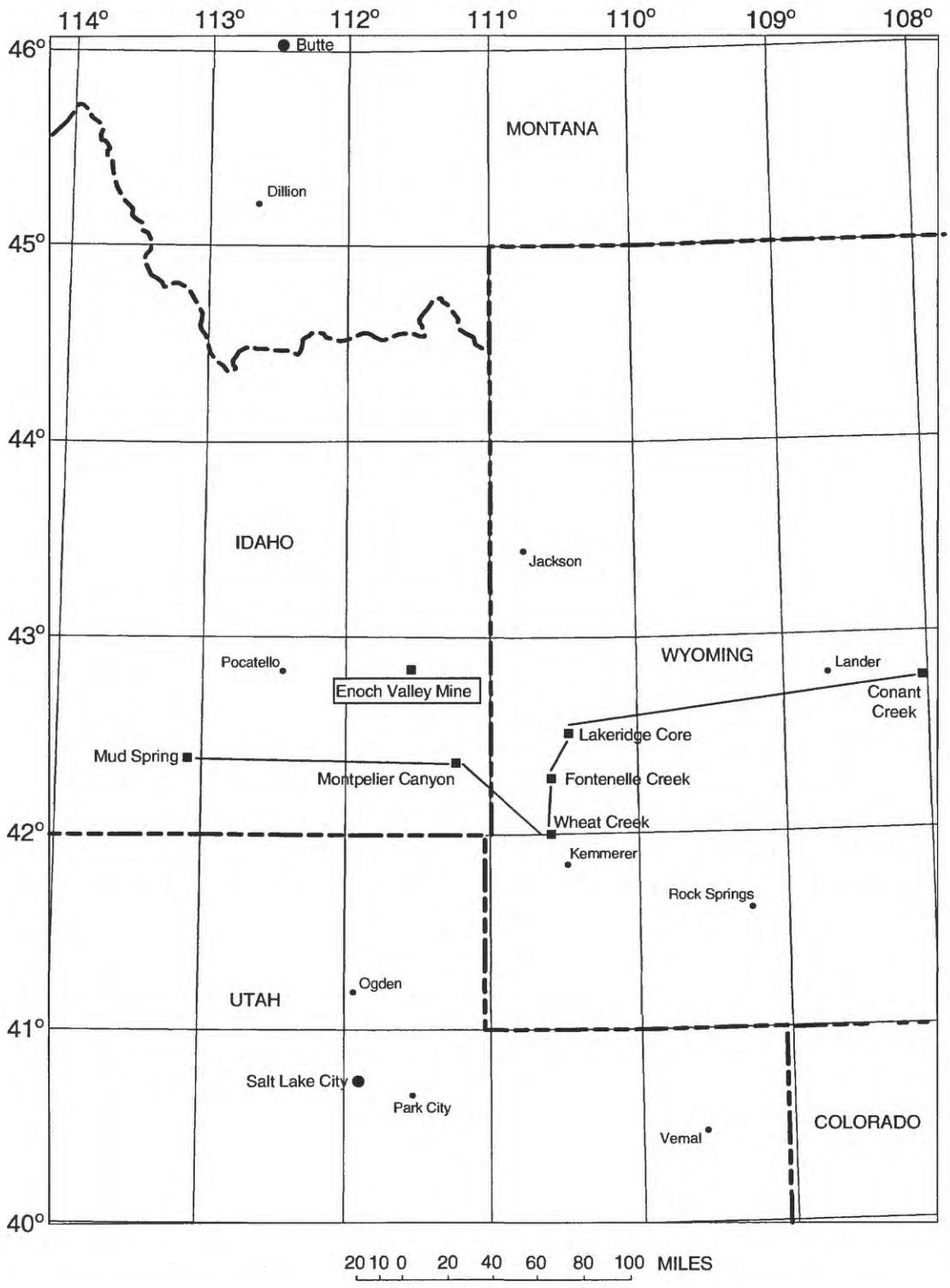

Figure 1. Location map of the northwest U. S., showing the Enoch Valley mine and sections analyzed earlier for their chemical composition (Piper and Medrano, 1994; Medrano and Piper, 1995). Closed squres give location of Enoch Valley mine and other sites reported by Medrano and Piper.

troubling, particularly as concerns their introduction into and possible deleterious impact on the modern environment, a possible impact that has prompted this study, of which this manuscript is a small part.

GEOLOGIC SETTING AND SAMPLING

Geologic and Oceanographic Setting

The Phosphoria Basin was located in what is now eastern Idaho, western Wyoming, northern Utah, northeastern Nevada and southwestern Montana. The sediment was deposited in an interior sag basin (Wardlaw and Collinson, 1986), located along the western margin of the North American craton. Paleomagnetic data (Sheldon, 1964) indicate that the basin lay at much lower latitude, at 3° to 9° N, in Permian time (fig. 2). Deposition occurred over approximately 10 my., from the middle of the Leonardian to the middle of the Guadalupian stages (Wardlaw and Collinson, 1984; Murchey and Jones, 1992). The Meade Peak Member of the Phosphoria Formation, the most phosphatic enriched member of the formation and the unit examined in this report accumulated over a period of approximately 7.2 my.

Paleontologic evidence suggests that the sediment accumulated at an ocean depth of a few hundred meters, possibly as shallow as 200 meters (Yochelson, 1968). The sediment now consists of carbonaceous and phosphatic mudstone, phosphorite, carbonates of both calcite and dolomite, and dark gray chert (McKelvey and others, 1959). At other sites (fig, 1) examined for their geochemistry (Medrano and Piper, 1992, 1995; Piper and Medrano, 1994), Conant Creek, the easternmost site in central Wyoming, is mainly a carbonate facies, possibly of shallow-water origin; Mud Spring, more than 500 km to the west, is predominantly a mudstone facies, possibly deposited in deeper water (McKelvey and others, 1959). The Phosphoria Formation at the Enoch Valley Mine and at other sites examined are located between the two east-west extremes and consist of these components plus major phosphate and chert units. This lithology has suggested to many geologists that the deposit accumulated under conditions of intense primary productivity. The total duration of deposition, which allows calculation of rates of reactions, albeit in a general way, however, suggests that primary productivity in the basin could have been typical of ocean-margin basins of today, perhaps no more than moderate (Piper and Isaacs, 1996), that is, in the range of 0.5 gr carbon/m^2 per day. The major difference with similar basins in the modern ocean was an extremely low rate of accumulation of terrigenous debris in the Phosphoria Basin, comparable to its rate of accumulation in the central Pacific Ocean today (Piper and Medrano, 1994). This resulted in an extremely limited dilution of the seawater-derived (i.e., marine) fraction by terrigenous debris, producing a deposit quite unlike any sedimentary unit accumulating along the margins of the ocean today, in both its areal extent and composition.

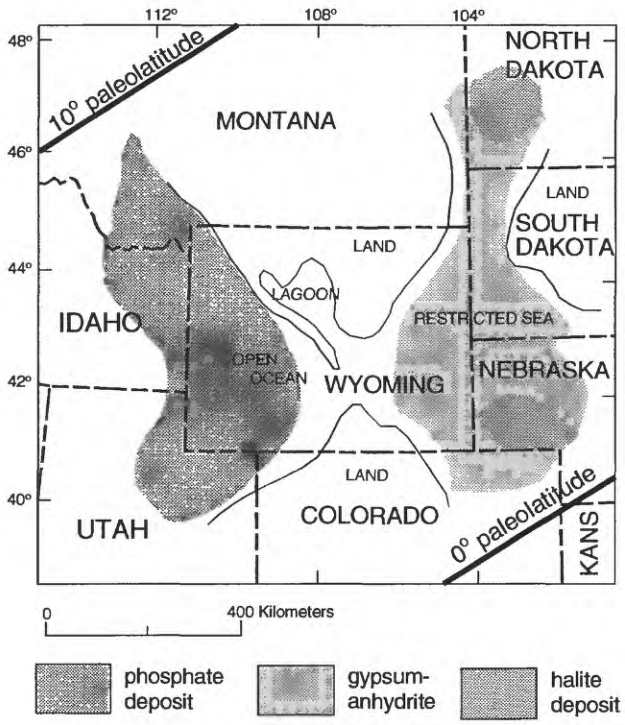

Figure 2. Map of northwest U.S. showing extent of the Phosphoria Formation, location of evaporite deposits to the east, and paleolatitudes during Permian time. In the land areas of Montana and central Wyoming, deposits include red beds. Figure is adapted from Sheldon (1964).

Sample Selection

The Enoch Valley mine, on the South Rasmussen Leases I-7958 and I-23658 (T6S, R43E, section 16, SE1/4 of the NW1/4), at latitude 42° 53.109' N and 111°24.745' W (fig. 1), was described and sampled in 1992 with great assistance from mine personnel. A stratigraphic section, showing sample positions, was constructed from field descriptions and

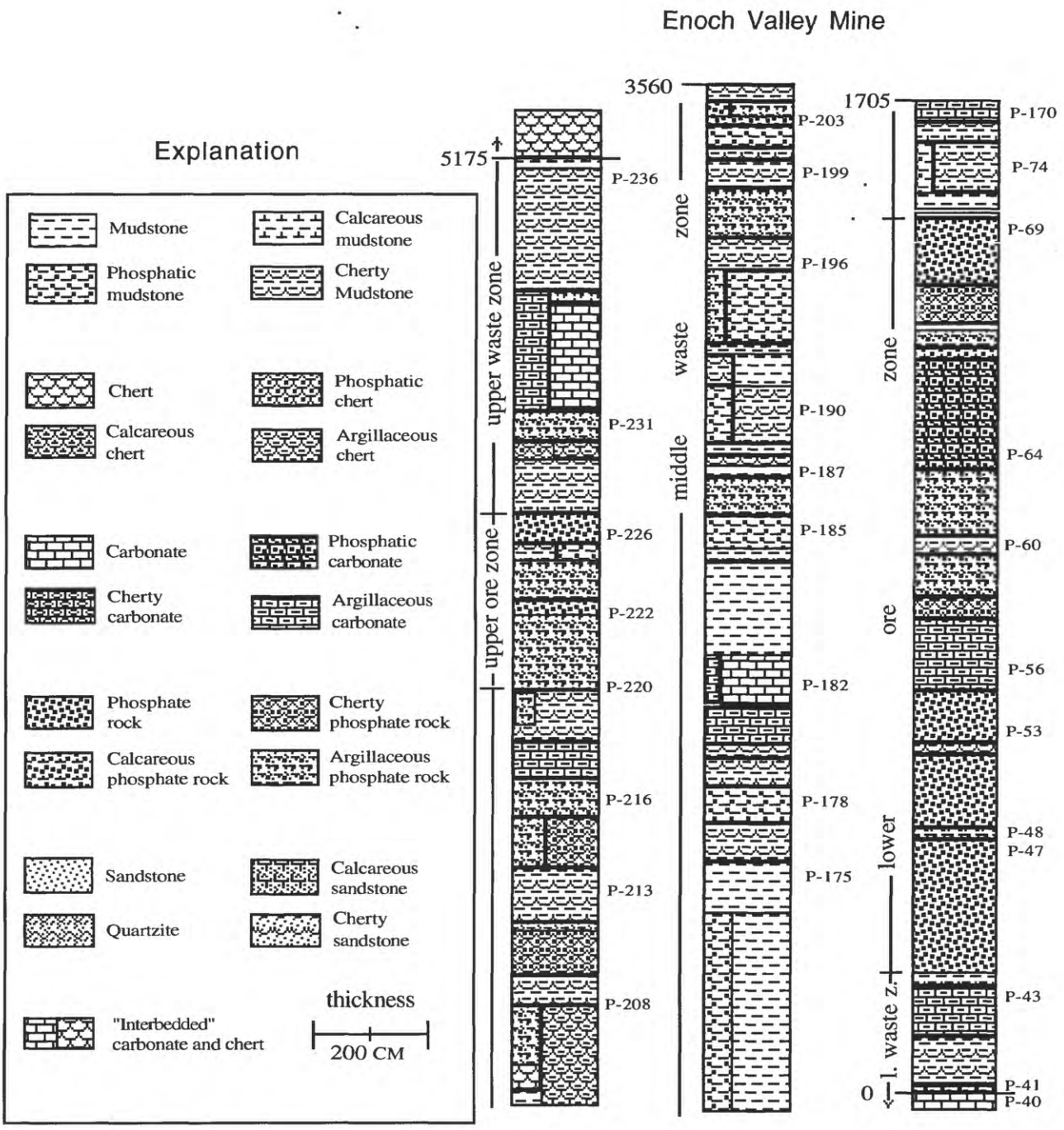

Figure 3. Stratigraphic column of the Meade Peak Member of the Phosphoria Formation at the Enoch Valley Mine. Thicknesses (0 to 5175) are in centimeters; sample numbers are prefaced with a "P". The carbonate below 0 cm is the Grandeur Formation; the chert above 5175 cm is the Rex Chert Member of the Phosphoria Formation. No distinction has been made between calcite and dolomite in this figure, although the carbonate is predominantly dolomite.

Table 1. Detection limits, accuracy and precision for elements analyzed by the different analytical techniques, determined by repeated analysis of rock standards, by the Branch of Geochemistry (Baedecker, 1987; Lichte and others, 1987a, 1987b; Arbogast and others, 1990).

Analytical Technique	Detection Limit	Accuracy	Precision
ICP-AES	Limits of detection, in weight percent, in parentheses: Al_2O_3 (0.09), CaO (0.07), Fe_2O_3 (0.07), K_2O (0.1), MgO (0.08), Na_2O (0.1), P_2O_5 (0.02), and TiO_2 (0.02). Limit of detection in parts per million in parentheses: Ag (2), As (10), Au (8), Ba (1), Be (1), Bi (10), Cd (2), Ce (4), Co (1), Cr (1), Cu (1), Eu (2), Ga (4), Ho (4), La (2), Li (2), Mn (10), Mo (2), Nb (4), Nd (4), Ni (2), Pb (4), Sc (2), Sn (10), Sr (2), Ta (40), Th (4), U (100), V (2), Y (2), Yb (1), and Zn (2)	Standards analyzed varied 0.5 to 10 % from the proposed value	±2 to 10 percent for concentrations greater than 10 times the lower limit of detection
XRF	Limits of detection and concentration range SiO_2 0.10% to 99.0% Al_2O_3 0.10% to 28.0% Fe_2O_3 0.04% to 28.0% MgO 0.10% to 60.0% CaO 0.02% to 60.0% Na_2O 0.15% to 30.0% K_2O 0.02% to 30.0% TiO_2 0.02% to 10.0% P_2O_5 0.05% to 50.0% MnO 0.01% to 15.0% LOI 0.01% to 100.0%	Standards analyzed varied 0.5 to 3 % from the proposed value	Precision is better than ±5 percent and, depending on the element, as low as ±0.2 percent
ICP-MS	Limits of detection in parts per million: La (0.002), Ce (0.002), Pr (0.002), Nd (0.009), Sm (0.006), Eu (0.003), Gd (0.011), Tb (0.002), Dy (0.007), Ho (0.002), Er (0.007), Tm (0.002), Yb (0.006), Lu (0.002).	Accuracy similar to ICP-AES and neutron activation analysis (INAA)	The average RSD for the REE is 2.5%. They range from 1.7% to 5.1%.
INAA	Limits of detection in parts per million: La (0.02), Ce (0.5), Nd (2), Sm (0.5), Eu (0.02), Tb (0.1), Yb (0.2), Lu (0.01), Hf (0.1), Se (1), Sb (0.1), Th (0.1), U (0.5).	Accuracy similar to ICP-AES and ICP-MS	The average RSD is 5%. They range from 3% to 10%.
Combustion (total carbon)	Limit of detection and concentration range C 0.05% to 30%	Standard: MAG-1, $\overline{X}$ = 2.28%, n = 12, s = 0.009%, proposed value: 2.15±0.40%	RSD is ≤ 5% for samples with > 0.01% C or an absolute standard deviation of 0.05% C, whichever is greater.
Combustion	Limit of detection and concentration range S 0.05% to 30%	Standard: SDO-1, $\overline{X}$ = 5.44%, n = 10, proposed value: 5.35±0.44%	RSD for standard is 0.2%
Coulometric titration (carbonate carbon)	Limit of detection and concentration range CO_2 0.01% to 50.0%	Standard: GSP-1, $\overline{X}$ = 0.10±0.003%, n = 12, proposed value: 0.11%	RSD is < 5% for concentration range of 0.01% to 36%.
Hydride-generation atomic absorption	Limit of detection Se 0.1ppm.		RSD is 2.0% for solution concentration of 50 ppb.
Ion-selective electrode	Limit of detection and concentration range F 100ppm to 2.7%	Standard: GSP-1, $\overline{X}$ = 3240 ppm, n = 23, proposed value: 3630 ppm	RSD for standard is 11%.

measurements (fig. 3). Samples were collected from the lower level of the mine, from a trench made by mine personnel. The samples come mainly from the Meade Peak Phosphatic Shale Member and one sample from the underlying Grandeur Formation. Chemical analyses were completed in 1993, but publication was delayed by Agency reorganization and individual reassignment.

ANALYTICAL TECHNIQUES AND DATA EVALUATION

Major-Element-Oxide Analyses

The analyzed portion of these samples are aliquots of ground powders (to 200 mesh) dried at 60°C. Major-element oxides (table 1) were measured by inductively-coupled plasma-atomic emission spectroscopy (ICP-AES) after acid digestion (Lichte and others, 1987a). Selected samples from cores collected by the Monsanto Company (now Solutia Inc.) were analyzed by wavelength-dispersive X-ray fluorescence spectroscopy (XRF; Taggart and others, 1987). Loss on ignition at 925°C was measured on the samples which were analyzed by XRF.

Major-element data are used to determine the normative components of each sample. The procedure is discussed in detail by Medrano and Piper (1995), but also below. As each successive calculation compounds any error in the original data, evaluating the quality of the major-element data (table 2) becomes crucial. In the worst case, total CaO is used to calculate the concentration of calcite, but only after adjusting, in order, for the CaO contribution by the detrital fraction, the CaO contribution by apatite, and the CaO contribution by dolomite. Thus, the uncertainty in the calculation of calcite in a sample is dependent upon the uncertainty in the measurements of CaO, as well as of Al_2O_3 (used to calculate the concentration of the detrital fraction), P_2O_5 (used to calculate the concentration of apatite), and MgO (used to calculate the concentration of dolomite).

The limit of detection and the precision and accuracy of each analytical technique has been determined in the U. S. Geological Survey laboratory by a comparison of repeated analyses of standard samples by several different analytical techniques (table 1). Here it is determined in a somewhat different way, from a comparison of carbon measured by ignition with carbon calculated by summing the carbon concentration in the detrital fraction, apatite, dolomite, calcite, and organic matter (fig. 4), based on their stoichiometries (table 3). The correlation between the two carbon values and extrapolation of the curve to zero, suggest that the accuracy of each element analysis given in table 1 represents an upper limit.

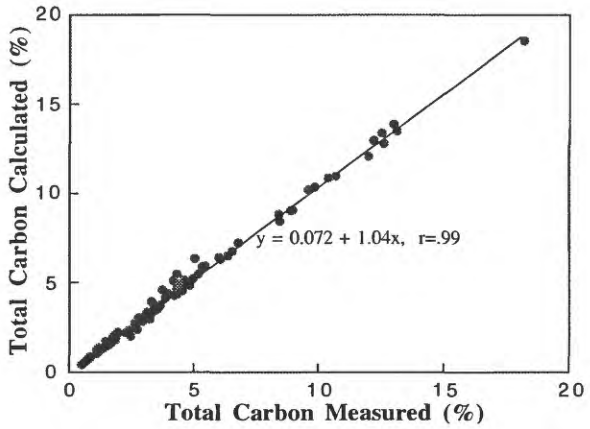

Figure 4. Relation between total carbon measured (table 2) and total carbon calculated, which is based on the stoichiometry and concentration of each carbon-bearing component (table 3).

The quality of data for the Phosphoria Formation has been evaluated further by comparing analyses of individual elements made by more than one technique (Medrano and Piper, 1995). Ideally, the analytical results of multiple techniques should agree closely. In earlier work (Medrano and Piper, 1995; Piper and Isaacs, 1995) x-y plots of individual elements measured by different techniques showed agreement within 5 percent of the one-to-one line in 75 percent of the cases. This procedure does not identify which technique is in error; rather, it establishes that a finite systematic error exists in one or, possibly, both analyses. Analytical results for P_2O_5, measured by wet chemistry and listed by Sheldon and others (1953, 1963), Smart and others (1954), and McKelvey and others (1959) for Mud Spring, Conant Creek, and Lakeridge sections, are in excellent agreement with more recent measurements made by XRF (Medrano and Piper, 1995). In contrast, the ICP-AES data for the Wheat Creek and Fontenelle Creek sections are higher by approximately 13 percent and 9 percent, respectively, than the XRF data. These deviations suggest a possible systematic error in the ICP-AES data for P_2O_5, an error that the Enoch

Table 2a. Concentration of major-element oxides, organic carbon, F, and S, P-series of samples. All values are in percent, except for MnO, which is reported in parts per million.

	P-238	P-237	P-236	P-235	P-234	P-233	P-232	P-231	P-230	P-229	P-228	P-227	P-226	P-225	P-224	P-223	P-222	P-221	P-220	P-219	P-218	P-217	P-216	P-215
Al_2O_3--	1.0	11.2	11.2	11.2	11.2	14.4	1.5	8.3	4.5	9.1	1.4	10.4	0.51	10.2	1.1	6.4	0.51	1.6	3.8	8.9	3.6	5.7	8.5	7.6
CaO----	0.41	6.9	2.8	2.1	0.80	6.6	30.8	16.8	35.0	1.3	42.0	2.7	51.8	7.0	50.4	23.8	50.4	46.2	35.0	11.9	37.8	21.0	16.8	13.8
Fe_2O_3--	0.46	3.6	3.7	3.7	3.7	4.4	0.49	2.1	1.2	2.3	0.44	3.3	0.13	4.9	0.36	1.6	0.20	0.49	1.2	2.6	1.2	1.9	2.6	3.2
K_2O----	0.18	2.8	2.5	2.5	1.8	3.1	0.25	1.6	0.96	1.5	0.27	1.9	0.10	1.5	0.22	1.0	0.10	0.30	0.73	2.2	0.71	1.0	1.9	1.9
MgO---	0.08	1.3	0.95	0.83	0.75	1.2	18.2	0.56	0.35	0.60	0.13	0.66	0.15	0.50	0.20	0.40	0.13	0.36	0.46	0.56	5.1	12.4	0.7	0.48
Na_2O---	0.04	0.13	0.54	0.96	1.1	0.54	0.22	0.98	0.62	0.90	0.27	1.2	0.15	2.0	0.19	0.97	0.16	0.19	0.36	1.0	0.86	1.3	1.0	0.77
P_2O_5---	0.25	4.1	1.6	1.3	0.50	4.1	0.64	11.2	22.9	0.78	29.8	1.5	39.0	4.6	36.7	16.5	36.7	32.1	25.2	7.3	0.16	0.21	10.1	10.3
TiO_2----	0.02	0.35	0.33	0.38	0.45	0.23	0.05	0.22	0.07	0.28	0.03	0.33	0.01	0.37	0.03	0.05	0.01	0.05	0.08	0.17	0.08	0.13	0.12	0.15
MnO---	5.2	81.4	142	111	2320	167	916	55.5	19.4	51.7	23.2	219	20.7	878	31.0	335	12.9	19.4	58.1	31.0	219	916	81.4	14.2
CO_2----	0.05	0.2	0.08	0.04	0.04	0.17	40.4	0.43	0.9	0.04	0.93	0.07	1.5	0.2	1.3	0.69	1.4	1.42	1.0	0.36	32.5	27.3	0.46	0.26
Org. C--	0.46	3.8	1.8	1.4	0.81	1.8	1.18	1.3	3.05	0.61	1.2	1.1	1.5	0.74	1.4	1.4	1.4	5.04	4.5	2.7	0.98	0.95	4.2	2.9
F--------	0.03	0.64	0.28	0.22	0.12	0.64	0.1	1.5	2.84	0.25	5.8	0.33	4.0	0.71	4.2	3.6	3.8	2.14	2.9	1.0	0.05	0.03	1.4	1.0
S--------	0.03	0.38	0.16	0.09	0.04	0.14	0.001	0.15	0.42	0.02	0.22	0.1	0.17	0.05	0.17	0.11	0.15	0.52	0.45	0.22	0.5	0.06	0.43	0.29
H_2O^+---	0.72	3.6	3.2	3.0		4.1									1.0						1.0			2.8
H_2O^----	0.34	3.5	2.4	1.7		2.5									0.56						0.42			1.9

	P-214	P-213	P-212	P-211	P-210	P-209	P-208	P-206	P-207	P-205	P-204	P-203	P-202	P-201	P-200	P-199	P-198	P-197	P-195	P-196	P-194	P-193	P-192	P-191
Al_2O_3--	6.6	11.3	3.2	7.0	1.3	10.0	9.5	6.2	8.1	9.6	7.2	1.5	8.5	9.5	11.3	10.6	9.5	6.9	4.5	9.4	4.2	11.0	7.6	1.6
CaO----	18.2	3.5	36.4	22.4	43.4	2.5	7.4	10.1	6.0	6.9	25.2	44.8	15.4	7.1	1.2	4.2	12.0	0.35	15.4	11.1	36.3	0.56	30.8	44.8
Fe_2O_3--	2.7	4.6	1.7	2.0	0.90	3.4	3.2	2.0	2.3	3.2	1.6	0.53	2.6	3.0	3.9	3.4	3.6	1.4	22.9	3.2	1.9	2.0	2.4	1.3
K_2O----	1.5	2.7	0.82	1.7	0.20	2.2	2.1	1.3	1.7	1.6	1.5	0.34	1.9	1.9	2.1	2.7	2.1	2.1	0.98	2.4	1.0	2.8	1.6	0.3
MgO---	0.38	0.35	0.27	0.32	0.08	0.17	0.20	0.25	0.20	2.8	0.51	0.18	0.51	0.56	0.12	0.61	0.61	0.91	0.36	0.70	0.35	0.18	0.66	0.08
Na_2O---	0.88	1.3	0.55	1.1	0.49	1.9	2.2	1.3	1.6	2.0	0.93	0.49	1.2	1.4	2.6	1.2	0.90	0.58	0.51	1.0	0.78	1.6	0.73	0.67
P_2O_5---	12.6	1.9	25.2	12.6	32.1	1.3	4.8	6.4	3.9	1.8	15.8	32.1	10.1	4.4	0.73	2.5	8.7	18.8	11.5	6.9	25.2	0.46	18.6	32.1
TiO_2----	0.12	0.33	0.07	0.05	0.03	0.23	0.28	0.12	0.30	0.32	0.07	0.03	0.18	0.37	0.43	0.28	0.22	0.05	0.15	0.22	0.03	0.33	0.07	0.03
MnO---	284	31.0	800	50.4	63.3	284	2450	167	193	2320	111	36.2	34.9	112	2060	78.8	51.6	18.1	245	118	20.7	40.0	94.3	45.2
CO_2----	0.49	0.09	0.9	0.55	1.1	0.06	0.3	0.49	0.16	5.8	0.67	0.86	0.42	0.18	0.07	0.07	0.24	0.55	0.42	0.36	0.65	0.01	0.07	1.03
Org. C--	3.27	2.4	4.0	3.6	0.79	1.6	0.71	1.7	1.3	1.7	4.4	4.3	4.1	4.8	1.1	4.5	3.5	5.9	1.56	4.2	3.7	0.64	4.3	0.91
F--------	1.49	0.28	2.9	1.7	3.5	0.16	0.55	0.74	0.44	0.20	2.0	3.3	1.2	0.60	0.08	0.46	0.96	2.1	1.32	0.98	2.8	0.06	2.5	3.4
S--------	0.34	0.21	0.5	0.37	0.18	0.14	0.07	0.16	0.13	0.12	0.50	0.68	0.47	0.59	0.10	0.50	0.38	0.73	0.3	0.54	0.58	0.08	0.65	0.36
H_2O^+---			0.98				2.5						2.3			3.5				3.7				
H_2O^----			2.7				0.69						2.0			1.8				1.8				

	P-190	P-189	P-188	P-187	P-186	P-185	P-184	P-183	P-182	P-181	P-180	P-179	P-178	P-177	P-176	P-175	P-174	P-173	P-172	P-171	P-170	P-76	P-75	P-74
Al_2O_3--	8.9	10.2	10.6	10.4	7.0	6.4	10.6	8.7	1.5	2.1	10.6	11.7	10.2	8.7	10.6	11.2	10.4	0.19	0.53	10.2	3.0	10.2	11.7	8.5
CaO----	12.9	6.6	5.3	4.6	12.2	10.4	1.2	18.2	33.6	30.8	3.5	4.6	11.6	19.6	0.66	0.94	10.5	0.41	49.0	14.0	28.0	15.4	5.5	23.8
Fe_2O_3--	2.7	3.6	2.7	3.7	3.2	2.9	2.7	4.2	0.40	0.54	2.9	3.6	3.9	2.4	3.6	3.7	3.6	0.07	0.21	3.2	1.0	3.4	3.7	2.3
K_2O----	2.2	2.1	2.4	2.2	1.6	1.5	2.7	1.9	0.39	0.54	2.3	2.7	2.5	2.1	2.1	2.3	2.2	0.04	0.13	2.4	0.57	2.7	1.9	1.9
MgO---	0.46	0.20	0.36	0.38	0.93	0.91	0.32	0.71	18.2	15.8	0.38	0.48	0.66	0.63	0.20	0.25	0.60	0.08	4.0	1.8	14.3	0.68	2.8	0.40
Na_2O---	1.3	1.6	1.6	1.5	0.28	0.24	1.6	0.69	0.12	0.19	1.6	1.5	0.77	0.66	2.2	2.0	1.3	0.12	0.11	0.80	0.85	0.80	3.0	1.3
P_2O_5---	9.4	4.6	4.4	3.9	9.4	8.5	0.66	12.6	0.16	0.32	2.0	2.5	7.6	12.6	0.23	0.41	6.4	0.05	0.48	6.2	0.09	9.4	0.30	14.9
TiO_2----	0.15	0.33	0.33	0.32	0.20	0.20	0.40	0.17	0.05	0.05	0.32	0.32	0.23	0.13	0.35	0.37	0.28	0.01	0.02	0.30	0.10	0.20	0.38	0.07
MnO---	42.6	258	37.5	142	16.8	15.5	29.7	51.7	219	491	112	516	477	38.7	154	32.3	245	12.9	193	91.7	258	47.8	1420	63.3
CO_2----	0.12	0.18	0.09	0.08	0.23	0.17	0.04	0.45	42.8	40.4	0.08	0.2	0.26	0.42	0.03	0.03	0.8	0.11	40.8	4.3	36	0.42	6.5	0.58
Org. C--	3.6	1.1	3.3	3.1	18.1	1.9	2.2	6.2	0.87	0.98	3.5	2.9	3.4	3.6	1.6	1.7	2.7	1.7	2.0	7.8	0.88	6.4	0.69	3.8
F--------	1.0	0.58	0.60	0.33	1.2	1.2	0.09	1.7	0.04	0.06	0.24	0.34	0.99	1.6	0.03	0.07	0.77	0.03	0.05	0.78	0.02	1.3	0.03	1.8
S--------	0.40	0.10	0.34	0.34	2.0	2.7	0.28	0.80	0.01	0.01	0.36	0.32	0.40	0.42	0.14	0.16	0.29	0.15	0.14	0.89	0.03	0.8	0.02	0.47
H_2O^+---	2.6						2.9			1.0			3.9									4.5		
H_2O^----	2.7						1.1			0.38			1.8									2.9		

Table 2a. Cont.

	P-73	P-72	P-71	P-70	P-69	P-68	P-67	P-66	P-64	P-63	P-62	P-61	P-60	P-59	P-58	P-57	P-56	P-55	P-54	P-53	P-52	P-51	P-50	P-49
Al_2O_3--	14.2	16.9	8.5	11.2	1.4	2.1	6.2	4.9	1.0	4.5	0.34	4.0	9.8	4.5	7.2	3.2	2.7	1.2	0.42	1.5	10.2	1.7	8.6	5.7
CaO----	2.5	1.1	23.8	7.8	46.2	37.8	21.0	33.6	37.8	29.4	49.0	33.6	4.6	35.0	16.8	26.6	28.0	44.8	50.4	43.4	5.0	44.8	15.4	29.4
Fe_2O_3--	2.9	3.2	2.9	4.3	0.47	0.79	2.0	1.3	0.17	1.2	0.41	1.4	3.1	1.4	2.4	0.87	0.81	0.54	0.20	0.54	2.7	0.63	1.0	1.7
K_2O----	4.2	4.2	2.2	2.5	0.40	0.55	1.9	1.5	0.43	1.5	0.10	1.3	2.9	1.5	2.3	0.92	0.77	0.37	0.14	0.48	3.0	0.58	3.7	1.8
MgO---	0.36	0.18	0.65	0.20	0.25	0.30	1.2	0.51	11.6	1.0	0.17	0.35	1.8	0.43	0.25	15.8	15.8	0.20	0.15	0.22	0.28	0.25	10.4	2.7
Na_2O---	0.62	1.1	0.86	2.2	0.62	0.55	0.63	0.70	0.24	0.71	0.28	0.62	1.9	0.62	1.2	0.78	0.80	0.40	0.32	0.30	2.0	0.34	0.27	0.93
P_2O_5---	0.37	0.66	15.6	4.8	32.1	27.5	13.3	22.2	12.8	19.9	36.7	21.1	1.1	20.9	11.7	2.3	1.6	34.4	36.7	32.1	2.8	32.1	0.14	17.2
TiO_2----	0.22	0.17	0.08	0.28	0.03	0.07	0.17	0.03	0.02	0.03	0.01	0.08	0.40	0.05	0.27	0.10	0.08	0.05	0.02	0.05	0.43	0.05	0.12	0.03
MnO---	2066	207	65.9	516	5.2	258	43.9	20.7	168	46.5	5.2	16.8	129	16.8	27.1	297	206	16.8	5.2	5.2	516	10.3	167	49.1
CO_2----	0.11	0.08	0.83	0.22	1.2	0.90	2.1	1.1	28.5	2.6	1.3	0.85	3.8	0.79	0.41	33.0	35.4	1.2	1.2	1.1	0.14	1.2	20.2	5.9
Org. C--	8.4	0.76	4.3	3.4	5.0	4.7	5.5	4.3	1.2	2.5	4.8	4.0	1.7	4.8	2.5	0.60	0.75	3.1	4.3	3.11	3.2	2.8	1.3	2.7
F--------	0.04	0.1	2	0.58	3.4	5.5	1.8	2.8	1.3	2.6	3.5	2.3	0.13	2.3	1.3	0.28	0.11	3.2	3.3	3.32	0.30	3.3	0.52	2.4
S--------	0.92	0.04	0.53	0.35	0.87	0.67	0.70	0.55	0.04	0.32	0.70	0.57	0.17	0.77	0.34	0.01	0.01	0.47	0.62	0.45	0.38	0.44	0.01	0.61
H_2O^+---	5.1					2.1			0.66						2.1				1.7					
H_2O^----	3.6					1.5			0.36						1.1				1.2					

	P-48	P-47	P-46	P-45	P-44	P-43	P-42	P-41	P-40
Al_2O_3--	2.8	0.89	0.70	1.6	9.3	4.0	10.4	0.09	0.11
CaO----	37.8	47.6	49.0	43.4	4.5	21.0	2.5	32.2	33.6
Fe_2O_3--	3.9	1.3	0.76	0.81	3.0	1.0	4.2	0.09	0.10
K_2O----	0.95	0.30	0.25	0.53	2.8	1.0	2.9	0.01	0.01
MgO---	0.58	0.22	0.23	0.43	2.2	12.8	0.95	19.9	21.6
Na_2O---	0.82	0.96	1.0	0.90	0.15	0.65	0.13	0.05	0.05
P_2O_5---	27.5	34.4	34.4	29.8	1.3	0.07	1.4	0.37	0.39
TiO_2----	0.08	0.03	0.03	0.05	0.40	0.12	0.40	0.01	0.01
MnO---	76.2	18.1	23.2	12.9	168	181	581	349	659
CO_2----	1.8	1.9	2.06	1.4	2.9	29.2	0.22	46	46.4
Org. C--	2.3	2.1	2.20	4.0	2.1	0.92	0.75	0.05	0.35
F--------	5.5	3.8	3.72	3.2	0.36	0.06	0.62	0.06	0.06
S--------	0.76	1.1	0.98	1.2	0.28	0.04	0.09	0.01	0.01
H_2O^+---	1.9						2.1		
H_2O^----	0.71						2.7		

Table 2b. Concentration, in percent, of major-element oxides measured by XRF plus loss on ignition (LOI), E-series of samples.

	E35-38	E35-34	E35-30	E35-26	E35-22	E34-63	E34-59	E34-55	E34-51	E34-47	E8-38	E8-35	E8-32	E8-29	E8-26
SiO_2----	4.27	11.9	56.3	9.85	30.1	4.45	15.5	19.3	9.81	21.6	12.6	22.2	60.1	17.8	22.6
Al_2O_3--	0.52	1.75	8.63	1.44	4.6	0.5	2.35	3.11	1.42	3.61	1.71	3.07	9.7	2.86	3.6
CaO----	48.2	41.6	8.14	44	29.6	47	35.6	23.1	44.5	34.4	41.3	31.3	6.34	36.6	36.8
Fe_2O_3--	0.29	0.82	3.05	0.63	1.75	0.2	1.17	1.51	0.62	1.51	0.88	1.6	3.17	1.19	1.26
K_2O----	0.2	0.62	3.05	0.54	1.58	0.19	0.85	1.02	0.57	1.38	0.62	1.08	3.42	1.08	1.34
MgO---	0.28	0.52	2.99	0.43	0.78	0.11	0.29	14.1	0.1	0.25	0.3	0.19	0.31	0.18	0.19
Na2O---	0.29	0.6	1.62	0.55	1.03	0.26	0.55	0.86	0.67	0.82	0.42	0.54	1.45	0.52	0.73
P_2O_5---	33.9	27.4	1.26	30.1	19.3	33.3	25.8	0.1	31.1	23.6	28.1	23.3	4.03	26.2	25
TiO_2----	0.036	0.132	0.636	0.106	0.351	0.034	0.173	0.246	0.105	0.274	0.13	0.221	0.724	0.208	0.267
MnO---															
CO_2----															
Org. C--															
F--------															
S--------															
LOI---	11.9	15	11.8	12	9.6	14.2	17.1	35.6	10.8	12.3	13.8	16.6	10.7	13.2	7.3

Table 3. Formulas used to calculate the normative components and total CO_2, based on measured concentrations of major-element oxides (table 2). The amount of H_2O in organic matter was selected to give a carbon concentration of 71.6% and is not intended to imply a concentration of hydrogen or oxygen in the organic component as shown.

Component	Formula	Stoichiometry
Detritus----------	$6.0 \times Al_2O_3$	$Mg_{.3}Na_{.44}K_{.86}Fe_{.7}Al_{2.4}Si_{10}O_{25.6}{\cdot}5.7(H_2O)$
Biogenic silica---------	$SiO_2 - 3.5 \times Al_2O_3$	SiO_2
Apatite----------	$(P_2O_5 - 0.01 \times Al_2O_3) \div 0.40$	$Ca_5(PO_4)_{2.7}(CO_3)_{0.4}F$
Dolomite----------	$(MgO - 0.07 \times Al_2O_3) \div 0.22$	$MgCa(CO_3)_2$
Calcite----------	$(CaO - 0.15 \times Al_2O_3 - 1.37 \times MgO - 1.38 \times P_2O_5) \div 0.56$	$CaCO_3$
Organic matter---------	Organic Carbon x 1.4	$C_4(H_2O)$
ΣCO_2----------	0.48 x Dolomite + 0.01 x Apatite + 0.44 x Calcite + 2.62 x Organic Matter	CO_2

Valley data might also have. However, the other sections give far better results. The carbon plot (fig. 4) certainly suggests that the Enoch Valley data are much better as well. The analyses of the other major oxides also are in close agreement (Medrano and Piper, 1995).

Trace-Element Analyses

Trace elements were determined by ICP-AES (table 4) and the rare earth elements (REE) by inductively coupled plasma-mass spectroscopy (ICP-MS; table 4). Selenium was measured by hydride-generation atomic absorption spectrometry in the XRAL laboratory at Don Mills, Ontario, Canada. The range of detection, precision, and accuracy of each analytical technique is given in table 1. The trace elements—Bi, Nb, Sn, Ta—were below their detection level in most samples and have not been reported for the other samples.

La analyses give an excellent measure of the quality of trace-element data. It was analyzed by the two techniques—ICP-MS and ICP-AES—and was significantly above the detection limit. The plot of La (fig. 5a) gives similar results to the x-y plots for the major elements analyzed by both ICP-AES and XRF, $\sigma \geq 0.98$, and a similarly small deviation of ≤5 percent from the 1:1 curve, as reported earlier.

For several of the plots of the data and for a statistical analysis of the data, the $\log_{10}$ of the measured values has been used rather than the raw data. In the case of trace elements, linear plots of the raw data invariably show increasing scatter at high concentration levels; the data are heteroscedastic. That is, residuals of variance are higher at high concentrations

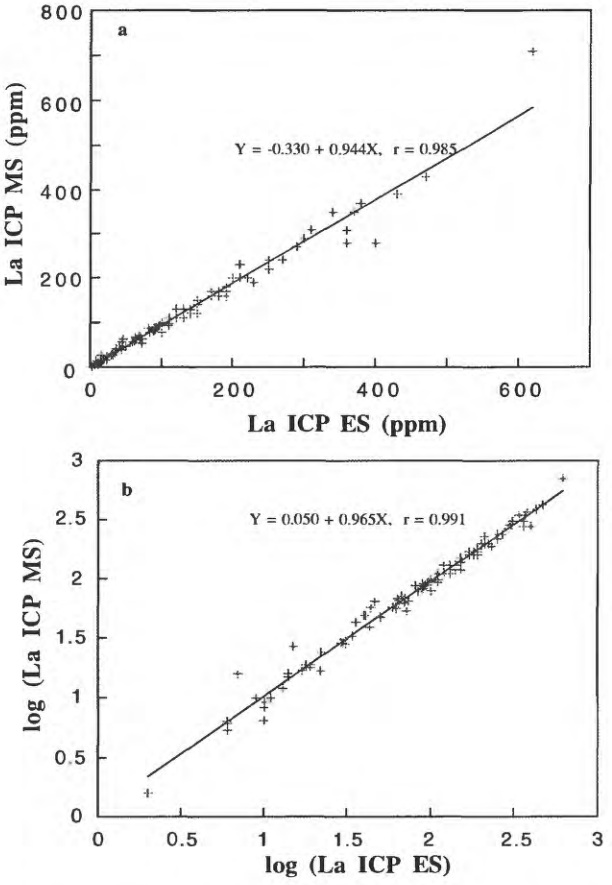

Figure 5. Relation between La measured by ICP-AES and ICP-MS. Values are plotted in (a); $\log_{10}$ of the values are plotted in (b).

Table 4a. Minor-element concentrations, in parts per million, measured by ICP-AES and AA, in the case of Se (P-series of samples).

	P-238	P-237	P-236	P-235	P-234	P-233	P-232	P-231	P-230	P-229	P-228	P-227	P-226	P-225	P-224	P-223	P-222	P-221	P-220	P-219	P-218	P-217	P-216	P-215
Ag-------	2	2	2	2	2	2	2	2	2	2	2	6	2	9	5	8	2	5	9	15	2	2	9	12
As-------	10	36	10	24	24	19	10	10	10	10	10	10	10	61	10	20	10	10	10	25	10	10	23	37
Ba-------	42	310	330	330	310	360	44	280	350	200	56	280	98	240	94	160	75	130	130	260	96	130	270	270
Cd------	1	37	32	22	12	9	10	12	44	18	16	28	30	50	29	32	32	160	100	53	22	28	50	69
Co------	41	7	13	16	16	14	13	6	8	11	7	11	6	21	6	8	6	9	9	11	7	12	12	7
Cr-------	180	2000	650	710	180	970	100	420	490	530	310	450	620	520	930	750	470	1100	1700	1700	160	220	2200	1400
Cu------	9	110	39	52	23	54	15	31	47	25	19	43	32	57	38	60	15	120	110	130	13	26	160	85
La-------	7	81	44	41	36	120	14	170	620	15	130	46	69	63	310	180	210	72	220	89	11	19	110	140
Li-------	11	41	25	25	19	32	5	19	12	16	2	24	2	17	4	13	2	12	16	27	2	5	35	24
Mo------	2	2	6	14	2	8	2	4	9	16	2	18	2	38	7	10	2	2	5	22	2	2	16	2
Ni-------	25	270	140	120	240	260	56	120	110	160	52	180	26	350	41	130	26	73	84	97	41	95	240	120
Pb------	24	37	12	12	14	12	2	2	8	9	2	13	2	21	8	9	2	2	8	17	44	2	11	8
Sc-------	1	11	11	11	11	14	1	8	14	6	1	10	1	9	5	10	5	1	8	10	1	6	10	11
Se-------	6.4	10	122	12.7	11	16.7	7.2	25.7	44.5	5.4	1.9	101	1	46.1	2.7	36.1	5.2	23	28	74.9	20.4	18.3	49.2	5.6
Sr-------	28	160	88	75	63	170	240	330	920	56	590	81	1100	150	960	490	980	930	920	330	360	190	590	600
V-------	48	480	230	220	130	160	29	110	100	160	87	200	430	860	260	530	210	1100	740	730	130	210	280	250
Y--------	20	150	64	61	42	180	16	270	970	25	180	87	120	91	550	320	410	130	410	150	10	16	200	250
Zn-------	94	1300	790	410	770	830	200	660	610	890	280	1200	250	2700	380	910	270	680	690	530	270	470	920	740
U--------	4.34	58.4	16.8	13.1	4.55	36.6	3.16	52.1	88.7	7.28	59.2	10.9	110	16.2	120	46.4	134	119	76.8	39.5	1.65	2.49	34.1	49.9
La-------	16	88	57	49	43	130	16	170	710	27	130	64	63	68	310	170	230	54	200	91	10	19	110	130
Ce-------	6.1	66	70	56	76	94	8.2	95	160	29	32	99	10	54	52	76	46	14	44	52	17	27	52	58
Pr-------	3.4	15	11	9.3	10	20	2.1	30	100	4.9	19	18	5.9	13	35	27	32	6.3	23	15	2.3	4.0	16	19
Nd------	13	58	39	35	37	73	8.2	120	410	19	74	76	24	54	140	110	140	25	94	61	7.8	15	66	73
Sm------	2.4	12	8.3	7.3	7.7	14	1.2	23	69	4.2	12	16	4.2	10	24	22	23	4.2	17	11	1.6	3.0	11	13
Eu-------	0.59	2.7	1.9	1.5	1.9	3.4	0.30	5.6	17	0.77	3.1	3.6	1.1	2.2	6.1	4.8	5.8	1.1	4.2	2.6	0.35	0.73	2.7	3.3
Gd------	2.7	13	8.4	8	7.0	16	1.6	25	77	3.3	13	12	6.0	9.6	33	24	25	5.4	22	10	1.9	3.0	11	16
Tb-------	0.34	2	1.3	1.2	1.2	2.4	0.20	3.9	12	0.55	1.9	2.2	0.91	1.6	4.7	3.5	4.2	0.79	3.4	1.9	0.24	0.46	2.0	2.4
Dy-------	2.2	13	7.8	7.3	7.4	15	1.4	25	78	4.0	13	14	6.6	11	31	26	31	6.4	24	13	1.5	3.4	14	16
Ho-------	0.42	2.9	1.7	1.5	1.5	3.3	0.32	5.0	17	0.72	2.7	2.4	1.5	2.1	8	5.4	6.7	1.6	5.6	2.8	0.31	0.58	3.3	3.7
Er-------	1.3	9.4	5.4	4.9	4.5	10	0.89	15	52	2.3	8.3	6.8	5.0	6.6	26	18	21	4.9	20	8.7	1	1.7	10	12
Tm------	0.18	1.3	0.79	0.75	0.66	1.4	0.15	1.9	7.1	0.36	1.2	0.84	0.70	0.93	3.7	2.6	3.0	0.73	2.6	1.3	0.16	0.27	1.5	1.7
Yb-------	1	8.8	5.4	4.5	4.4	8.7	0.85	11	42	2.6	6.7	5.0	4.1	5.9	24	15	18	4.5	17	7.7	1.1	1.8	9.0	11

	P-214	P-213	P-212	P-211	P-210	P-209	P-208	P-206	P-207	P-205	P-204	P-203	P-202	P-201	P-200	P-199	P-198	P-197	P-195	P-196	P-194	P-193	P-192	P-191
Ag-------	13	9	6	10	2	2	2	5	4	5	8	5	11	14	4	12	7	10	29	8	2	2	11	2
As-------	31	51	20	28	10	22	33	10	22	23	10	10	21	27	42	37	33	30	400	36	10	25	31	23
Ba-------	210	280	210	260	130	240	250	210	230	200	290	130	280	340	240	370	330	360	170	290	170	250	260	76
Cd------	36	26	27	20	6	8	12	8	5	21	26	16	24	81	51	28	41	77	83	59	21	6	89	21
Co------	11	12	28	12	16	12	14	12	20	14	7	19	7	10	16	8	8	8	13	10	11	11	13	23
Cr-------	1300	840	980	440	390	340	210	280	480	320	1700	600	2300	2100	220	2400	2500	1700	2200	3500	2000	450	2000	560
Cu------	160	110	92	89	28	57	60	42	74	58	160	62	170	110	35	63	230	360	250	200	130	18	190	20
La------	97	67	210	170	200	31	64	91	50	50	340	200	180	92	34	110	270	400	290	250	370	9	300	170
Li-------	18	15	10	10	2	6	7	7	8	7	28	6	27	27	4	31	33	47	18	40	17	11	34	2
Mo------	33	37	25	32	8	24	22	21	6	23	26	8	39	45	11	40	12	9	340	96	14	13	52	5
Ni------	280	290	330	220	62	210	450	150	150	380	220	130	260	240	340	270	210	190	780	380	68	44	200	52
Pb------	2	13	2	9	2	14	11	2	8	2	2	2	11	13	12	15	9	12	23	17	4	14	13	2
Sc------	7	12	9	6	6	8	11	7	6	10	6	5	12	10	9	11	13	6	8	12	7	6	7	4
Se-------	19.5	31	7.5	24.9	4	7.6	11.5	11.4	11.4	43.5	19.4	9	90.3	33.2	10.9	28.6	40.5	19.7	406	88.7	19.2	35.1	71.1	25
Sr-------	770	150	1500	820	1400	110	240	360	210	170	890	1400	500	240	78	150	410	1200	620	420	1200	76	1400	1600
V-------	360	290	130	180	60	100	100	95	99	200	210	74	280	780	300	380	330	350	530	650	110	97	280	95
Y--------	170	88	400	300	330	37	79	130	64	60	560	310	290	150	32	160	410	560	330	370	460	9	350	200
Zn-------	1300	1500	1200	1300	420	1000	1200	590	730	1000	890	340	810	910	920	620	870	790	3800	1300	110	120	1200	480
U--------	41.5	13.2	51.2	37.2	38.1	5.12	9.11	24.3	11.8	10.3	44.2	49.7	36.7	24.5	5.95	23.8	36.2	59.7	61.7	55.5	53.8	4.51	55.3	56.5
La-------	94	71	200	160	200	31	65	86	48	47	350	200	160	89	33	98	240	280	270	240	350	10	290	160
Ce-------	47	79	46	58	49	47	94	52	60	54	98	40	66	69	58	72	97	67	120	98	71	16	85	46
Pr-------	16	15	24	22	29	7.3	15	12	11	8.5	47	25	22	14	7.6	17	36	37	54	37	44	2.4	35	27
Nd------	66	58	91	89	120	30	56	48	44	33	190	110	84	57	30	65	140	160	220	140	180	8.7	130	110
Sm-------	13	11	16	15	22	5.7	12	8.6	9.9	6.7	33	17	15	11	5.7	13	26	24	39	25	27	1.8	22	18
Eu-------	3.1	2.5	4	3.7	5.6	1.4	2.6	2.1	2.1	1.3	8.1	4.4	3.7	2.6	1.3	3.1	6.2	6.5	8.1	6	6.8	0.38	5.4	4.2
Gd------	14	10	21	17	25	4.9	12	8.8	8.2	5.7	37	20	19	11	4.2	14	27	27	36	30	28	1.3	25	17
Tb-------	2.1	1.8	3.1	2.8	3.8	0.85	1.8	1.4	1.3	0.88	5.7	3.0	2.7	1.9	0.76	2.1	4.4	4.5	5.1	4.3	4.6	0.21	3.7	2.7
Dy-------	16	11	21	19	27	6.0	11	9.9	9.2	6.2	42	21	18	13	5.4	14	32	31	33	27	32	1.7	29	17
Ho-------	3.1	2.3	5.3	4.6	5.5	1.2	2.2	2.2	1.6	1.3	9.1	4.8	4.2	2.8	1.0	3	6.4	6.8	6.4	6.2	7.0	0.40	5.9	3.5
Er------	10	6.8	17	15	18	3.2	6.7	6.7	5.0	3.9	29	15	13	9.2	3.2	9.5	20	21	17	19	20	1.3	18	9.2
Tm------	1.4	0.92	2.5	2.1	2.4	0.50	0.95	0.97	0.69	0.58	3.9	2.0	1.8	1.3	0.48	1.4	2.6	2.8	2.1	2.7	2.7	0.22	2.5	1.3
Yb------	8.4	5.8	16	13	14	3.2	6	6.3	4.2	3.6	23	12	11	8.4	3.3	8	15	17	11	16	16	1.8	15	6.7

Table 4a. Cont.

	P-190	P-189	P-188	P-187	P-186	P-185	P-184	P-183	P-182	P-181	P-180	P-179	P-178	P-177	P-176	P-175	P-174	P-173	P-172	P-171	P-170	P-76	P-75	P-74
Ag-------	8	6	7	7	15	19	9	14	2	2	5	11	5	2	2	4	5	4	2	13	2	15	2	6
As-------	30	36	37	39	34	42	27	60	10	10	38	44	49	31	35	36	41	10	10	35	10	51	60	34
Ba-------	270	200	310	310	160	180	270	250	21	36	380	340	290	270	270	290	290	22	17	260	37	280	120	290
Cd------	86	45	75	55	120	61	14	85	5	8	16	30	27	10	4	1	5	1	8	58	14	46	21	5
Co------	12	15	7	12	4	4	6	10	5	18	9	18	22	13	14	9	12	52	14	6	7	4	32	12
Cr-------	2100	650	1400	1500	8400	10000	800	3300	160	280	1000	1400	3500	2700	460	680	2000	86	250	3200	190	3600	290	910
Cu------	99	62	91	140	540	310	34	230	6	12	81	83	150	170	42	51	110	9	21	180	17	200	30	140
La-------	190	100	140	130	360	360	30	190	10	19	130	100	100	140	18	22	120	2	10	150	10	180	29	140
Li-------	25	11	14	17	69	72	11	39	2	2	17	24	46	35	8	10	24	2	2	40	2	41	6	17
Mo------	13	35	30	42	83	150	24	12	2	2	10	62	51	12	34	24	28	2	10	100	10	67	21	18
Ni-------	220	480	190	180	370	500	130	430	16	42	180	410	440	210	210	150	230	26	54	480	45	450	350	230
Pb------	15	8	13	12	21	29	12	8	2	2	8	17	11	11	11	12	9	9	2	15	2	14	9	9
Sc-------	11	11	11	10	13	13	6	12	1	1	11	14	16	12	7	7	11	1	1	14	1	15	8	6
Sc-------	27.4	183	44.5	52.4	72.6	127	168	7.4	52	3.2	95.8	2.9	41.9	39.5	24	36.1	96.8	5.4	10.8	56	24.5	124	10.7	85.5
Sr-------	510	320	390	450	510	520	100	790	230	240	210	260	530	840	68	80	560	73	660	590	180	630	77	910
V-------	190	200	150	260	570	640	130	410	46	96	250	680	500	250	140	150	230	12	79	460	180	490	220	120
Y--------	230	100	120	140	480	470	18	230	7	14	120	120	130	140	10	14	130	< 4	7	190	5	240	15	150
Zn-------	690	2100	380	280	280	140	280	1200	110	180	660	1300	1500	820	980	700	940	50	140	1500	270	1300	950	820
U--------	30.2	16.0	16.8	17.4	69.0	85.5	5.64	47.6	1.05	2.12	20.3	29.7	34.5	29.0	3.75	4.82	17.7	0.26	2.31	35.2	0.845	47.6	3.56	23.3
La-------	170	95	130	130	280	310	29	170	8.4	18	110	97	99	130	19	24	110	1.6	6.5	150	9.3	170	29	120
Ce-------	69	69	92	82	62	60	39	55	5.4	9.4	78	78	62	56	37	43	56	0.7	2.6	56	15	58	51	49
Pr-------	23	14	19	18	38	44	5.4	22	1.3	2.4	20	19	16	22	4.3	5.7	18	0.3	0.9	22	2.0	23	6.5	18
Nd------	83	52	74	70	150	180	19	87	4.8	8.5	73	80	61	88	15	24	68	0.9	3.7	82	7.9	86	22	73
Sm------	14	9.1	11	12	25	28	3.7	14	0.81	1.6	13	14	11	14	3.8	4.7	13	0.19	0.63	14	1.5	15	5.0	12
Eu-------	3.4	2.2	2.5	2.9	5.9	6.8	0.66	3.6	0.19	0.35	2.9	3.5	2.6	3.2	0.56	0.98	2.9	0.03	0.12	3.6	0.28	3.7	0.87	2.7
Gd------	17	8.1	10	12	26	29	3.1	16	0.8	1.4	13	14	12	13	1.9	3.7	10	0.2	0.5	15	1.1	18	3.8	12
Tb-------	2.4	1.4	1.7	2.0	3.9	4.6	0.45	2.3	0.07	0.2	2.0	2.3	1.7	2.0	0.39	0.61	1.6	0.01	0.08	2.4	0.17	2.5	0.66	1.7
Dy-------	15	9.9	12	13	29	31	2.9	18	0.76	1.4	13	15	11	14	3.2	4.0	13	0.15	0.77	17	1.3	17	4.2	12
Ho-------	3.4	2.0	2.3	2.7	6.0	6.8	0.63	3.6	0.14	0.29	2.6	3.0	2.5	2.7	0.57	0.73	2.6	0.05	0.13	3.5	0.27	3.7	0.73	2.5
Er-------	11	6.3	7.3	8.4	19	21	2	11	0.45	0.88	8.8	8.8	7.8	7.7	1.8	2.2	8.2	0.12	0.37	11	0.81	12	2.3	7.5
Tm------	1.5	0.92	1.1	1.1	2.5	2.8	0.34	1.5	0.06	0.13	1.1	1.3	1.1	1.1	0.32	0.36	1.1	0.015	0.06	1.5	0.12	1.6	0.37	1.1
Yb-------	8.8	5.8	6.3	7.0	15	16	2.3	9.5	0.43	0.79	7.4	7.8	7	6.2	2.3	2.3	6.5	0.09	0.37	9.9	1.0	9.9	2.4	6.4

	P-73	P-72	P-71	P-70	P-69	P-68	P-67	P-66	P-64	P-63	P-62	P-61	P-60	P-59	P-58	P-57	P-56	P-55	P-54	P-53	P-52	P-51	P-50	P-49
Ag-------	10	17	10	9	8	10	36	21	4	18	7	15	8	11	10	2	2	6	2	10	8	7	11	16
As-------	65	82	53	82	10	10	40	51	10	24	10	35	43	46	35	10	10	10	10	10	44	10	27	42
Ba-------	100	100	270	120	110	110	210	200	40	140	58	150	250	170	220	50	59	100	46	66	260	77	53	170
Cd------	10	1	7	7	10	140	280	230	31	58	150	350	150	280	160	130	71	200	180	220	97	250	120	39
Co------	8	11	6	27	4	4	5	5	6	6	13	4	5	3	6	8	8	4	4	5	11	15	4	3
Cr-------	550	2300	2500	870	1300	950	1800	1700	260	970	370	1400	490	1200	750	140	110	690	230	790	540	1000	380	1600
Cu------	330	60	200	140	140	160	280	210	20	83	27	170	67	190	88	16	16	96	20	70	120	100	40	110
La------	31	17	190	70	380	430	230	470	110	190	150	140	43	100	73	22	13	88	90	64	62	120	6	150
Li-------	2	5	33	4	7	7	32	29	2	12	2	19	7	15	10	2	2	5	2	6	9	9	9	27
Mo------	37	26	73	37	13	26	120	77	6	33	7	46	70	30	82	9	10	8	9	12	130	25	10	33
Ni-------	740	180	380	430	140	230	340	260	45	180	130	170	220	170	160	67	48	77	73	99	550	86	480	220
Pb------	23	30	11	9	2	9	16	14	2	9	2	16	13	18	10	2	4	4	2	2	16	9	2	12
Sc------	5	1	9	10	5	11	9	6	1	6	1	5	7	4	6	1	1	1	1	1	6	1	1	8
Se-------	169	153	173	115	24.1	32.4	108	64.3	2.6	41.7	42.5	32.6	287	100	72	8.5	11.7	48.1	70.1	21.4	96	59.2	25	43.1
Sr-------	69	41	890	270	1600	1200	660	1300	750	1000	1400	860	130	900	450	210	180	1100	1000	850	140	810	81	700
V-------	130	230	270	260	120	800	2200	1400	140	910	640	2700	1300	2800	2200	370	340	1800	750	1800	1300	1400	1100	440
Y-------	21	11	210	79	430	620	330	630	140	240	200	190	41	140	92	22	12	130	130	91	62	170	4	200
Zn-------	1200	910	1100	1300	420	980	2800	2100	310	1400	1500	2700	2700	2400	2300	870	800	1500	1400	1600	3400	1800	8900	2000
U------	5.71	1.77	41.5	15.3	57.1	127	70.8	141	27.8	107	73.6	178	11.4	200	75.7	9.25	6.89	194	135	118	31.2	169	1.45	49.3
La------	28	17	160	69	370	390	190	430	93	180	120	130	39	79	64	17	12	81	83	62	56	110	5.4	140
Ce-------	39	26	47	58	51	63	59	78	16	47	16	38	54	29	50	19	14	16	15	17	67	24	11	42
Pr------	6.2	4.1	22	13	45	43	29	52	9.5	20	12	15	7.8	10	9.9	2.9	2.1	8.6	8.6	6.8	13	11	1.0	15
Nd------	23	16	89	51	190	160	110	210	36	75	52	67	31	46	38	11	8.7	33	33	28	57	45	4.3	64
Sm------	4.6	3.1	14	9.6	29	28	21	32	5.9	14	7.5	10	6.1	7.9	7.5	2.4	1.6	5.8	5.4	4.8	11	8.0	0.69	10
Eu-------	1	0.72	3.1	2.2	6.8	7.2	5.2	8.2	1.5	3.5	1.9	2.6	1.4	1.9	1.7	0.50	0.34	1.4	1.4	1.1	2.4	1.9	0.08	2.5
Gd------	3.9	2.1	13	8.6	31	38	23	37	8.3	13	8.8	11	4.8	8.2	7.8	2.0	1.5	6.2	7.5	5.0	9.1	8.3	0.4	11
Tb-------	0.56	0.29	2.1	1.5	4.4	5.3	3.5	5.8	1.1	2.4	1.4	1.7	0.78	1.3	1.2	0.33	0.22	0.96	0.98	0.80	1.4	1.3	0.08	1.7
Dy------	3	1.5	15	9.2	31	34	24	40	7.2	18	11	13	6.6	9.4	7.6	2.4	1.7	7.8	6.9	5.7	9.2	10	0.81	12
Ho-------	0.56	0.27	3.1	2.0	6.7	8.3	5.1	9.2	1.8	4.0	2.5	2.9	1.2	2.1	1.6	0.53	0.35	1.7	1.7	1.3	1.7	2.4	0.17	2.8
Er------	1.6	0.94	9.8	5.9	20	26	16	29	5.4	12	8.0	9.8	3.5	6.6	5.3	1.7	0.95	5.9	5.2	4.7	4.5	7.4	0.40	8.9
Tm------	0.23	0.12	1.4	0.78	2.7	3.7	2.0	3.9	0.81	1.7	1.1	1.4	0.59	0.94	0.77	0.24	0.15	0.87	0.76	0.63	0.58	1.1	0.08	1.2
Yb------	1.4	0.65	8.4	4.4	16	23	13	24	5	10	7.1	8.6	4.0	5.8	4.9	1.6	1.0	5.7	4.5	4.0	3.7	6.7	0.59	7.8

Table 4a. Cont.

	P-48	P-47	P-46	P-45	P-44	P-43	P-42	P-41	P-40
Ag-------	15	2	2	7	6	2	2	2	2
As-------	140	44	29	23	39	25	40	10	10
Ba-------	120	170	140	92	270	100	230	22	60
Cd-----	46	30	43	76	160	150	40	23	37
Co------	7	9	16	21	30	41	33	9	13
Cr-------	760	630	790	1400	820	75	480	21	34
Cu------	58	53	78	100	110	7	32	1	4
La------	250	190	130	83	59	14	40	6	6
Li-------	12	7	8	13	38	8	38	2	2
Mo------	61	29	17	5	130	9	7	1	5
Ni------	370	120	87	130	360	99	690	23	42
Pb------	8	2	9	15	14		130		
Sc------	6	1	1	1	9	1	9	1	1
Se-------	14	13.4	15.7	12.8	74.7	6.9	1	0.7	1
Sr-------	910	1300	1400	1200	93	100	91	160	150
V-------	890	950	1400	2900	1400	380	880	44	85
Y-------	350	250	170	120	73	12	46	5	5
Zn-------	2600	1200	1100	1500	4100	1100	3100	200	260
U------	52.9	133	155	89.9	32.5	2.64	9.91	5.47	4.89
La------	220	160	110	78	57	15	49	6.4	6.2
Ce-------	55	30	18	18	74	22	64	1.9	1.6
Pr------	24	17	11	8.9	13	3.0	9.7	0.9	0.7
Nd------	89	67	44	37	54	11	35	2.6	2.4
Sm------	15	11	6.9	5.9	9.9	2.4	7.2	0.36	0.30
Eu-------	3.8	2.6	1.6	1.5	2.3	0.47	1.5	0.11	0.08
Gd------	20	13	7.8	6.9	8.6	2.0	7.2	0.4	0.4
Tb-------	2.7	2.0	1.2	1.0	1.7	0.32	1.1	0.06	0.04
Dy------	18	14	8.7	7.3	11	2.2	6.9	0.49	0.44
Ho------	4.5	3.2	2.0	1.7	2.1	0.44	1.5	0.13	0.10
Er------	14	11	6.8	5.5	6.2	1.6	4.6	0.34	0.30
Tm------	2	1.5	0.97	0.79	0.90	0.23	0.72	0.05	0.04
Yb------	12	8.8	6.0	4.8	5.5	1.4	4.6	0.33	0.34

Table 4b. Trace-element concentrations, in parts per million, measured by INAA (the rare-earth elements, Hf, Sb, and Se) and by ICP-AES (all other trace elements).

	E35-38	E35-34	E35-30	E35-26	E35-22	E34-63	E34-59	E34-55	E34-51	E34-47	E8-38	E8-35	E8-32	E8-29	E8-26
Ag-------	2.2	7.1	2.5	9.1	3	1.8	9.5	1.9	1.8	3	11.8	8.1	15.9	5.5	3.2
As-------	3	18	42	12	23	5	20	20	8	18	14	30	46	14	20
B--------	5	26	30	21	35	5	38	5	27	40	32	43	70	38	35
Ba-------	140	177	271	184	225	149	207	242	185	298	216	228	361	260	223
Cd-----	56	240	128	57	138	63	196	71	166	297	169	182	109	155	161
Co------	0.9	2.6	6.7	1.6	3.8	0.8	1.1	5.9	2.2	4	0.8	0.9	2.3	0.7	1.7
Cr-------	220	750	360	370	500	250	900	130	350	590	940	830	750	550	430
Cu------	23.9	111	61.6	51.1	43.4	28.1	128	18.6	50.2	52.2	92.4	94.9	71.4	69.5	65.5
Hf------	0.7	1.7	7.6	1.5	4.9	0.4	1.9	3	2.4	3.5	1.9	3	8.2	2.4	3.9
Mo------	11	130	66	64	54	1	49	34	11	16	1	35	20	1	16
Ni------	89	370	207	137	151	66	158	96	168	250	135	91	164	58	97
Pb------	6	14	5	6	9	3	13	1	7	10	13	10	1	8	10
Sb------	2.2	6.1	12	3.7	7.2	2.2	8.6	5.5	3.1	6.1	5.2	12	13	5.9	7.2
Sc------	1.86	3.89	7.29	2.25	4.29	2.42	4.17	2.1	2.64	4.75	3.15	4.36	9.45	4.45	5.32
Se-------	20	99	190	57	110	220	240	41	110	110	36	200	600	150	34
Sr-------	1230	919	179	979	677	1170	834	148	940	806	799	612	189	611	660
Th------	0.4	1.4	7.7	1.2	3.9	0.6	1.9	2.8	1.5	3.5	1.5	2.9	8.5	2.6	4
V-------	850	2920	709	1550	1330	978	3340	549	1710	1640	1470	2960	1640	2020	1070
Y-------	143	199	76	93	93	192	193	14	112	138	233	227	136	141	132
Zn-------	1650	7850	4490	1360	3420	936	4150	1110	3990	3650	1420	1190	1780	1400	2460
U------	80.8	173	21.3	100	71.3	114	194	1.3	152	118	93.1	167	27.8	140	136
La------	88	126	54.4	51.6	58.9	113	123	8.9	68.3	85.3	148	137	89	81.7	98.9
Ce-------	16	27	72	14	34	20	28	16	20	34	33	37	62	30	46
Nd------	40	67	51	31	36	55	67	7	41	51	78	76	61	50	61
Sm------	5.21	9.15	9.93	4.27	5.73	7.4	9.95	1.29	6.3	7.82	11.3	10.7	9.71	7.06	9.57
Eu-------	0.95	1.82	1.92	0.82	1.17	1.43	2.07	0.3	0.93	1.58	2.38	2.24	2.13	1.55	1.82
Tb-------	0.8	1.5	1.8	0.6	0.6	1.1	1.4	0.1	0.8	1.2	1.8	1.4	1.4	0.8	1.5
Yb------	4.58	6.88	3.48	3.18	3.74	6.16	6.86	0.75	3.82	5.51	7.09	7.52	6.81	5.54	6.01
Lu------	0.81	1.17	0.5	0.53	0.61	1.1	1.14	0.13		0.92	1.16	1.24	1.13	0.95	0.94

than at low concentrations, rather than showing a normal distribution over the full range of concentrations. Such a distribution violates the assumption of homoscedasticity, or normal distribution of residuals, an assumption made in the calculation of the test of significance. This is clearly seen in the plot of U versus apatite and the plot of the $\log_{10}$ of measured values (fig. 6), but also in the La versus La plots, even though the correlation of the two La measurements is 0.98 (fig. 5a and 5b). Of course, an equally strong reason for plotting the data in this way is that the graph gives equal weight to samples with low elemental concentrations as it gives to samples with high elemental concentrations.

Miscellaneous Analyses

Total sulfur and total carbon, evolved as oxides during combustion, were measured by absorption of infrared radiation (table 1; Jackson and others, 1987). Carbonate carbon was measured as CO_2 by coulometric titration (Jackson and others, 1987).

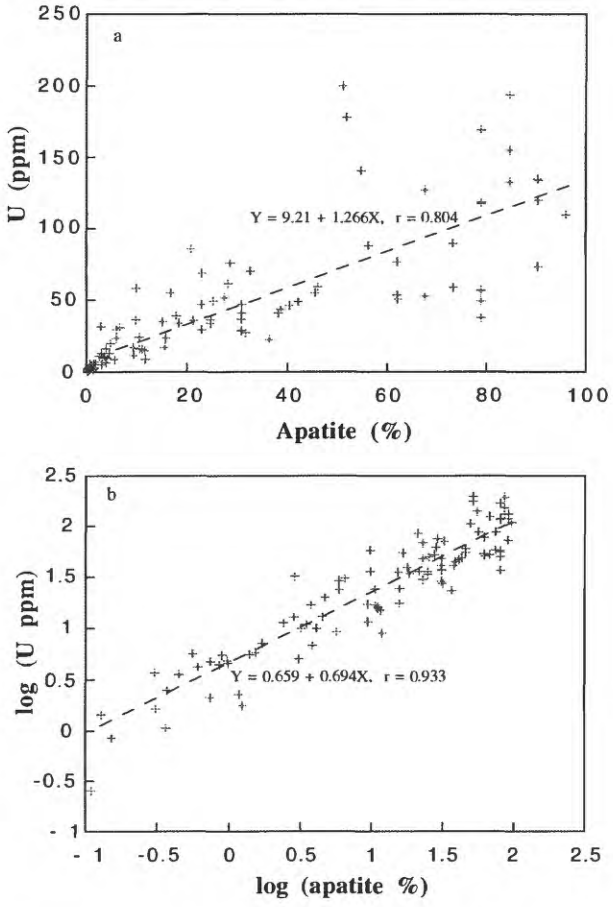

Figure 6. Relation between U and apatite. Measured values are plotted in (a) and $\log_{10}$ of values are plotted in (b).

Fluorine was determined by ion-selective electrode following $LiBO_2$ fusion and HNO_3 dissolution (Bodkin, 1977; Cremer and others, 1984). Ranges of detection, precision, and accuracy are given in table 1 and the results listed in tables 2 and 4.

NORMATIVE CALCULATION OF ROCK COMPONENTS

The Phosphoria Formation is composed of two sediment fractions, a marine fraction derived from seawater and a detrital fraction of terrigenous origin (Piper and Medrano, 1994). The major rock components (table 5) are terrigenous debris (the detrital fraction) and chert, dolomite, calcite, apatite, and organic matter (the marine fraction). Earlier studies show that they have relatively constant major-oxide compositions at the individual sites, and the detrital fraction also has a constant trace-element composition. The major-element oxide composition of the bulk sediment is used to calculate the concentration of these components in each sample (table 5). The procedure is somewhat analogous to a calculation of the salts that might be obtained from evaporation of seawater, based on measurements of the dissolved ions that are actually present in seawater.

Studies of modern and ancient sediments have shown that Al_2O_3 is the diagnostic major-element oxide of detrital material, being hosted essentially totally in this fraction of sediment (Isaacs, 1980 and references therein). The concentration of P_2O_5 is diagnostic of apatite, after making a correction for a P_2O_5 contribution by the detrital fraction. MgO is diagnostic of dolomite, after making a similar correction. CaO is diagnostic of calcite, but here the correction for contributions by the detrital fraction, dolomite, and apatite are significant. SiO_2 is diagnostic of biogenic silica, now opal-CT or even quartz; again following a correction for the detrital contribution to the bulk-content measurement of silica. And finally, organic carbon measures singularly the concentration of organic matter in each sample. Metal sulfides and (or) possibly oxides may also be present, but their contribution to the bulk, major-element-oxide composition of the sediment is minor.

The concentration of Al_2O_3 in the detrital fraction itself and the concentration of the diagnostic element oxides of each of the other major mineral components can be determined from x-y plots. These plots can then give the concentration of each component on a sample-by sample basis.

Table 5. Unit thicknesses (in centimeters) and lithology of samples. Concentrations of components are in percent. Lithologic description is taken from field notes and may not match exactly concentration of components. Residual is an estimate of biogenic silica, based on the deficit of oxides and elements (tables 2 and 4) and corrected for the detrital contribution of SiO_2 (table 3). E series of samples are from cores collected by Solutia Inc. Blanks in columns 5 through 11 represent no data.

	Thickness (cm)	Position/Cumulative thickness (cm)	Lithology	Detritus	Apatite	Dolomite	Calcite	Organic Matter	Residual	Biogenic Silica
P-238--------		at 5190	Rex Chert Member	6.0	0.6	0.1	0.0	0.6	92.3	
P-237--------	8.8	5173	organic rich mudstone	66.9	10.0	2.3	0.0	5.3	17.5	
P-236--------	50.3	5164	mudstone/chert (interbedded)	66.9	3.8	0.7	0.0	2.5	29.0	
P-235--------	87.1	5114	siltstone	66.9	2.9	0.2	0.0	2.0	31.1	
P-234--------	86.3	5027	mudstone	66.9	1.0	0.0	0.0	1.1		
P-233--------		at 4925	siltstone at top	86.2	10.0	1.0	0.0	2.5	5.2	
P-232--------	218.1	4941		9.1	1.6	82.4	8.3	1.7		
P-231--------	4.0	4722	phosphorite (coarse grained)	49.9	27.9	0.0	0.6	1.8		
P-230--------	42.3	4718	organic rich siltstone	27.2	57.2	0.1	5.4	4.3		
P-229--------	20.8	4676	chert	54.4	1.7	0.0	0.0	0.9		
P-228--------	9.6	4655	phosphorite (coarse grained)	8.3	74.4	0.2	1.8	1.7		
P-227--------	92.7	4646	mudstone	62.4	3.5	0.0	0.0	1.6		
P-226--------	46.3	4553	phosphorite (medium/coarse grained)	3.1	97.4	0.5	0.0	2.1		
P-225--------	27.2	4507	siltstone (laminated)	61.2	11.2	0.0	0.0	1.0		
P-224--------	51.9	4480	phosphorite	6.6	91.6	0.6	0.0	2.0	-2.3	
P-223--------	14.4	4428	phosphorite (nodular)	38.5	41.1	0.0	0.6	1.9		
P-222--------	28.8	4413	phosphorite	3.1	91.6	0.4	0.1	1.9		
P-221--------		at 4375		9.6	80.2	1.1	3.1	7.1		
P-220--------	133.4	4384	Upper ore (at 4275 cm)	22.7	62.9	0.9	0.0	6.3		
P-219--------	91.1	4251	phos. mudstone (at 4245 cm)	53.3	18.1	0.0	1.2	3.7		
P-218--------	43.9	4160	limestone	21.5	0.3	22.2	54.1	1.4	2.0	
P-217--------	22.4	4116	siltstone	34.0	0.4	54.7	5.9	1.3		
P-216--------	64.7	4094	phos. mudstone	51.0	25.0	0.2	3.2	5.8		
P-215--------	29.6	4029	organic rich phosphorite	45.3	25.6	0.0	0.0	4.0	24.9	
P-214--------	54.3	3999	organic rich phosphorite	39.7	31.3	0.0	0.1	4.6		
P-213--------	67.1	3945	cherty mudstone	68.0	4.5	0.0	0.0	3.3		
P-212--------	8.0	3878	sandy phosphorite	19.3	62.9	0.2	2.6	5.7	7.1	
P-211--------	62.3	3870	organic rich phosphorite, shaley	41.9	31.3	0.0	7.5	5.0		
P-210--------	22.4	3808	phosphorite	7.8	80.2	0.0	0.0	1.1		
P-209--------	38.4	3785	phosphatic mud	60.1	3.1	0.0	0.0	2.3		
P-208--------	17.6	3747	mudstone	56.7	11.8	0.0	0.0	1.0	32.1	
P-206--------	171.8	3729	siltstone (fossiliferous at 3715 cm)	37.4	15.9	0.0	0.8	2.3		
P-207--------		at 3575	siltstone	48.8	9.5	0.0	0.0	1.9		
P-205--------	24.0	3558	mudstone	57.8	4.2	9.7	0.3	2.3		
P-204--------	22.4	3534	siltstone w/ phosphorite interbeds	43.1	39.3	0.1	4.6	6.2		
P-203--------	5.6	3511	phosphorite	8.7	80.2	0.4	1.1	5.9		
P-202--------	67.9	3506	phos. siltstone	51.0	25.0	0.0	0.8	5.7	17.8	
P-201--------	40.7	3438	cherty mudstone	56.7	10.6	0.0	0.0	6.7		

Table 5. Cont.

	Thickness (cm)	Position/Cum-mulative thick-ness (cm)	Lithology	Detritus	Apatite	Dolomite	Calcite	Organic Matter	Residual	Biogenic Silica
P-200--------	20.0	3397	mudstone	68.0	1.5	0.0	0.0	1.5		
P-199--------	46.3	3377	siltstone	63.5	6.0	0.0	0.0	6.3	24.6	
P-198--------		at 3335	argil. phosphorite	56.7	21.5	0.0	0.0	4.9		
P-197--------	87.9	3331	argil. phosphorite (at 3250 cm)	41.3	46.8	2.0	0.0	8.2		
P-195--------				27.2	28.5	0.2	0.0	2.2		
P-196--------	62.3	3243	phos. siltstone (at 3190 cm)	56.7	16.9	0.2	0.6	5.9	18.8	
P-194--------	127.8	3180	mudstone w/ phos. lens (at 3060 cm)	24.9	62.9	0.3	2.3	5.2		
P-193--------	24.0	3053	silty mudstone	65.8	0.9	0.0	0.0	0.9		
P-192--------	62.3	3029	siltstone w/ phos. lens	45.3	46.2	0.6	7.5	6.0		
P-191--------			phosphate lens of P-190	9.9	80.1	0.0	1.3	1.3		
P-190--------	102.3	2966	phos. siltstone (orbiq. brachiopods)	53.3	23.3	0.0	0.0	5.1	18.8	
P-189--------	24.0	2864	mudstone	61.2	11.2	0.0	0.0	1.6		
P-188--------			shale unit	63.5	10.6	0.0	0.0	4.6		
P-187--------	25.6	2840	shale unit	62.4	9.5	0.0	0.0	4.3		
P-186--------			E-Bed (top)	41.9	23.3	2.0	0.0	25.4		
P-185--------	130.2	2814	E-Bed (bottom)	38.5	21.0	2.1	0.0	2.6		
P-184--------		at 2680	organic siltstone	63.5	1.4	0.0	0.0	3.1	35.4	
P-183--------	183.8	2684	organic siltstone w/ phos. lens	52.2	31.3	0.5	0.0	8.7		
P-182--------	84.7	2500	carbonate	8.7	0.4	82.4	14.5	1.2		
P-181--------	57.5	2416	siltstone	12.5	0.7	70.9	15.2	1.4	-1.4	
P-180--------	16.0	2358	organic silty mudstone	63.5	4.8	0.0	0.0	4.9		
P-179--------	47.9	2342	mudstone	70.3	6.0	0.0	0.0	4.1		
P-178--------		at 2290	phos. mudstone	61.2	18.6	0.0	0.0	4.8	14.4	
P-177--------	67.9	2294	phos. mudstone (at 2235 cm)	52.2	31.3	0.1	2.1	4.7		
P-176--------	75.9	2226	Cherty siltstone	63.5	0.3	0.0	0.0	2.2		
P-175--------		at 2145	mudstone	66.9	0.8	0.0	0.0	2.3		
P-174--------	91.9	2150	mudstone (at 2070 cm)	62.4	15.8	0.0	0.5	3.8		
P-173--------			chert concretion	1.1	0.1	0.3	0.4	2.4		
P-172--------			limestone concretion	3.2	1.2	17.9	76.4	2.8		
P-171--------	355.6	2059	mudstone (concretionary)	61.2	15.2	5.0	4.7	10.9		
P-170--------	34.4	1703	silty carbonate (?)	18.1	0.2	63.8	14.4	1.2		
P-76---------		at 1660	waste	61.2	23.2	0.0	2.1	9.0	2.8	
P-75---------	28.8	at 1645	marker bed above C	70.3	0.5	9.1	1.2	1.0		
P-74---------	90.3	1640	argil. phosphorite	51.0	37.0	0.0	4.1	5.3		
P-73---------	2.4	1550	mudstone	85.0	0.6	0.0	0.2	11.8	3.9	
P-72---------	2.4	1547	buddingtonite	101.4	1.2	0.0	0.0	1.1		
P-71---------		at 1542	P 70 interbed phosphorite	51.0	38.7	0.2	2.2	6.0		
P-70---------	8.0	at 1540	mudstone	66.9	11.7	0.0	0.0	4.7		
P-69---------		at 1533	C unit (phosphorite)	8.5	80.2	0.7	3.4	7.0		
P-68---------		at 1475	C Unit (phosphorite)	12.5	68.7	0.7	0.0	6.6	6.1	
E34-63[a]-----		at1410	C Unit (mudstone)	3.0	81.2	0.3	3.1			2.7

Table 5. Cont.

	Thickness (cm)	Position/Cumulative thickness (cm)		Lithology	Detritus	Apatite	Dolomite	Calcite	Organic Matter	Residual	Biogenic Silica
P-67---------		at 1350		C unit (cherty phosphorite)	37.4	33.1	3.7	1.5	7.7		
P-66---------	270.1	at 1295		C unit (phosphorite)	29.5	55.4	0.8	4.1	6.0		
E34-59[a]----		at 1290		C Unit (phos. mudstone)	14.1	62.9	0.6	0.3			7.3
P-64---------	197.5		1267	false cap (phos. carbonate)	6.0	32.1	52.4	7.4	1.6	-0.2	
E34-55[a]----		at 1258		dolomite	18.7	0.2	63.1	6.0			8.4
P-63---------		at 1100		phosphorite	27.2	49.7	3.2	1.0	3.5		
P-62---------		at 1065		phosphorite	2.0	91.6	0.6	0.0	6.8		
E34-51[a]----		at 1040		phosphorite	8.5	76.5	0.0	3.9			4.8
E35-38[a]----		at 1025		phos. mudstone	3.1	83.6	1.1	3.4			2.5
E8-38[a]------		at 991		phosphorite	10.3	69.2	0.8	5.0			6.6
E34-47[a]----		at 980		phos. mudstone	21.7	57.5	0.0	3.5			9.0
E35-34[a]----		at 968		argil. carbonate	10.5	1.8	66.8	6.7			5.8
P-61---------	122.2	at 965		argil. phosphorite	23.8	52.3	0.3	7.4	5.5		
P-60---------	29.6	at 930		lower waste (phos. mudstone)	59.0	2.5	5.2	0.4	2.3		
E8-35[a]-----		at 929		phos. mudstone	18.4	57.4	0.0	0.0			11.5
E35-30[a]----		at 925		mudstone	51.8	2.9	10.9	3.5			26.1
P-59---------		at 900		upper B	27.2	51.7	0.5	10.2	6.7		
E35-26[a]----		at 863		argil. phosphorite	8.6	74.1	1.5	4.7			4.8
E35-22[a]----		at 816		argil. carbonate	27.6	47.5	2.1	4.0			14.0
P-58---------	113.5	at 810		upper B (argil. phosphorite)	43.1	28.9	0.0	0.0	3.5	23.8	
P-57---------		at 790		B Parting	19.3	5.7	70.6	2.8	0.8		
E8-32[a]-----		at 775		mudstone	58.2	0.0	9.6	0.1			26.2
P-56---------	115.9	at 700		B parting (argil. carbonate)	15.9	3.8	70.7	7.1	1.0		
P-55---------		at 685		lower B	7.3	85.4	0.5	0.0	4.3		
E8-29[a]-----		at 662		phos. mudstone	17.2	64.4	0.0	1.4			7.8
P-54---------		at 645			2.5	91.2	0.5	0.1	6.0	-4.1	
E8-26[a]-----		at 630		argil. phosphorite	21.6	61.5	0.0	4.6			10.0
P-53---------	85.5	at 615		low B (phosphorite)	9.0	79.8	0.5	0.0	4.4		
P-52---------	22.4		603	mud parting	61.2	6.6	0.0	0.0	4.4		
P-51---------	83.9		580	lower B (phosphorite)	10.0	79.8	0.6	0.9	3.9		
P-50---------	0.8		496	Peanut Butter Seam	51.3	0.1	44.8	0.8	1.8		
P-49---------	40.0		496	lower B (argil. phosphorite)	34.0	42.6	10.3	3.6	3.8		
P-48---------	16.0		456	A cap/snails	17.0	68.5	1.7	0.0	3.2	1.4	
P-47---------		at 452		A bed	5.3	85.5	0.7	0.5	3.0		
P-46---------		at 445		A bed	4.2	85.5	0.8	2.9	3.1		
P-45---------		at 380		A bed	9.5	74.0	1.5	3.6	5.5		
P-44---------	255.2		440	A bed (phosphorite)	55.6	2.9	6.9	0.0	3.0		
P-43---------	90.0		185	Footwall mud (silty)	23.8	0.1	56.8	5.5	1.3		
P-42---------	84.0		95	Footwall mud	62.4	3.1	1.0	0.0	1.1	33.3	
P-41---------	11.2		11	Fish scale (dolomite)	0.6	0.9	90.4	7.5	0.1		
P-40---------				Grandeur Fm. (dolomite)	0.7	1.0	97.9	5.8	0.5		

[a] The E-series samples were positioned, relative to the P-series samples, based on measured distances from tentatively identified prominent carbonate units.

The validity of the assumption of constant compositions can be evaluated from these plots. For example, if two element oxides correlate strongly and their relation extrapolates to the origin, the two elements are essentially entirely in that one component; their element-to-element ratio in that component is relatively constant and, therefore, the composition of the component itself is constant. A graph of element oxides in which the data scatter below a well-defined maximum curve further defines the partitioning of element oxides between components. Extrapolation of the maximum curve to one of the axes can identify the concentration of one element oxide in one of the components; extrapolation to the second axis may define the second oxide concentration in another single component. A strongly defined minimum of a plot of two element oxides, that extrapolates to the origin, also can identify the major-element-oxide ratio of the two element oxides in a component. That is, the minimum line represents a constant element-oxide to element-oxide ratio in the one component. The strengths of these minima and of the maxima should reflect the constancy of composition in each component.

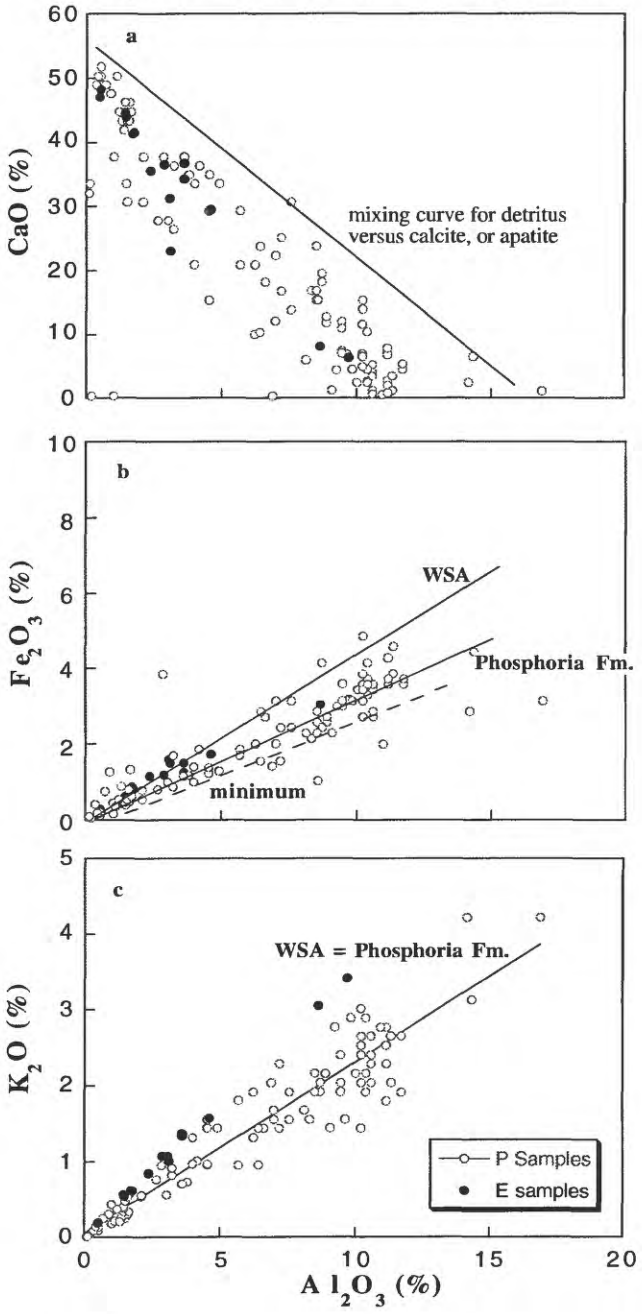

Figure 7. Relation between Al_2O_3 and (a) CaO, (b) Fe_2O_3, and (c) K_2O. Curves labeled WSA give relations for World Shale Average; those labeled Phosphoria Fm. are from Medrano and Piper (1995).

In the same way, the minima of plots of trace elements versus Al_2O_3, or versus the concentration of the detrital fraction itself, can identify the trace-element concentration of this fraction. The excursion of data from the minima gives the concentration of each trace element in the marine fraction of sediment on a sample-by-sample basis.

The purpose of these plots and calculations is two-fold. (1) The present partition of trace elements between the different components of sediment should largely determine their introduction into the groundwater system via weathering. The more labile or easily leached components, such as metal sulfides and organic matter, will release their complement of trace elements to solution more easily, more quickly, than the relatively insoluble components, such as terrigenous debris and apatite. And (2) the fraction of trace elements in excess of that contributed by the detrital fraction alone represents the marine fraction of trace elements. This fraction defines the chemical environment of deposition (Piper, 1991 and 1994; Piper and Medrano, 1994): specifically, primary productivity in the photic zone and redox conditions of the water column.

Detrital Component

The detrital fraction is a mineral mix of detrital quartz, clay minerals, feldspars, micas, and minor amounts of accessory minerals such as zircon and rutile (Gulbrandsen, 1960). Even so, it can be treated here as a single entity. The earlier studies of the Phosphoria Formation (Medrano and Piper, 1992, 1995; Piper and Medrano, 1994) established that this sediment fraction has a constant composition at any

Table 6. Major-oxide and minor-element composition of terrigenous (i.e., detrital) fraction. All values are in parts per million. Blanks indicate that no value was listed, or that it could not be determined.

	World Shale Average[1]	North American Shale Composite[2]	Phosphoria Fm. (Medrano and Piper, 1995)	Value from minimum line (this study)	Value used in calculations (this study)
			Major-oxides		
SiO_2	58.4	64.8	58.3	58.3	58.3
Al_2O_3	15.1	16.9	16.7	16.7	16.7
Fe_2O_3	6.84	6.29	6.2	4.5	6.2
MgO	2.49	2.85	1.2	1.14	1.2
CaO	3.09	3.58	2.5	3.58	2.5
Na_2O	1.3	1.13			
K_2O	3.19	3.94	4.2	4.17	4.2
TiO_2	0.77	0.79	0.48	0.48	0.48
P_2O_5	0.16	0.14	0.17	0.23	0.17
CO_2	2.63[3]				
			Minor elements		
Ag	0.05-0.90		0.48		0.48[1]
As	13	28.4	32		32
Ba	546	636	429		430
Cd	0.8		0.8		0.8[1]
Co	19	25.7	20		20
Cr	83	124.5	83	115	83[1]
Cu	35		35	34	35
Ga	18				17
Li	76				76[1]
Mn	600	600		168	
Mo	0.7-2.0			2.0	2
Ni	42	58	59	165	165
Pb	21.6		10	5	10
Sc	13	14.9	15		15
Se	1.0			1.5	1.5
Sr	24-359	142	70	70	70
Th	12	12.3	7		12
V	98-2600		180	160	160
Zn	100		60	300	100[1]
			Rare Earth Elements		
Y	27	27			36
La	41	32	43	38	41
Ce	83	70	93	58-80	83
Pr	10.1	7.9	10.6	8.5	10
Nd	38	31	41	32	36
Sm	7.5	5.7	7.6	6.6	7.6
Eu	1.61	1.24	1.65	1.5	1.6
Gd	6.35	5.21	6.9	5.9	6.35
Tb	1.23	0.85	1.13[1]	0.85-1.28	1.15
Dy	5.5		5.5[1]	5.3-8.7	5.5[1]
Ho	1.34	1.04	1.38	0.85-1.55	1.34[1]
Er	3.75	3.4	4.5	3.1-4.65	3.75
Tm	0.63	0.5	0.70	0.5-0.7	0.63
Yb	3.53	3.1	4.1	3.1-4.6	3.53

[1] World Shale Average (major-element oxides,Turekian and Wedepohl, 1961; minor elements, Wedepohl, 1969-1978; rare-earth elements, Piper, 1974)

[2] North American Shale Composite (major and minor elements on a volatile free basis: Gromet and others, 1984; rare-earth elements, Haskin and Haskin, 1966)

[3] CO_2, Wedepohl, 1969-1978

one site, despite its complex mineral assemblage; that it seems to have remained largely non-reactive during its earlier passage through the ocean; and that the source of material remained unchanged even into the Triassic Period, with the deposition of the overlying Dinwoody Formation (McKelvey and others, 1959; Peterson, 1980). The Enoch Valley samples support this interpretation and the procedure, that is, the proportionality constant, for calculating its abundance (table 3). No effort has been made to explain variations in the composition of this fraction of the sediment between the different sites studied, particularly its mineralogy, but clearly such a study could give important information, for example, about the dispersal of sediment during deposition and the history of burial.

The maximum of the plot of Al_2O_3 versus CaO (fig. 7) is strongly defined; it extrapolates to an Al_2O_3 concentration of 16.6 percent at a CaO concentration of zero to one percent. This gives the Al_2O_3 concentration in the detrital fraction (table 6), a value that closely approximates its concentration in this fraction at other sites (table 6). The plots of Al_2O_3 versus Fe_2O_3 and K_2O (fig. 7) further suggest a constant composition for the detrital fraction and one that approaches the composition of WSA (Wedepohl, 1969-1978).

As at other sites, several trace elements also correlate with Al_2O_3 (table 7) and further suggest a concentration for the detrital fraction similar to that of WSA (table 6). These include Th, Ba, Li, and Sc. The correlations are not as strong as observed for the other sections, except for Th, measured only in the E series of samples (table 4; fig. 8) by INAA and not included in the other tables.

An alternative approach to ascertain those elements hosted by the detrital fraction is by factor analysis (table 8). Results of this calculation show that seven factors account for 97% of the variability; with

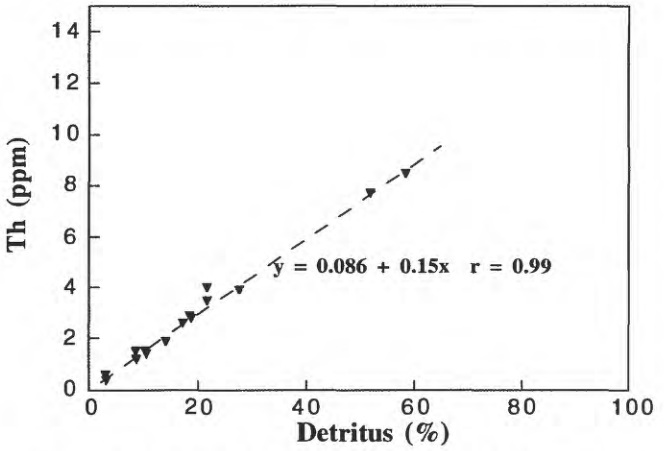

Figure 8. Relation between detritus and Th. Samples include only the E-series. Detritus equals 6 times Al_2O_3, measured by XRF (table 2). Th is measure by INAA (table 4).

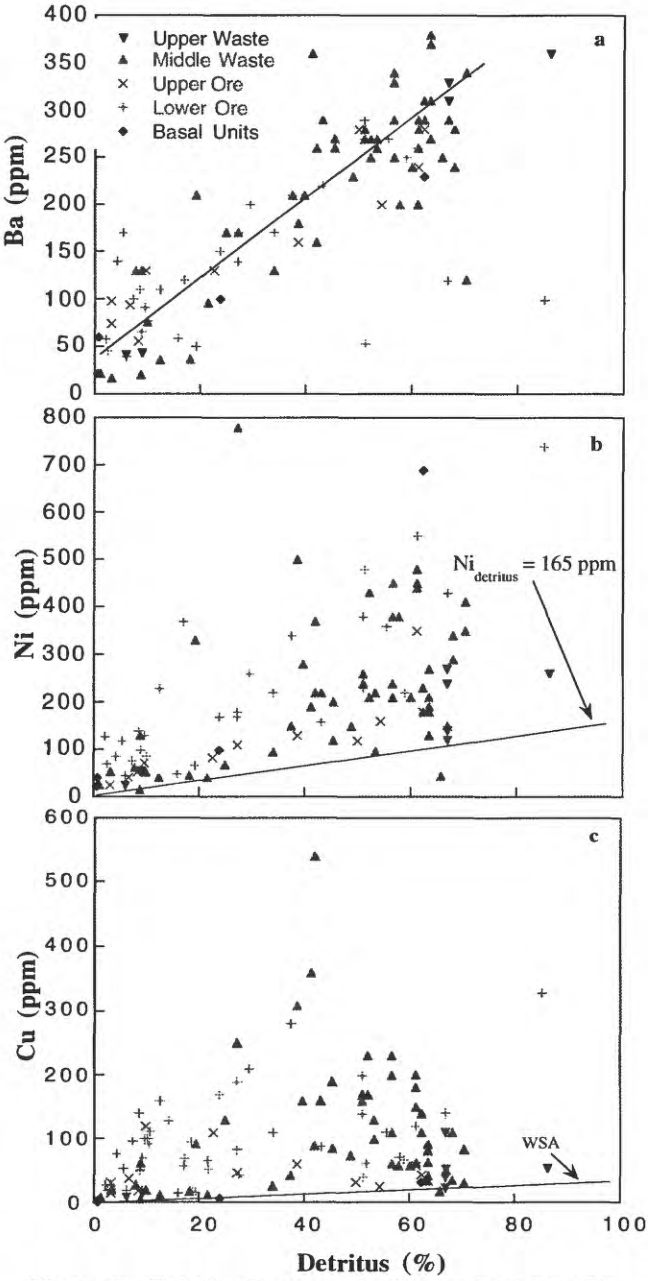

Figure 9. Relation between detritus and (a) Ba, (b) Ni, and (c) Cu. Curve in (a) is least squares best fit; curves in (b) and (c) give values for the detrital fraction (table 6), when extrapolated to 100 percent.

Table 7. Correlation coefficients for the log of trace-element, major-element, and major-element-oxide concentrations (table 5a). The La* was measured by ICP-AES and the other by ICP-MS.

	Al_2O_3	CaO	Fe_2O_3	K_2O	MgO	Na_2O	P_2O_5	TiO_2	MnO	CO_2	Org. C	F	S	Ag	As	Ba	Cd	Co	Cr	Cu	La*
Al_2O_3	1																				
CaO	-0.64	1																			
Fe_2O_3	0.88	-0.54	1																		
K_2O	0.97	-0.59	0.85	1																	
MgO	0.07	-0.13	-0.07	0.10	1																
Na_2O	0.61	-0.33	0.61	0.58	-0.15	1															
P_2O_5	-0.38	0.60	-0.23	-0.33	-0.49	-0.13	1														
TiO_2	0.88	-0.68	0.83	0.84	0.07	0.57	-0.49	1													
MnO	0.45	-0.29	0.40	0.37	0.38	0.35	-0.54	0.50	1												
CO_2	-0.52	0.66	-0.54	-0.47	0.68	-0.35	-0.02	-0.50	0.29	1											
Org. C	0.07	0.25	0.10	0.16	-0.20	0.02	0.52	0.05	-0.28	-0.13	1										
F	-0.34	0.60	-0.22	-0.28	-0.43	-0.18	0.96	-0.48	-0.53	0.01	0.49	1									
S	0.00	0.21	0.16	0.06	-0.53	0.09	0.64	-0.08	-0.46	-0.31	0.79	0.54	1								
Ag	0.29	0.06	0.33	0.37	-0.12	0.17	0.32	0.13	-0.17	-0.15	0.59	0.34	0.49	1							
As	0.55	-0.32	0.74	0.60	-0.14	0.41	-0.03	0.49	0.22	-0.35	0.21	-0.03	0.28	0.53	1						
Ba	0.75	-0.45	0.76	0.72	-0.32	0.58	0.12	0.64	0.09	-0.68	0.32	0.12	0.42	0.29	0.45	1					
Cd	-0.13	0.38	-0.07	-0.03	0.07	-0.09	0.44	-0.08	-0.26	0.19	0.42	0.47	0.34	0.44	0.06	0.04	1				
Co	0.14	0.32	0.25	0.05	-0.14	0.11	-0.25	0.22	0.42	-0.21	-0.35	-0.28	-0.23	-0.35	0.09	0.1o	-0.38	1			
Cr	0.34	0.03	0.40	0.38	-0.25	0.07	0.46	0.18	-0.34	-0.37	0.70	0.46	0.69	0.66	0.47	0.52	0.27	-0.23	1		
Cu	0.41	0.02	0.47	0.47	-0.25	0.23	0.45	0.24	-0.16	-0.32	0.79	0.44	0.72	0.73	0.54	0.56	0.38	-0.21	0.84	1	
La*	-0.05	0.40	0.09	-0.03	-0.40	0.03	0.85	-0.22	-0.38	-0.55	0.48	0.83	0.73	0.45	0.17	0.39	0.38	-0.25	0.65	0.64	1
Li	0.62	-0.29	0.63	0.63	-0.06	0.16	0.17	0.47	-0.11	-0.47	0.46	0.22	0.43	0.48	0.45	0.75	0.21	-0.02	0.76	0.69	0.43
Mo	0.44	-0.13	0.56	0.51	-0.14	0.42	0.13	0.39	0.07	-0.26	0.39	0.12	0.42	0.65	0.66	0.43	0.26	-0.10	0.53	0.65	0.33
Ni	0.68	-0.31	0.77	0.72	-0.10	0.43	0.02	0.62	0.35	-0.38	0.39	0.06	0.36	0.55	0.73	0.62	0.19	0.10	0.49	0.68	0.28
Pb	0.60	-0.51	0.62	0.62	-0.14	0.20	-0.18	0.54	0.09	-0.53	0.12	-0.16	0.26	0.33	0.58	0.52	0.05	0.10	0.41	0.40	0.04
Sc	0.73	-0.37	0.75	0.67	-0.21	0.47	0.07	0.62	0.23	-0.55	0.30	0.07	0.34	0.32	0.46	0.83	0.00	0.10	0.52	0.53	0.44
Se	0.39	-0.12	0.43	0.44	-0.05	0.34	-0.01	0.33	-0.05	-0.20	0.37	-0.03	0.33	0.52	0.42	0.29	0.18	-0.25	0.40	0.49	0.16
Sr	-0.53	0.80	-0.39	-0.48	-0.21	-0.20	0.86	-0.66	-0.48	0.32	0.53	0.82	0.58	0.26	-0.14	-0.12	0.40	-0.31	0.35	0.35	0.74
V	-0.01	0.22	0.07	0.12	-0.06	0.00	0.37	0.03	-0.27	0.05	0.39	0.41	0.40	0.53	0.32	0.13	0.78	-0.30	0.40	0.47	0.27
Y	-0.10	0.39	-.04	-0.08	-0.44	-0.04	0.88	-0.26	-0.42	-0.17	0.59	0.86	0.70	0.42	0.09	0.39	0.39	-0.21	0.61	0.60	0.98
Zn	0.31	0.01	0.40	0.40	-0.08	0.27	0.19	0.28	0.13	-0.06	0.24	0.27	0.20	0.46	0.51	0.32	0.49	-0.04	0.19	0.42	0.18
U	-0.30	0.49	-0.16	-0.23	-0.48	-0.16	0.94	-0.38	-0.59	-0.09	0.58	0.90	0.71	0.38	0.03	0.22	0.58	-0.31	0.53	0.53	0.83
La	0.03	0.34	0.11	-0.02	-0.44	0.03	0.83	-0.20	-0.38	-0.21	0.59	0.81	0.70	0.42	0.15	0.43	0.34	-0.20	0.64	0.62	0.99
Ce	0.64	-0.24	0.71	0.60	-0.33	0.51	0.28	0.51	0.13	-0.53	0.31	0.28	0.43	0.34	0.45	0.83	0.13	0.05	0.50	0.57	0.62
Eu	0.14	0.17	0.22	0.12	-0.49	0.14	0.72	-0.02	-0.26	-0.35	0.50	0.69	0.67	0.40	0.22	0.56	0.25	-0.10	0.61	0.61	0.93
Yb	0.06	0.26	0.51	0.06	-0.46	0.10	0.78	-0.09	-0.34	-0.66	0.40	0.78	0.67	0.39	0.14	0.54	0.38	-0.18	0.60	0.60	0.95

	Li	Mo	Ni	Pb	Sc	Se	Sr	V	Y	Zn	U	La	Ce	Eu	Yb
Li	1														
Mo	0.46	1													
Ni	0.61	0.70	1												
Pb	0.57	0.41	0.51	1											
Sc	0.69	0.46	0.65	0.48	1										
Se	0.33	0.60	0.41	0.32	0.29	1									
Sr	0.00	0.04	-0.14	-0.36	-0.10	-0.03	1								
V	0.31	0.42	0.32	0.27	-0.02	0.28	0.24	1							
Y	0.44	0.25	0.22	0.03	0.42	0.08	0.72	0.27	1						
Zn	0.30	0.50	0.67	0.27	0.21	0.32	0.02	0.67	0.16	1					
U	0.30	0.21	0.09	-0.03	0.14	0.07	0.75	0.55	0.87	0.28	1				
La	0.46	0.31	0.28	0.07	0.48	0.13	0.68	0.23	0.98	0.16	0.82	1			
Ce	0.61	0.47	0.64	0.42	0.86	0.29	0.03	0.10	0.59	-0.35	0.32	0.66	1		
Eu	0.51	0.34	0.36	0.19	0.61	0.16	0.52	0.17	0.94	0.18	0.76	0.96	0.79	1	
Yb	0.51	0.30	0.31	0.12	0.56	0.09	0.60	0.26	0.96	0.21	0.80	0.97	0.73	0.96	1

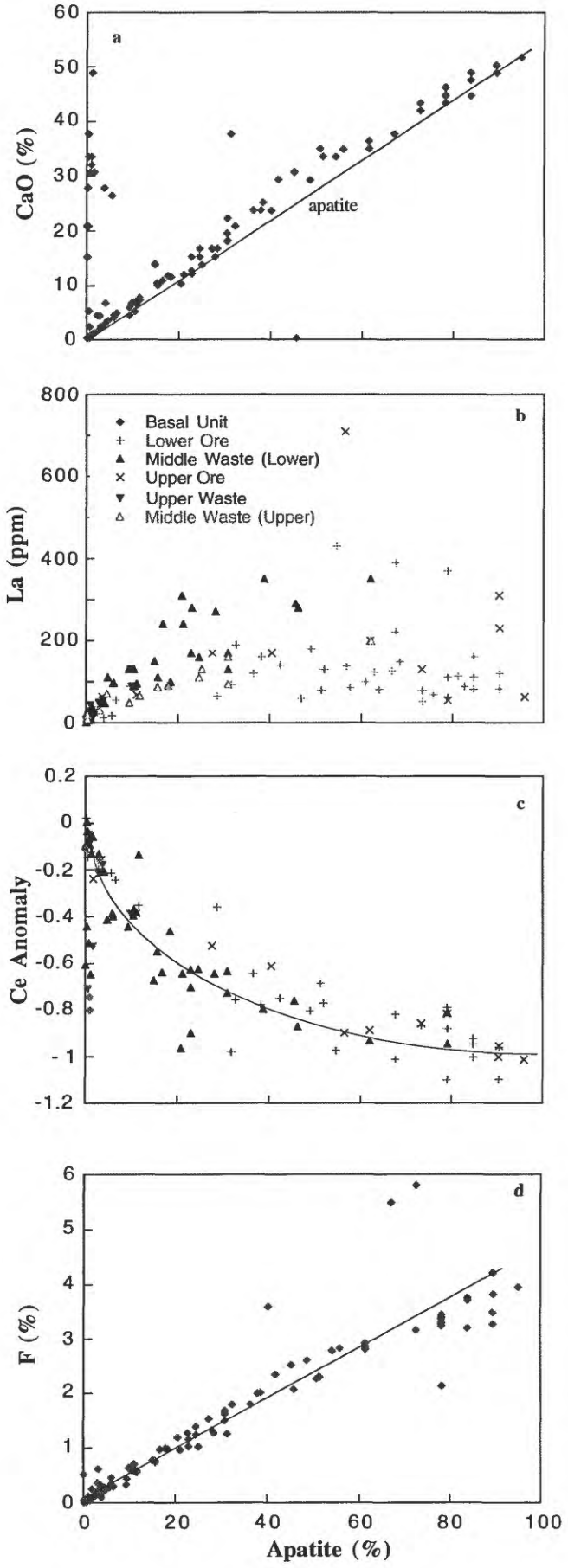

factors six and seven characterized by a single element, Na_2O in the case of factor six and Co in the case of factor seven. Factor two has a strong detritus loading of 0.96, along with the oxides that correlate with Al_2O_3 (fig. 7, table 7). Several of the trace elements also show strong loadings on this factor. Somewhat unexpected are the strong loadings of Ni and Ce, suggesting that a significant portion of these elements are hosted by the detrital fraction.

The concentrations in the detrital fraction of trace elements that show no correlation with the detrital fraction itself are determined from the detritus versus trace-element minima (fig. 9). Except for Ni, their concentrations in this fraction, based on these minima, also closely approach their concentrations in WSA (table 6). In the case of many such trace elements, which include Cd, Cr, Cu, Mo, Ni, Sb, Se, U, V, and Zn, the detrital contribution to the bulk concentration is small in most samples (fig. 9). This *excess* is interpreted to represent the bulk marine fraction of trace elements, which should be hosted by the marine components of the sediment.

Marine Components

Apatite

Apatite is the carbonate fluorapatite, francolite (McClellan and Lehr, 1969). A CO_3^{2-} concentration of 2.3 percent (table 3) is taken from Gulbrandsen (1970). The fluoride content is between 3.5 and 4 percent (fig. 10d), greater than the value of 3.43 per-percent reported by McClellan and Lehr (1969). A $CaO:P_2O_5$ ratio of 1.36 (fig. 10a) is similar to that reported for the other sites examined by Medrano and Piper (1992, 1995). Clearly, CaO is present in other components, but extrapolation of the extrema to the origin supports the interpretation that P_2O_5 is present predominantly in the apatite component. I have assigned a P_2O_5 concentration of 0.16 percent to the detrital fraction (table 3 and 6), based on its concentration in WSA (Wedepohl, 1969-78).

Trace elements that are incorporated into apatite (tables 7 and 8) include U (fig. 6), Y, and the REE (fig. 10b) exclusive of Ce. However, the Ce anomaly exhibits a strongly negative correlation with apatite (fig. 10c). Because the Ce anomaly versus apatite

Figure 10. Relation between apatite and CaO (a), La (b), Ce anomaly (c), and F (d). Curve in (a) is a best-fit minimum; curves in (c) and (d) are log and linear best fits, respectively.

Table 8. Varimax orthogonal transformation solution, principal component factor extraction method, using Statview^{tm} II software. Values greater than 0.50 are in bold, except in the case of the Ce anomaly, which is calculated for each sample as a negative value (see Figure 5 for details of the calculation).

	Factor 1	Factor 2	Factor 3	Factor 4	Factor 5	Factor 6	Factor 7
Detritus	-0.079	**0.96**	-0.016	0.053	0.012	0.091	-0.002
Apatite	**0.84**	-0.37	0.20	-0.12	0.15	0.016	-0.032
Dolomite	-0.32	-0.41	0.26	**0.67**	-0.17	-0.18	0.058
Calcite	-0.078	-0.40	-0.096	**0.69**	0.13	0.20	0.049
Org. Matter	0.49	0.042	0.19	0.12	**0.64**	-0.12	-0.19
Al_2O_3	-0.078	**0.96**	0.018	0.053	0.12	0.092	-0.002
CaO	0.38	-0.69	0.20	0.40	0.055	0.178	-0.026
Fe_2O_3	0.056	**0.90**	0.10	-0.06	0.17	0.12	0.21
K_2O	-0.093	**0.91**	0.14	0.066	0.20	0.080	-0.038
MgO	-0.45	0.031	0.14	**0.82**	-0.17	-0.086	-0.091
Na_2O	-0.010	**0.58**	-0.008	-0.14	0.086	**0.67**	-0.025
P_2O_5	**0.84**	-0.38	0.21	-0.013	0.16	0.029	0.034
TiO_2	-0.24	**0.91**	0.097	-0.085	-0.017	0.058	-0.015
MnO	-0.34	0.44	-0.026	0.33	-0.27	0.29	0.49
Sulfur	**0.64**	0.031	0.13	-0.19	**0.56**	-0.084	-0.095
Fluorine	**0.82**	-0.35	0.29	-0.085	0.11	-0.011	-0.037
Ag	0.29	0.22	0.44	-0.019	**0.61**	0.072	-0.068
As	0.035	**0.53**	0.31	-0.12	0.47	0.079	0.39
Ba	0.41	**0.80**	0.021	-0.18	0.084	0.018	-0.073
Cd	0.30	-0.11	**0.81**	0.10	0.005	-0.064	-0.27
Co	-0.13	0.18	-0.23	-0.19	-0.24	-0.082	**0.74**
Cr	**0.53**	0.32	0.14	0.017	**0.62**	-0.30	-0.092
Cu	**0.51**	0.37	0.29	0.057	**0.63**	-0.073	-0.005
Ga	0.20	**0.68**	0.013	0.17	0.19	-0.36	-0.038
Li	0.39	**0.65**	0.17	0.071	0.28	-0.39	-0.080
Mo	0.19	0.43	0.38	-0.029	**0.53**	0.24	0.12
Ni	0.19	**0.68**	0.39	0.025	0.32	0.093	0.33
Pb	-0.018	**0.64**	0.18	-0.19	0.25	-0.35	0.089
Sc	0.46	**0.81**	-0.069	0.001	0.046	0.033	0.027
Se	-0.003	0.34	0.18	0.010	**0.61**	0.28	-0.24
Sr	**0.69**	-0.56	0.10	0.18	0.26	0.096	-0.033
V	0.15	-0.026	**0.89**	-0.12	0.23	-0.12	-0.13
Y	**0.98**	-0.035	0.10	-0.012	0.13	-0.062	-0.043
Zn	0.11	0.26	**0.80**	-0.084	0.097	0.22	0.21
U	**0.81**	-0.26	0.36	-0.18	0.16	-0.11	-0.13
La	**0.98**	0.037	0.062	0.001	0.15	-0.018	-0.023
Ce	**0.65**	**0.72**	0.051	-0.055	-0.033	0.16	0.028
Pr	**0.95**	0.23	0.012	-0.041	0.11	0.015	0.013
Nd	**0.96**	0.20	0.025	-0.047	0.12	0.018	0.009
Sm	**0.94**	0.27	0.022	-0.070	0.080	0.034	0.017
Eu	**0.95**	0.23	0.011	-0.067	0.083	0.010	0.009
Gd	**0.97**	0.17	0.028	-0.041	0.065	-0.016	0.007
Tb	**0.97**	0.21	0.053	-0.066	0.054	-0.001	0.007
Dy	**0.97**	0.17	0.068	-0.042	0.063	0.00	-0.018
Ho	**0.98**	0.13	0.086	-0.037	0.063	-0.013	-0.031
Er	**0.98**	0.12	0.085	-0.053	0.066	-0.018	-0.044
Tm	**0.98**	0.13	0.093	-0.054	0.053	-0.018	-0.050
Yb	**0.97**	0.14	0.11	-0.050	0.036	-0.012	-0.078
Ce Anomaly	**-0.69**	0.62	-0.025	-0.039	-0.23	0.18	0.049

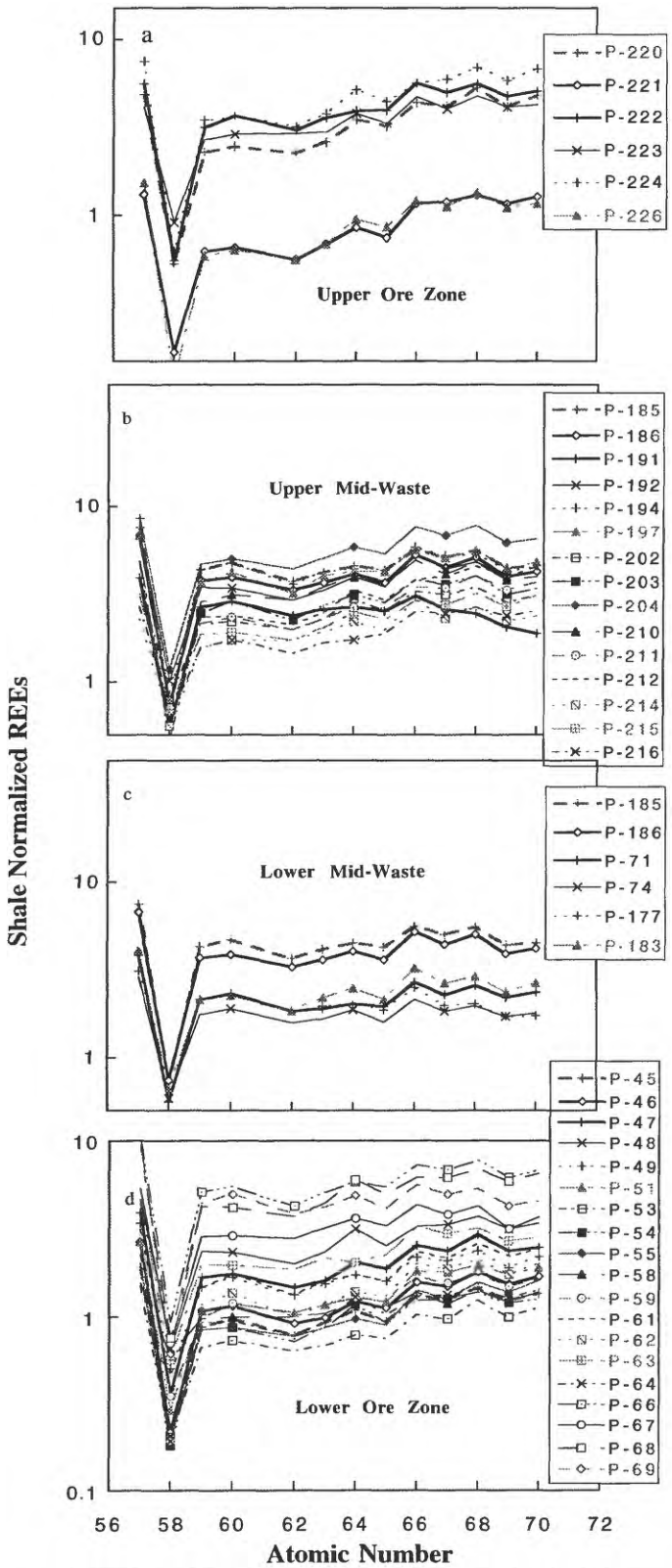

Figure 11. Atomic number versus normalized REEs (the REE pattern) for samples with greater than 10 percent apatite. See Figure 3 for zone identification and sample location. Y-axes are the same in all figures.

correlation is logarithmic and the REE are hosted predominantly by this component, the apatite Ce anomaly must be invariant. Its extrapolation to zero, at zero percent apatite, further gives the Ce anomaly for the detrital fraction, a well-documented value for terrigenous debris (Wedepohl, 1969-78; Piper, 1974).

These same relations are seen in the REE patterns of the samples (figs. 11 and 12). The samples are divided into the ore and waste zones of the deposit (fig. 3; table 5) and then according to their concentrations of apatite, less than or greater than 10 percent apatite. The patterns of samples with greater than 10 percent apatite all are similar, although samples from the ore zones seem to have a slight enrichment of the heavy REE, relative to samples from the waste zones (fig. 11). They all have a similar, strongly developed Ce anomaly. The patterns of the samples with less than 10 percent apatite show somewhat different patterns (fig. 12). The samples with the lowest bulk concentrations, normalized values less than 0.5, correspond to the carbonate enriched samples. They too have strong negative Ce anomalies, but no consistency in a heavy REE enrichment. The Ce anomalies become weaker as the overall concentrations increase to normalized values of one. These samples are composed dominantly of the detrital fraction. The anomalies then increase slightly as REE concentrations increase (normalized values greater than 1), owing to an increase in apatite in the range of 1 to 10 percent, for example, samples P-238, P-199, and P-44.

Pelletal apatite from the Peru shelf has a much lower REE concentration (La normalized = 1.1) and a less negative Ce anomaly (approximately - 0.2). The presence of significant pyrite and/or glauconite in this material, commonly in concentric zones (Piper and others, 1988), may account for this difference. The ubiquitous association of these other two marine components with apatite in the modern environment and their intimate intergrowth, versus their seemingly lower abundances in fossil apatite, is a rather intriguing problem. Apatite formation in both ancient and modern deposits occurred in the sediment (Kolodny, 1981). The region of sulfate reduction in the sediment column, underlying the region of denitrification, seldom must have extended into the surface and near-surface sediment region of apatite precipitation, but only in the case of the ancient deposit. It would seem to follow that the chemical fronts within the ancient sediment column may have been

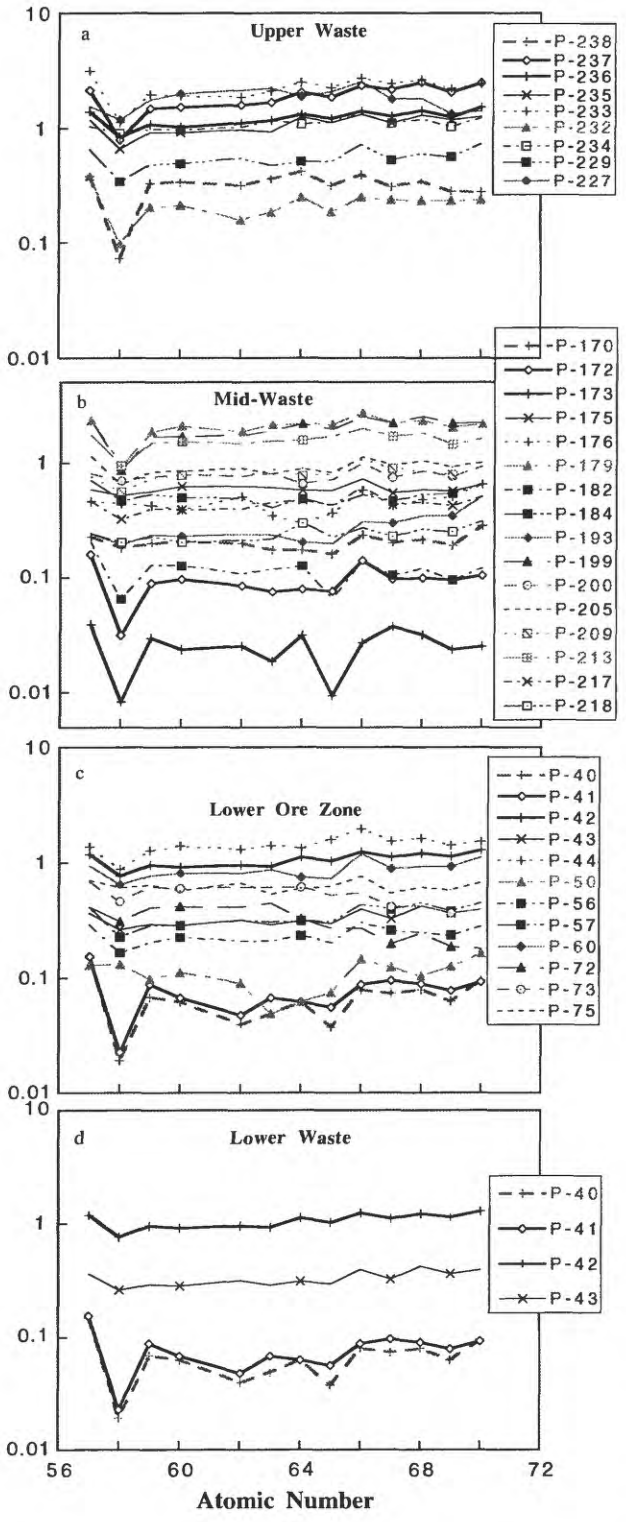

Figure 12. Atomic number versus normalized REEs (the REE pattern) for samples with less than 10 percent apatite. See Figure 3 for zone identification. Y-axes are the same in all figures, but are different from those in Figure 11.

much more stable than in the sediment now accumulating on the Peru Shelf. A high-velocity, bottom current on the Peru Self, at the depth of phosphatization (Arthur and others, 1998), is surely a major factor in driving temporally variable depths of chemical boundaries even within the sediment.

Carbonate Minerals

Calcite and dolomite are calculated assuming they are stoichiometric (table 3). This is suggested by the plot of MgO and CaO versus CO_2 (fig. 13). However, this plot is complicated by both CaO and MgO being present in the detrital fraction (table 3)

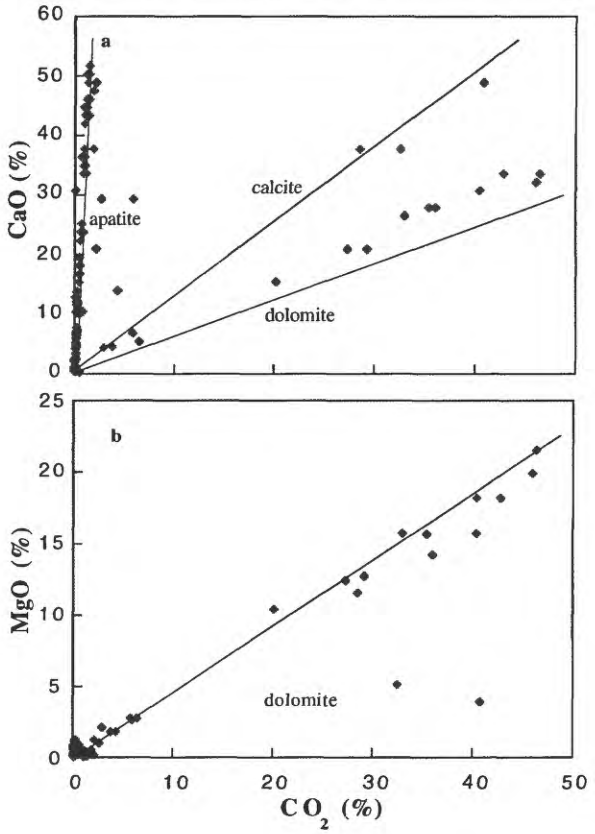

Figure 13. Relation between CO_2 and (a) CaO and (b) MgO. Labeled curves represent stoichiometric components (table 3).

and CaO being present mostly in the apatite component (fig. 10). Even so, the correlation between carbon measured and carbon calculated (fig. 4), where dolomite and calcite represent the dominant hosts of carbon, supports the assumption of a stoichiometric composition for both. Both are present in this section of the Phosphoria Formation, with dolomite dominant in almost all samples (table 5).

Table 9. Concentrations of trace elements in deep-ocean seawater (in ppb)(Boyle and others, 1976, 1977; Bruland, 1983; de Baar and others, 1985), marine plankton (in ppm) (Martin and Knauer, 1973; Elderfield and others, 1981; Brumsack, 1983; Collier, 1984, 1985; Palmer, 1985), and mass weight ratios with phosphorus.

Element	Seawater Content	δ -Seawater Weight Ratio	Organic-Matter Content	Element:P Ratio Organic Matter	Biogenic Carbonate Content	Biogenic Silica Content
Cd------	0.10	1.3×10^{-3}	12	1.2×10^{-3}		
Co------	0.0012	--	<1	--		
Cr------	0.22	0.95×10^{-3}	2.0	0.26×10^{-3}		
Cu------	0.18	1.1×10^{-3}	11	1.4×10^{-3}	0.50	7
Mo-----	10.60	--	2	0.26×10^{-3}		
Ni------	0.59	5.3×10^{-3}	7.5	1.0×10^{-3}		
Se------	0.13	1.5×10^{-3}	3.0	0.40×10^{-3}		
U-------	3.00	--	1(?)	--		
V-------	1.80	1.1×10^{-3}	3.0	0.40×10^{-3}		
Zn-----	0.52	6.1×10^{-3}	110	14.00×10^{-3}		7
La-----	0.0052				0.185	5.8
Ce-----					0.133	8.2
Nd-----					0.162	6.7

The trace element content of these two components is quite low (tables 7 and 8), a probable reflection of the very low concentration of trace elements in marine calcite (table 9). Nonetheless, the samples with little or no apatite that have strong Ce anomalies (fig. 10) tend to have high concentrations of dolomite and calcite (fig. 14); a reflection of the seawater anomaly (Piper, 1974), the negative Ce anomaly of marine calcite, but a low overall concentration of REEs (Palmer, 1985). Except for the "false cap" (table 5), the carbonate versus Ce anomaly relation is smooth, only slightly more negative than the Ce anomaly of modern marine calcite. The seemingly unusually strongly negative Ce anomaly for the "false cap" is attributed to its relatively high concentration of apatite (table 5). For the other carbonate-enriched units, precipitation within the sediment pore water of dolomite and the limestone concretion does not seem to have altered significantly the REE pattern or concentrations of REEs present in the original accumulating carbonate phases.

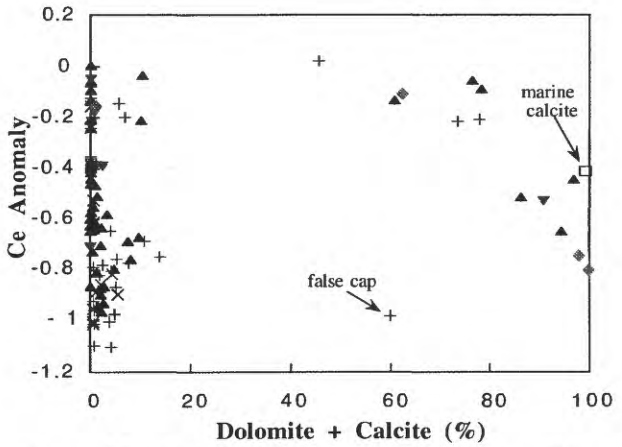

Figure 14. Relation between carbonates—calcite plus dolomite—and the Ce anomaly. See Figure 9 for identification of symbols. Marine calcite value is from Palmer (1985).

This distribution of the Ce anomalies (fig. 14) suggests that the occurrences of apatite and dolomite (and/ or calcite) are essentially mutually exclusive.

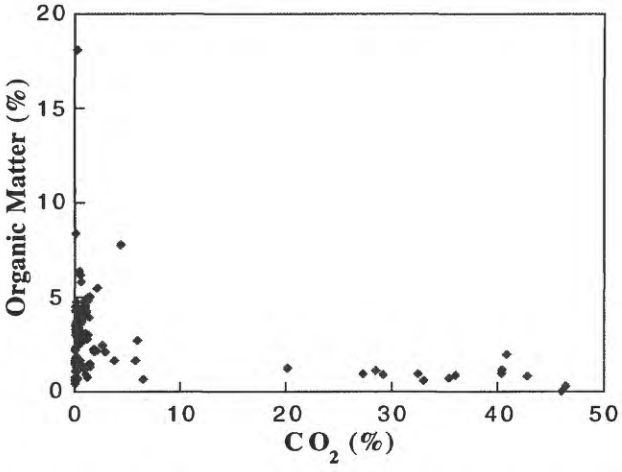

Figure 15. Relation between CO_2 (i.e., carbonate minerals) and organic matter. The relation shows two distinct populations, suggesting the two components are virtually mutually exclusive.

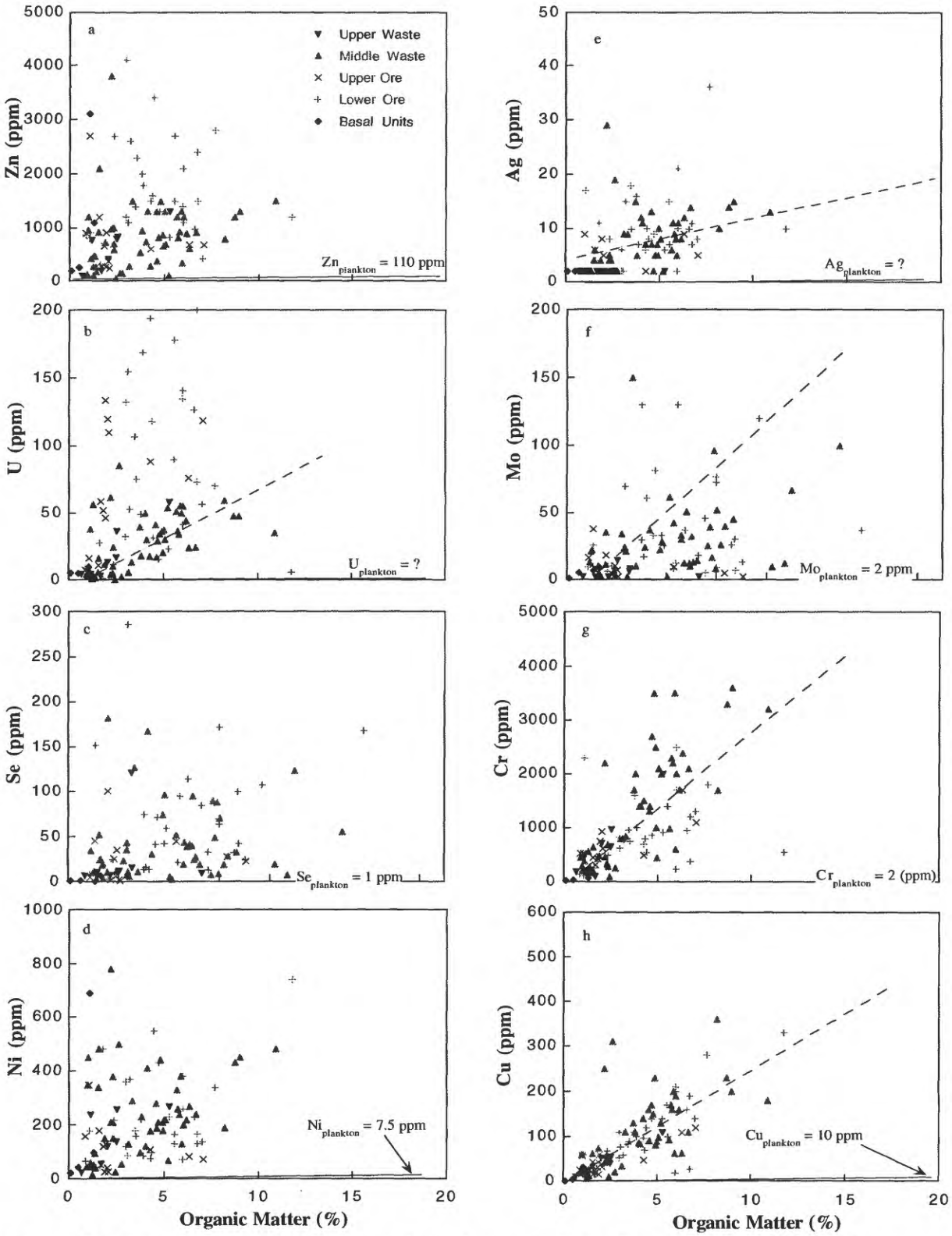

Figure 16. Relation between trace elements and organic matter. Broken lines are least-square, best-fit curves and include all data, except in the case of U, for which only the waste samples are included. Solid curves give the metal:organic-matter ratio for plankton (table 9).

This interpretation is supported by the relation between CO_2 and CaO (fig. 13a). The relation between CO_2, or carbonate minerals, and organic matter further exhibits a mutually exclusive distribution (fig. 15). The samples are distributed between two distinct populations, rather than merely showing a negative correlation.

Organic Matter

The proportionality constant used to convert organic carbon to organic matter of 1.4 (table 3) has been taken from Powell and others (1975). Other values are published in the literature, for example, by Isaacs (1980), but the value from Powell and others (1975) was used by Medrano and Piper (1995) and gave excellent closure for the sum of the major components to 100 percent for all sites studied. Again, the plot of the two carbon values (fig. 4) supports this value of 1.4 for the Enoch Valley samples as well as for the other five sites examined by Medrano and Piper (1995).

Factor analysis (table 8) shows a strong loading on factor five of trace elements—Ag, Cr, Cu, Mo, Se and, less so, Ni and As—the factor with the strongest loading for organic matter. Organic matter has only a slightly less strong loading on factor one, as do Cu and Cr, the factor which might be called the apatite factor. However, the grouping of the trace elements and sulfur on factor five as well suggests an association predominantly with organic matter. Conversely, the near absence of REE, Y, and Sr loadings on factor five, but strongly on factor one, supports their association with apatite, an association reported by others (Wright and others, 1987).

These relations demonstrate the strength of factor analysis over the calculation of simple linear correlation coefficients. The rather strong positive relation between the 3+-valence REEs (all REEs except Ce) with organic matter, that is, organic carbon (table 7), suggests, at first, that the REEs might be associated with this component as well as with apatite. Clearly, this is not the case. Those correlation merely reflect the correlation between P_2O_5 and organic carbon and the loading of apatite and less so organic matter on factor one, along with those of the REEs (table 8). The near total absence of REE loadings on factor five would seem to preclude any association between them and organic matter.

The plot of trace elements versus organic matter requires a strong trace-element enrichment in the residual organic matter, over their concentrations in the original organic matter, shown by Piper (1994) and Piper and Medrano (1994) to have been approximately equal to that of modern planktonic debris (table 9; fig. 16). If, indeed, these elements had a biogenic source, as discussed below, then much of the organic carbon must have been lost, probably during early diagenesis. The relations emphasize the contrast between the original composition of the planktonic source material of trace elements and the composition of the current residual organic-matter host, particularly for Ag, Cd, Cu, Mo, Ni, and Zn.

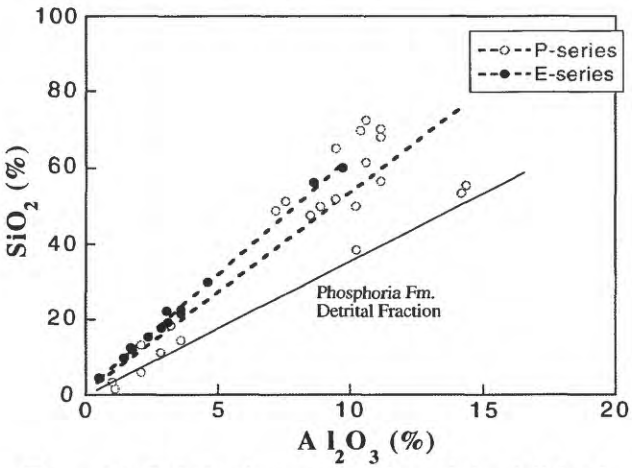

Figure 17. Relation between Al_2O_3 and the deficit of the sum of elements and oxides, except SiO_2 but including H_2O's (P-series, Meade Peak Member), i.e., the best estimate of total SiO_2 itself; and relation between Al_2O_3 and SiO_2 measured in the E-series (table 2). The curve labeled Phosphoria Fm. is from Medrano and Piper (1995). The broken curves are least-square, best-fit curves to the two series of samples. The data show rather close agreement suggesting the two series of samples indeed represent a single population.

Biogenic Silica

Total silica was not measured in the P-series of samples, precluding a direct calculation of biogenic silica. However, biogenic silica can be estimated from the deficit of the analyses (table 5). The estimate can then be compared to the silica values measured for the E-series of samples, for which Al_2O_3 and SiO_2 measurements are available (table 2b). The relation between Al_2O_3 and SiO_2, measured and estimated for these two groups of samples, is similar (fig. 17). Also, the minimum for the P-series of samples approaches the Al_2O_3:SiO_2 ratio of the detrital fraction measured for other sites (Medrano and Piper, 1995).

The trace-element content of biogenic silica is likely small (Martin and Knauer, 1973), similar to that of $CaCO_3$ (table 9), although Elderfield and others (1981) measured a La value of 5.8 ppm and Ce anomaly of – 0.2 in a single sample of marine planktonic silica.

Miscellaneous

Thin-section analyses of several samples reveal the presence of pyrite. I have also identified sphalerite under the scanning electron microscope. Unfortunately, it has proven impossible to calculate normative abundances of either. In the case of pyrite, an estimate of excess Fe_2O_3, i.e., in excess of the possibly maximum detrital contribution, can be obtained from a minimum for Al_2O_3 versus Fe_2O_3 (fig. 7b). Comparison of the "excess" iron values with sulfur fails to show any relation with the stoichiometry of pyrite (fig. 18). Thus, no attempt has been made to ascertain the trace-element composition of pyrite, although we might assume that its trace-element contribution to the total sample inventory is small; pyrite appears to constitute less than about 1 percent of the total sample.

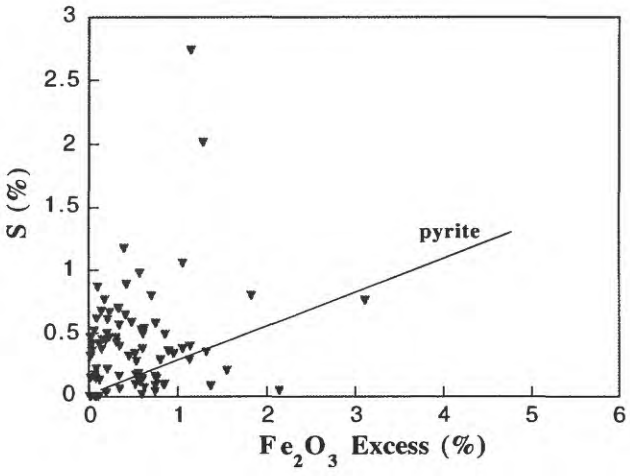

Figure 18. Relation between Fe_2O_3 in excess of a minimum for the Fe_2O_3 versus Al_2O_3 curve (fig. 6b) and total S. The curve represents the relation in FeS_2.

Summary

The overall calculations of the abundance of components were checked by the approach of their sum to 100 percent (table 5), despite exclusion of biogenic silica in the calculation. The sum exceeds 100 percent by more than 5 percent in only 2 samples. In both cases the samples are dominated by dolomite, suggesting that the MgO measurement by

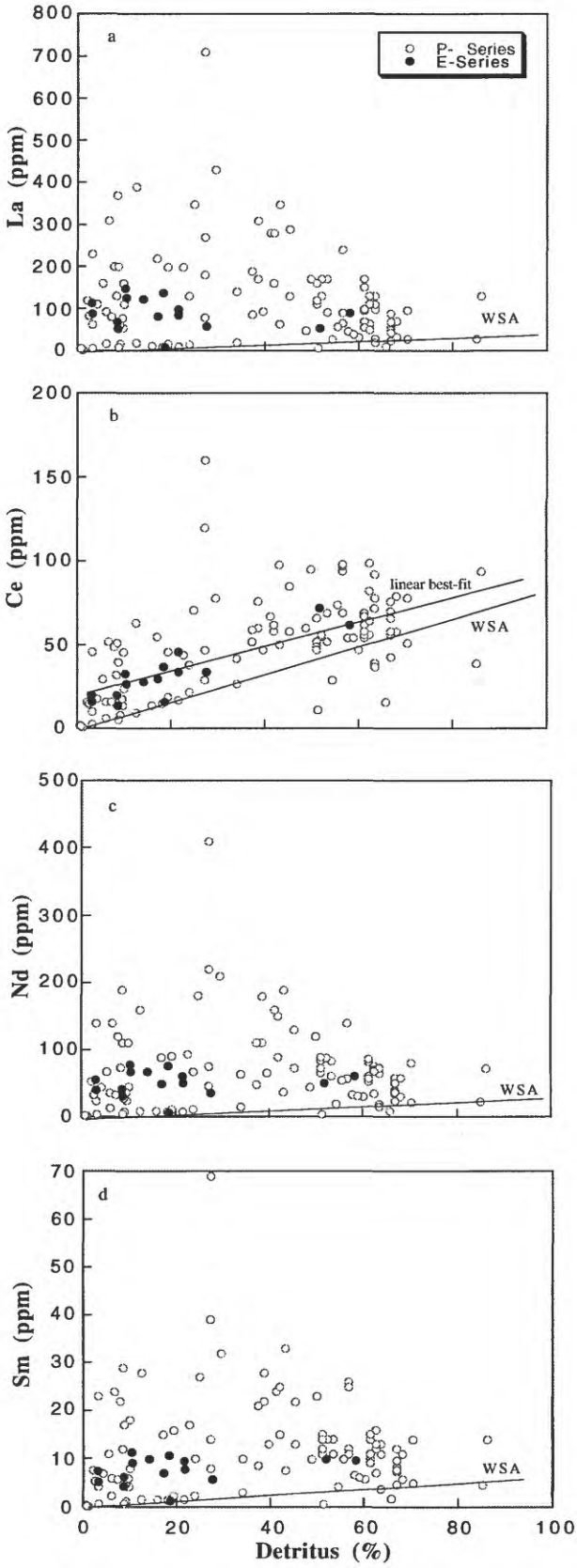

Figure 19. Relation between detritus and selected REE.

ICP-AES is slightly high. However, agreement of the values for carbon calculated and carbon measured, as discussed above, limits the uncertainty of that measurement. The close approach to 100 percent requires the absence of biogenic silica (opal-CT) in a few of the samples, but more importantly, it supports the overall calculations of the abundances of components throughout the stratigraphic section.

Calculation of the marine fraction of trace elements from minima of the trace-element versus detritus plots can be expressed by the following simple formula:

(1) $C = A - B \times$ (terrigenous fraction),

where A = total trace-element content of a sample (table 4), B = trace-element content of terrigenous material (table 6), and C = marine-derived, trace-element content in each sample. Correlations between bulk trace-element concentrations and the major components provide a check on the calculations of the marine fraction of trace elements. For example, Th correlates strongly with the detrital fraction; the heavy metals correlate strongly with organic matter and an undefined component (factor 3 in table 8), and the REEs, except for Ce, correlate with apatite. These same associations have been reported in earlier studies (Altschuler and others, 1967; Nissenbaum and Swaine, 1976; Wright and others, 1987). Because of the small contribution of the detrital fraction to the bulk concentration of most trace elements, any error in estimating the detrital composition of trace elements will little effect the calculation of trace-element concentrations in the marine fraction and the conclusions based on the distribution of trace elements in the marine fraction alone.

The REE content of the detrital fraction was suggested to be similar to that of the WSA (Piper, 1974), based on the close approach of the REE patterns to that of shale, for those samples composed dominantly of a detrital fraction (fig. 12). This relation can also be seen in the plots of the detrital fraction versus individual REE, for which the lowest measured values lie close to the relation for WSA (fig. 19). The interpretation that the detrital fraction has REE concentrations similar to those of WSA is further supported by the extrapolation of the apatite versus Ce anomaly curve to zero (fig. 10), by definition the anomaly of WSA, and the correlation between Ce and the detrital fraction, a relation that approximately parallels the relation of WSA (fig. 19b).

HOST PHASES OF TRACE ELEMENTS: PARTITIONING, WEATHERING, AND STRATIGRAPHIC DISTRIBUTION

Partitioning of trace elements between their current host components contributes to an estimate of the behavior of trace elements under conditions of weathering. The detrital fraction of trace elements has been shown above to be similar to that of the WSA. It is both source and host of several trace elements, as well as host of the major-element oxides. Although it is a minor host for most heavy metals and REE, it is a major host for Ba, Sc, Th, and possibly Ce, Ni (table 8), and Co (Medrano and Piper, 1995). These correlations and the approach of most to their relation in WSA further suggest that this sediment fraction has been largely non-reactive throughout its history.

The marine fractions of Ag, Cr, Cu, Mo, Se, and, less so, several other trace elements correlate with the organic-matter content (tables 7 and 8). Partitioning of trace elements into organic matter was reported by Leventhal (1989), Odermatt and Curiale (1991), and Piper and Isaacs (1995) for the Monterey Formation; by Swanson (1961) for Paleozoic organic-matter-enriched shales; and by Nissenbaum and Swaine (1976) for modern marine sediment. Lewan (1984), Moldowan and others (1986), and Odermatt and Curiale (1991) further examined the fractionation of metals between various phases of organic matter. For example, Lewan (1984) interpreted the V/(Ni+V) ratio in crude oils to reflect the Eh, pH, and sulfide activity of the depositional environment.

The REE and U are partitioned mostly into apatite (tables 6 and 8), similar to their partitioning in other phosphate deposits (Wright and others, 1987; Piper, 1991). Additional marine host phases might include glauconite and metal sulfides (Glenn and Arthur, 1988; Piper and others, 1988), predominantly iron sulfides. Pyrite is present in many sections of the Phosphoria Formation (Sheldon, 1963), but apparently only in minor amounts in Enoch Valley rocks (fig. 18). I have also detected trace amounts of sphalerite by microprobe in rocks from other sections.

The carbonate minerals host a minor fraction of trace elements (tables 8, and 9).

Partitioning of trace elements into marine host phases and, particularly, into organic matter occurs during diagenesis and, possibly, during later alteration of the originally deposited marine phases. Trace

elements commonly are enriched by more than 10-fold in the residual organic fraction over their concentrations in modern planktonic debris. As a result, the slopes of the trace-element/organic-matter curves (fig. 16) are unrelated to the composition of modern marine planktonic organic matter, a relation similar to that observed for other deposits (Calvert and Price, 1983; Piper, 1991; Piper and Isaacs, 1995). Yet, the trace-element/organic-matter relations probably did not change drastically during settling through the water column. Fisher and Wente (1993, p. 671) concluded from a study of particulate organic matter in the modern ocean that Am, Ag, and Sn are:

> "* * * retained sufficiently long, even by decomposing cells, to suggest that phytoplankton sinking as aggregates at rates of 100 m per day would effectively transport these metals hundreds of meters out of oceanic surface waters."

We might conclude from this finding that the current high trace-element content of sedimentary organic matter reflects uptake of trace elements by the residual organic phase. This interpretation parallels that advanced to explain the relation between C and S in organic matter of modern sediment (Mossmann and others, 1991). Also, apatite, which clearly precipitates within the upper few centimeters of the sediment (Kolodny, 1981; Burnett and others, 1988), must acquire its trace-element signal and, particularly, its REE signal from sediment pore water. Thus, the partitioning of trace elements among the different marine host phases of sediment (residual organic matter, apatite, and so on) reflects pore-water conditions, that is, diagenetic conditions.

In the case of organic matter, depth profiles of organic carbon in modern sedimentary environments (Douglas and others, 1986; Froelich and others, 1988; Calvert, 1990), which have organic-matter contents similar to that of the Phosphoria Formation, strongly suggest that much organic matter is lost during early diagenesis as HCO_3^-, rather than that trace elements are gained. Sediment-trap studies of pelagic environments further support the loss of organic matter during early diagenesis (Fischer and others, 1986; Baldwin and others, 1998). Settling particulate matter collected at greater than 3,000 m depth in the pelagic environment can have an organic-matter content approximately five times that of its detrital content, whereas surface sediment at the same sites has approximately 50-fold more detritus than organic matter. As much as 95 percent of the organic matter that rains out of the water column is thus, oxidized at and near the very surface. Ocean-margin areas have an even larger flux of organic matter to the sea floor owing to (1) a shallower sea floor (Suess, 1980; Sarnthein and others, 1988), (2) a higher primary productivity (Berger and others, 1988; Pedersen and Calvert, 1990), and (3) a positive relation between the relative rain rate of organic matter and primary productivity (Baines and others, 1994).

In oxic (Fischer and others, 1986) and mildly O_2-depleted environments (Shaw and others, 1990), a large fraction of associated trace elements is also lost. The content of trace elements in the Phosphoria Formation suggests that this may not have been the case for this deposit, as discussed below. However, here I am concerned with the trace-element composition of host components, not with the original source of trace elements and how well that source signal might have been retained in the rocks since their deposition.

If we can assume that the trace elements hosted by the different components (table 8) behave somewhat similar to the hosting components themselves, then we can estimate an order of reactivity of the trace elements under conditions of oxic weathering. This environment, which is far different from the O_2-depleted environment of deposition (discussed below), should largely account for the release of trace elements to solution. Clayton and King (1987), Clayton and Swetland (1978), and Littke and others (1991) have established an approximate order of weathering of host mineral components in shale formations of similar high organic-matter contents. The order of instability under conditions of subaerial weathering is roughly as follows:

> pyrite > organic matter > carbonates > apatite > chert > terrigenous debris.

I have estimated the positions of apatite and chert. Chert is likely a minor host of trace elements relative to other host phases (table 8 and 9), but perhaps more important than the carbonates. In positioning apatite, I have taken the constancy of its REE content (fig. 10; Piper and Medrano, 1995, fig. 7) to suggest that it is relatively non-reactive during weathering, slightly less so than chert and the detrital fraction (Littke and others, 1991).

Combining the order of weathering with the partitioning of trace elements (table 8) gives an order of release to ground water approximately as follows:

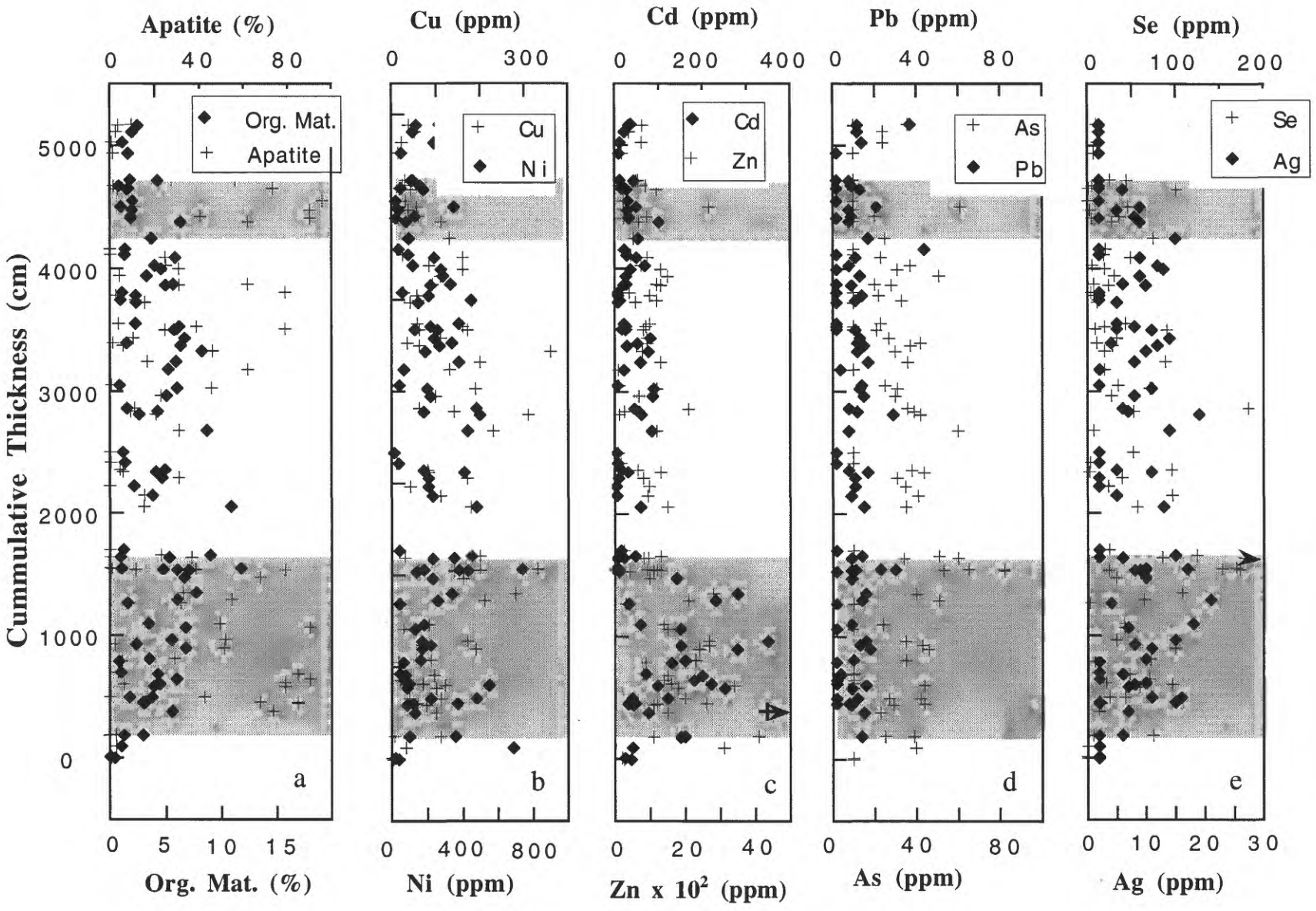

Figure 20. Distribution of components and trace elements versus stratigraphic depth (cm). Shaded areas are lower and upper ore zones, identified in figure 3.

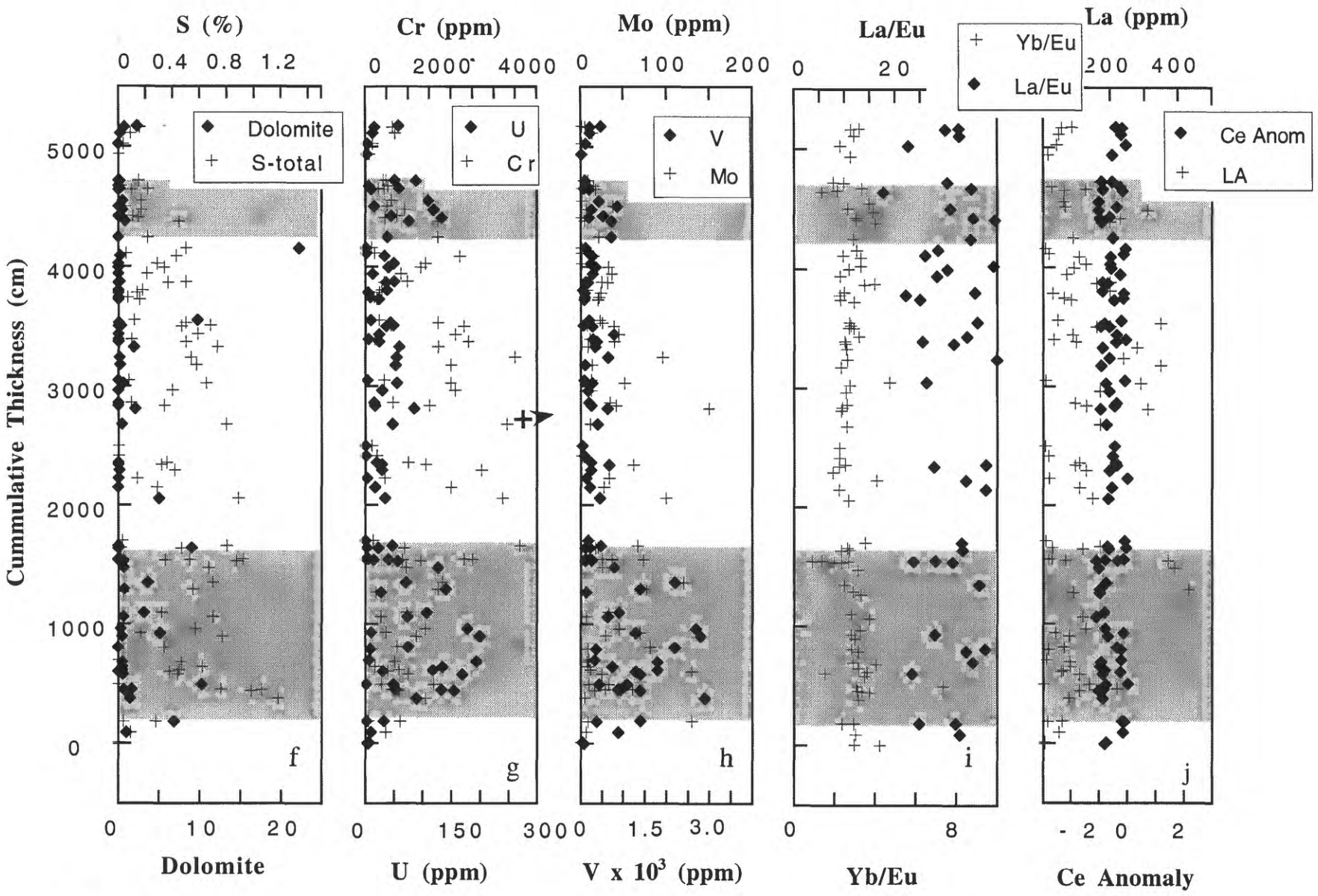

Figure 20. Cont.

Cr = Cu = Mo = Se > As >> U = REE >> Ba > Co > Th = Sc.

The behavior of any element once released to ground water, of course, will be influenced by its thermodynamic properties. Most of the trace elements are much more soluble under oxidizing than reducing conditions (table 10, p. 50) and should be held in solution once their host phase(s) is dissolved. They will remain in solution until they again have the opportunity to enter the food chain (Presser and Piper, 1998), accumulate in some O_2-depleted environment, or both.

Cd, V, and Zn are not included in the above sequence, as their host phase has not been identified. If ion-microprobe analysis, or some sequential leaching technique, determines that they are hosted largely by a sulfide phase, then they could be the most reactive of the elements examined here. Measurements of V in surface outcrop and in buried (40 ft) sections gave similar concentrations, which suggests that that will not be the case, at least for V (McKelvey and others, 1986). Also, Co is included, although it correlates with none of the major components at this site. At other sites, it correlates with the detrital fraction and has a concentration close to that of WSA (Medrano and Piper, 1995).

Several of the trace elements that have their strongest loadings on factors identified by one of the major components, nonetheless, also have significant loadings on Factor 3, the factor with Cd, V, and Zn. These include Ag, As, Cu, Mo, Ni, and U. The results of Desborough and others (1999) suggest that this second host component is pyrite. Clearly, its content and composition need to be ascertain.

The stratigraphic distributions of trace elements might also contribute to their introduction into ground water. Although As, Cu, and Se are enriched in the lower ore, they also achieve high concentrations in the middle waste and Cr is most enriched in the middle waste (fig. 20). Thus, As, Cr, Cu, and Se present perhaps the greatest impact to the environment, via transport by ground water flowing through mine tailings and unroofed, but unmined ore. Se represents perhaps the most severe problem, because of its biological uptake (USDOI, 1998). It is strongly bioreactive (Presser, 1994); has a very narrow range between the concentration at which it is an essential nutrient and the concentration at which it becomes a toxic nuisance (Presser and Piper, 1998); and is progressively enriched in the higher trophic levels (Presser and others, 1994). Its impact within other environments, for example, the San Joaquin Valley in California, where it is derived from similar rocks, albeit with lower Se concentrations (Piper and Isaacs, 1995), has been well documented (Presser and Ohlendorf, 1987; Skorupa, 1998). Certainly, other properties of Se and the other trace elements, such as their load and speciation in solution and the different levels of toxicity for various biota, will further determine their behavior in and impact upon the environment. Although the distribution of Se in this formation, its probable high degree of mobility under weathering conditions (Presser, 1994; Desborough and others, 1999), and its tendency to concentrate in biota account for the current attention on this element, we should not lose sight of the possibility that other trace elements strongly enriched in and weathered from the Phosphoria Formation, for example Cd, also may have a significant environmental impact.

SOURCE OF TRACE ELEMENTS: CHEMISTRY OF THE DEPOSITIONAL ENVIRONMENT

The sources of trace elements in this sedimentary deposit are the terrigenous and marine environments. The terrigenous-derived debris is represented by the detrital fraction. The seawater-derived marine fraction can be divided into a biogenic fraction derived from surface water and a hydrogenous fraction derived from bottom water. Two different approaches can be used to examine the contributions of trace elements by these multiple sources, despite complications introduced by the reactivity of the marine fraction during diagenesis. Both schemes assume that the composition of the detrital fraction was similar to that of WSA (table 6), that the composition of deposited organic matter was the same as that of modern plankton (table 9), and that the elemental content in excess of that contributed by these two sources can be attributed to a hydrogenous source.

The first approach computes the rate of accumulation of each element in the two marine fractions from the rate of accumulation of bulk sediment. By assuming a trace-element stoichiometry for Permian organic matter based on the trace-element content of modern plankton, similar to assuming a WSA composition for the detrital fraction, the rate of accumulation of organic matter required to supply each trace element to the sea floor can be calculated. These values are compared with the rate of accumulation of organic matter on the sea floor of different environments in the modern ocean. Those elements that give

disproportionately higher rates of accumulation than can be attributed to the flux of organic matter alone are then interpreted to have accumulated directly from seawater as a hydrogenous fraction, in addition to having accumulated as a biogenic fraction and a detrital fraction. That is, trace elements can have three sources—(1) a detrital, or terrigenous, source, (2) a marine organic, largely planktonic, source, and (3) a bottom-water, inorganic source.

The sediment accumulation rate in the Permian Formation (Piper and Medrano, 1995) is reported only as an average for the formation as a whole (Murchey and Jones, 1992) and imposes considerable limits on this first approach. However, the averages of accumulation rates of the marine-derived fraction of trace elements for the range of concentrations measured in these samples agree closely to accumulation rates expected for the Phosphoria Basin, based on geochemical conditions in what are considered to be similar environments of the modern ocean; for example, the ocean margins. The accumulation rate of the detrital fraction, by contrast, is far different from what might have been expected.

The second approach compares interelement ratios of trace elements in the marine fraction of the rocks with their ratios in modern plankton and seawater. From x-y plots, trace-element:trace-element ratios identify those elements that are enriched above a biogenic contribution. This procedure, which can be used in the absence of information about sediment-accumulation rates, points up the desirability of a master variable, or a single element, that defines the marine organic-matter source, just as Al_2O_3 defines the terrigenous source. In this discussion, we consider both Cu and Zn as master variables for the marine biogenic fraction.

Terrigenous Source

Ratios of major-element oxides to detritus indicate that the detrital fraction had a terrigenous source, as opposed to a marine volcaniclastic source. Plots of Al_2O_3 versus K_2O and Fe_2O_3 (fig. 7) and versus several trace elements (figs. 8, 9, and 19) fall along single trends that extrapolate to zero and have slopes approaching those for WSA, or exhibit strong minima. Thus, this fraction is a source phase, as well as a current host phase for these major-element oxides and trace elements. For the trace elements that do not correlate with detritus, their bulk content in most samples is large relative to the contribution by the detrital fraction, as determined from the detritus content of each sample and minima of detritus versus trace-element curves (fig. 9).

The trace elements that do not correlate with the detrital fraction itself (e.g., Cd, Cu, Cr), nonetheless, exhibit minima in minor-element versus detrital-fraction plots that are similar to their relations in WSA, that is, the curves extrapolate to the WSA values at 100 percent detrital fraction. However, it would be a mistake to assume that is the case for other sedimentary formations. Variations in the sedimentary rocks analyzed to obtain the WSA composition, or the composition of other standards (Wedepohl, 1969-78; Gromet and others, 1984) demonstrate that such an assumption is merely a first step in determining the composition of the detrital fraction of the sediment.

We can now estimate the rate of accumulation of this fraction. The length of time of deposition for the Meade Peak Member of the Phosphoria Formation was approximately 7.2 my. (Murchey and Jones, 1992). Making a best estimate for the amount of the detrital faction in this section of the Phosphoria Formation (table 5), I obtain an average accumulation rate of approximately 0.64 mg detritus/cm^2 per year. This rate is comparable to its rate of accumulation in the central Pacific Ocean today. It seems quite unlikely that the narrow shelf environments in the ocean today, commonly bordered by continental land masses of high relief, have comparable accumulation rates of terrigenous material. For example, in the Gulf of California, the rain rate into the Guaymas Basin is almost an order of magnitude higher (Thunell, 1998).

Marine Source

The original marine source phases of trace elements are (1) biogenic debris (organic matter, opal-A, and $CaCO_3$) and (2) hydrogenous material (trace-element precipitates and adsorbed phases, mostly from bottom water). Although several of these components may now also act as trace-element hosts, the initial trace-element composition of each of the two marine sources must be distinguished from that of the host phases if the seawater environment of deposition is to be deciphered.

Biogenic Source

The biogenic contribution of trace elements is determined prior to determining a possible hydrogenous contribution; then, the residual trace-element content is assigned to the hydrogenous source. The trace-element content of plankton, that is, the trace-element

stoichiometry of planktonic debris in the ocean today, varies considerably (Martin and Knauer, 1973; Eisler, 1981; Collier and Edmond, 1984), due to such natural factors as variations among species, location, growth rates, and seawater pH (Eisler, 1981). The care with

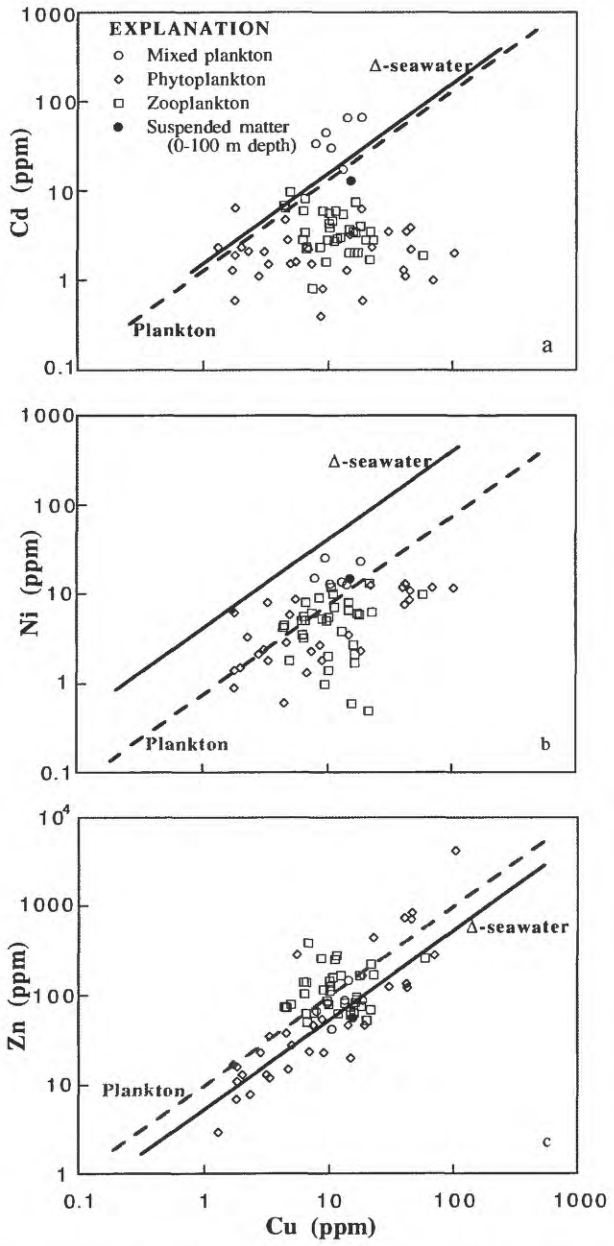

Figure 21. Relations between Cu and Cd, Ni, and Zn in plankton and seawater suspended phases (table 9). Broken curves are estimates of the average plankton value (Brumsack, 1983). The Δ-seawater values are calculated from the differences between concentrations of trace elements in the photic zone of the ocean and at an ocean depth of 500 to 2000 m.

which the samples used here to calculate a best estimate were collected and analyzed by Martin and Knauer, (1973), Collier and Edmond (1984), and Sherrell (1989) requires that the reported variations in the composition of plankton (fig. 21) are due to natural factors, rather than artifacts of sampling and analysis. The results indicate that we can not expect to obtain a single value for any trace-element content in samples of plankton. We might add that significant variations also are reported for the NO_3^- and PO_4^{3-} contents in plankton (Sverdrup and others, 1942; Collier and Edmond, 1984; Copin-Montegut and Copin-Montegurt, 1983), although certainly not as great as the variation of the trace elements (fig. 21). These ions constitute the major nutrients (Redfield and others, 1963), whose functions in plankton growth are well established. Given these variations, we chose to use the estimates of Brumsack (1986) rather than introduce a new set of values.

The magnitude of trace-element variations in plankton (fig. 21) can easily discourage further consideration of the data and their application to geochemical investigations of sedimentary rocks. However, two important aspects of the marine environment require examination of the contribution of organic debris to the accumulation of trace elements. First, rates of primary productivity throughout the ocean margin are relatively high (Berger and others, 1988), resulting in a large flux of organic matter to the sea floor (Calvert, 1990; Pedersen and Calvert, 1990; Baines and others, 1994). Second, a significant amount of the organic matter produced in the photic zone accumulates on the sea floor of ocean margins, owing to shallow water depths (Suess, 1980; Reimers and Suess, 1983). Thus, this fraction of sediment on ocean margins should represent a major sink for many trace elements in the oceans today (Collier and Edmond, 1984) and in ancient oceans as well.

The distributions of Cd, Cu, Cr, Ni, V, and Zn in the water column (fig. 22), relative to those of PO_4^{3-}, NO_3^-, and $Si(OH)_4$, reflect the importance, if not predominance, of plankton (that is, organic detritus) as a carrier of many metals from the photic zone to the sea floor. More importantly, the distributions of these elements provide a critical evaluation of the measured trace-element composition of plankton. NO_3^- and PO_4^{3-} are the limiting nutrients to phytoplankton productivity in the photic zone of the ocean today (Sverdrup and others, 1942; Broecker and Peng, 1982; Codispoti, 1989),

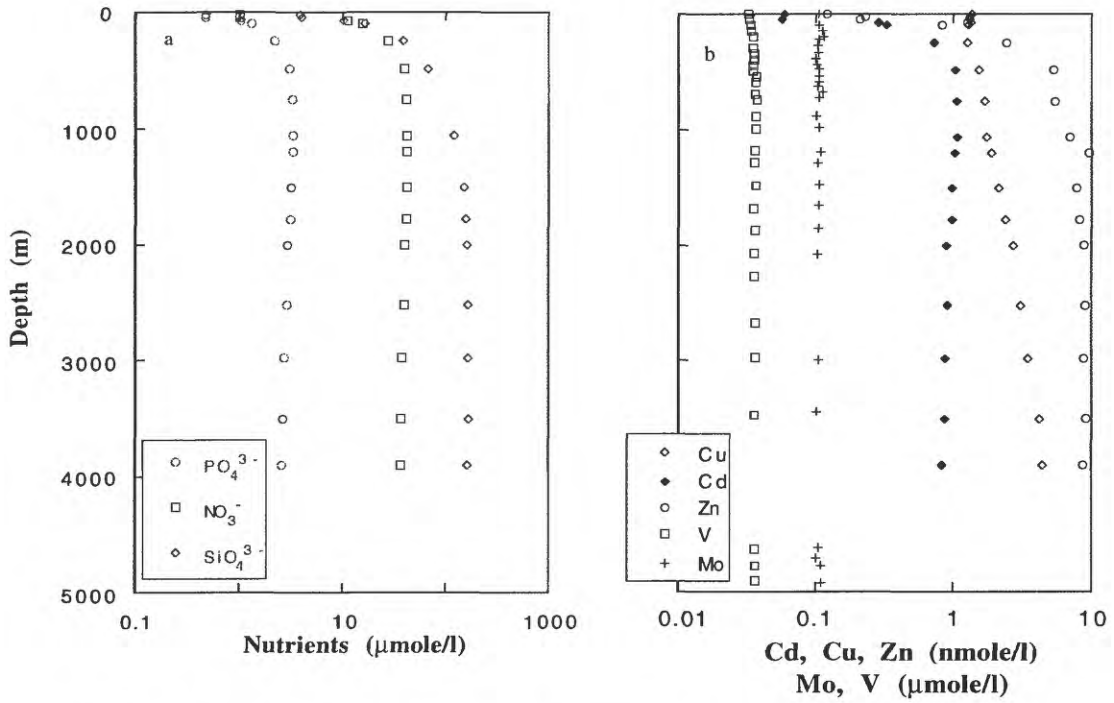

Figure 22. Depth profiles in the ocean of the major nutrients (a) and selected trace elements (b). Measurements are reported in Redfield and others (1963), Boyle and others (1976, 1977), Bruland (1983), and Collier (1984, 1985). Note the two scales for the x-axis in (b).

although $Si(OH)_4$ as well may be a limiting nutrient in some ocean-margin areas (Dugdale and Goering, 1970; Nelson and others, 1981). Iron also has been shown to limit primary productivity in selected areas of the ocean (Martin and Gordon, 1988; Coale and others, 1998). NO_3^- and PO_4^{3-} (and Fe and $Si(OH)_4$) are extracted from seawater in the photic zone during photosynthesis and returned to the ocean at depth by bacterial respiration. Only a small portion of the initial particulate form survives to the deep-ocean sea floor. As a result of their cycling through the water column, the NO_3^- and PO_4^{3-} concentrations in surface water are relatively low and even approach zero; their concentrations increase sharply below the photic zone to the thermocline and then remain relatively constant below approximately 500-m depth.

Many trace elements show a similar depth profile (fig. 22) and must, therefore, have a similar history. The variation in Cd content with depth parallels that of PO_4^{3-} concentration (Boyle and others, 1976), more so than those of the other trace elements. Zn- and Ni-depth profiles resemble that of $Si(OH)_4$ (Sclater and others, 1976; Bruland, 1983). For Zn, the Zn-$Si(OH)_4$ relation in seawater (Broecker and Peng, 1982) corresponds to a Zn content in opal of approximately 60 ppm. However, the measured Zn content of opal averages only 5 to 10 ppm (Martin and Knauer, 1973), much less than its bulk content in plankton of 110 ppm (table 9). Thus, the high Zn content in plankton (Collier and Edmond, 1984) and its much lower measured content in the siliceous fraction of plankton (Martin and Knauer, 1973) indicate that Zn and probably Ni as well are associated predominantly with the soft parts of organisms, similar to Cd.

The depth profiles of these trace elements in seawater, relative to that of PO_4^{3-}, can be used to evaluate their measured contents in plankton (table 9). The NO_3^-:PO_4^{3-} ratio, or δ–seawater $[NO_3^-]$,

$$(2) \qquad = \frac{NO_3^-(\text{deep ocean}) - NO_3^-(\text{photic zone})}{PO_4^{3-}(\text{deep ocean}) - PO_4^{3-}(\text{photic zone})},$$

based on the chemical profiles of these two ions in seawater (fig. 22), equals the average N:P atomic ratio of plankton of 15:1 (table 9). This agreement indicates that metabolic and advective processes dominate their distributions in the deep ocean. If this relation is also true for trace elements, δ-seawater values should equal the metal:P ratios in plankton as well. Although the two values for Cd closely approach each other, the δ–seawater values for Cr,

Ni, Se, and V are slightly higher, and for Zn lower, than the mean element:P ratios in plankton. The δ–seawater value for Cu also resembles the Cu:P ratio in plankton, although it is 2.5 times higher than the ratio in plankton when the Cu concentration in bottom water (fig. 22) is used in the calculation, rather than the Cu concentration at 2,000-m depth (table 9).

Boyle and others (1977) explain the distribution of Cu in the deep ocean by a combination of biologic and nonbiologic processes; the nonbiologic processes involve scavenging of Cu throughout the water column by settling particles and recycling of Cu into bottom water from oxic pelagic sediment. These and other nonmetabolic processes might also explain the high δ-seawater values for Cr, Ni, Se, and V, but their marine chemistry has not been examined as thoroughly as that of Cu. Nonetheless, the similarities of the seawater depth profiles of many metals to those of NO_3^-, PO_4^{3-}, and $Si(OH)_4$, and the fact that their Δ-seawater values are within a factor of 3 to 4 of the average compositional ratios in plankton (fig. 21; table 9), suggest that the elemental composition of plankton approximates the average composition of marine organic detritus settling into the deep ocean. Owing to the coarseness of our sampling of the Phosphoria Formation, as discussed below, only the average trace-element values of plankton are likely germane to our study, and these should be the values best given by seawater profiles. As noted earlier, Ni seems to be the exception (table 9).

Nonbiologic processes, which likely influence the distributions of many metals in the deep ocean, might contribute much less to metal distributions in the shallower continental shelf and slope environments. This reduced influence is suggested by the Cu distribution. Its δ–seawater value, based only on the uppermost 2,000 m of seawater (1.1×10^{-3}), is very close to the Cu:P ratio in plankton (1.4×10^{-3}). The δ–seawater value based on the very bottom water is 3.5×10^{-3}.

The distributions of Mo, U, and REE in seawater are little influenced by the biologic cycle. Mo and U concentrations are constant with depth (Broecker and Peng, 1982; Collier, 1985; Emerson and Huested, 1991). Mo is mildly bioreactive (table 9), but its uptake by plankton in the photic zone and the remineralization of planktonic debris at depth by bacteria are simply insufficient to measurably affect the vertical distribution of Mo in the water column (fig. 22). The content of Mo in plankton is estimated at about 2 ppm, but the Mo concentration in seawater is 10 ppb (table 9). As a result, oxidation of organic matter at depth increases the Mo concentration above its surface-water value by less than 2 percent, somewhat less than the precision of the analyses (Collier, 1985). This result is analogous to our inability to detect the change in Ca^{2+} concentration (Broecker and Peng, 1982), forced by phytoplankton precipitation of $CaCO_3$ in the photic zone, for example, by coccolithophorids, and dissolution at depth.

U too is apparently non-bioreactive. Similar to Mo, it is conservative in seawater, but it could likewise have a concentration in plankton of up to 1 ppm that would be undetected from seawater profiles alone. The REE concentrations in seawater increase with depth and are relatively high in handpicked diatom tests (Elderfield and others, 1981). However, their seawater profiles can be explained largely in terms of nonbiologic processes (de Baar and others, 1985; Sholkovitz and others, 1994). Although such an explanation suggests that the REE contents are very low in silica, possibly similar to their contents in biogenic calcite (Palmer, 1985), the elevated values of even single analyses suggest nonetheless that the REEs are bioreactive at an as yet undetermined level.

We present the trace-element contents of plankton below as single, well-defined values that we consider to be the best averages, as suggested by Brumsack (1986). However, they certainly are not well defined nor likely to be single values. Nonetheless, the successful application of this approach to ancient rocks (Piper, 1991; Piper and Isaacs, 1995, 1996) lends support to the values recommended by Brumsack (1986).

The sampling scheme alone should average out large short-term excursions from the assumed values. The samples that were ground were approximately 2 to 3 cm cubes. At the accumulation rate of the Phosphoria Formation of 1.6 mg/cm^2 per year, a sample with this thickness represents approximately 2500 years of history.

Before considering the trace elements, we calculate the accumulation rate of PO_4^{3-} in the Phosphoria Formation, relative to the current extraction via photosynthesis of PO_4^{3-} from the photic zone of the ocean. The duration of deposition for the Meade Peak Phosphatic Shale Member of the Phosphoria Formation (fig. 3), based on the conodont and brachiopod zones of Wardlaw and Collinson (1986)

and the time scale of Harland and others (1990), was approximately 7.2 my. The amount of P_2O_5 in the Meade Peak Member, at Enoch Valley, is estimated at 1370 gr P_2O_5 per cm^2 (table 5), giving a mean accumulation rate for P_2O_5 of 0.19 mg/cm^2 per year. Assuming a composition for settling organic matter which equaled that of modern plankton, the rate of accumulation of organic matter necessary to deliver P_2O_5 to the Phosphoria Sea floor would have been approximately 8 to 11 mg/cm^2 per year.

We can compare this accumulation rate with that for organic matter on the Peru Shelf, an environment often invoked as the modern analog to the Phosphoria Basin, owing to a sediment composition (Burnett and Froelich, 1988) similar to that of the Meade Peak Phosphatic Shale Member (McKelvey and others, 1959). Primary productivity of organic matter on this shelf is approximately 200 mg/cm^2 per year (Chavez and Barber, 1987), perhaps the highest rate of any region in the oceans today (Berger and others, 1988). Of this amount, approximately 15 to 45 percent settles out of the photic zone (Dugdale and Goering, 1970; Von Bockel, 1981). This amount greatly exceeds the required value for the Phosphoria Formation of 8 to 11 mg/cm^2 per year, suggesting that primary productivity in the Phosphoria Basin may have been significantly lower. Within the California Current, primary productivity averages approximately 75 mg organic matter/cm^2 per year (Eppley and others, 1986). Although its survival to approximately 4000-m depth is only about one to two percent (Baldwin and others, 1998), a great deal more, in the range of 10 to 20 percent, can be expected to survive to a few hundred meters depth (Sarnthein and others, 1988).

A lower level of primary productivity than along the coast of Peru is explained by the distribution of productivity in the oceans today (Berger and others, 1988). There and elsewhere along the continental margins of the oceans, the intensity of upwelling of nutrient enriched water from approximately 75 to 150-m depth, and thus the intensity of primary productivity, is driven by the intensity of the great ocean currents that sweep the shelves. No such currents are present in ocean-margin basins and there is no reason to suppose they were present in Permian time in the Phosphoria Basin. Primary productivity is in the range of 100 mg organic matter/cm^2 per year, or approximately one half that on the open shelf of the Peru margin.

In the Gulf of California, the flux of organic matter at 500-m depth averages approximately 20 mg organic matter/cm^2 per year, or 6.9 mg organic carbon/cm^2 per year (Thunell, 1998). Although a slightly higher value might be expected for the shallower Phosphoria Basin, the value for this modern ocean margin basin, nonetheless, is much closer to the above calculation than is the estimate for the open shelf along the coast of Peru.

The above calculation for the Phosphoria Basin ignores any loss of P_2O_5 during early diagenesis, which would, of course, require a higher rain rate of organic matter to the sea floor, perhaps at times as high as that of Peru Shelf (Chavez and Barber, 1987) or the very coastal waters of the Venezuela Shelf (Verela and others, 1997). Could the rate of primary productivity in the photic zone have an upper limit, past and present, that is represented by current primary productivity on the Peru Shelf? The depth of the photic zone on the Peru Shelf today is approximately 30 m (L.A. Codispoti, oral commun., 1992), limited by the high content of particulate organic matter in the water. Higher productivity would yield more organic matter within any volume of water in the photic zone, but limit even more the depth to the base of the photic zone. As this depth decreases relative to that of the mixed layer, phytoplankton growth per area of sea surface must decrease, owing largely to mixing below the photic zone. At some photic-zone depth versus mixed-layer depth, mixing will carry phytoplankton into the aphotic zone at a rate that must limit total productivity and the flux of organic matter to the sea floor. A second boundary condition is a photic zone equal to the mixing depth, or to the depth of the sea floor. Both the Phosphoria Sea and the Peru Shelf might have achieved a self-limiting maximum productivity of organic matter, approaching 200 mg/cm^2 per year. Whatever the exact level of primary productivity was in Permian time, it was surely moderate to high and it remained at that level for the phenomenal period of time of about 7.2 my, possibly increasing occasionally to this inferred maximum if indeed it is a maximum.

The ratio of the depth of the photic zone to that of the mixed layer likely influence other aspects of the flux of organic matter to the sea floor. For example, the loss of organic matter as the fecal debris of

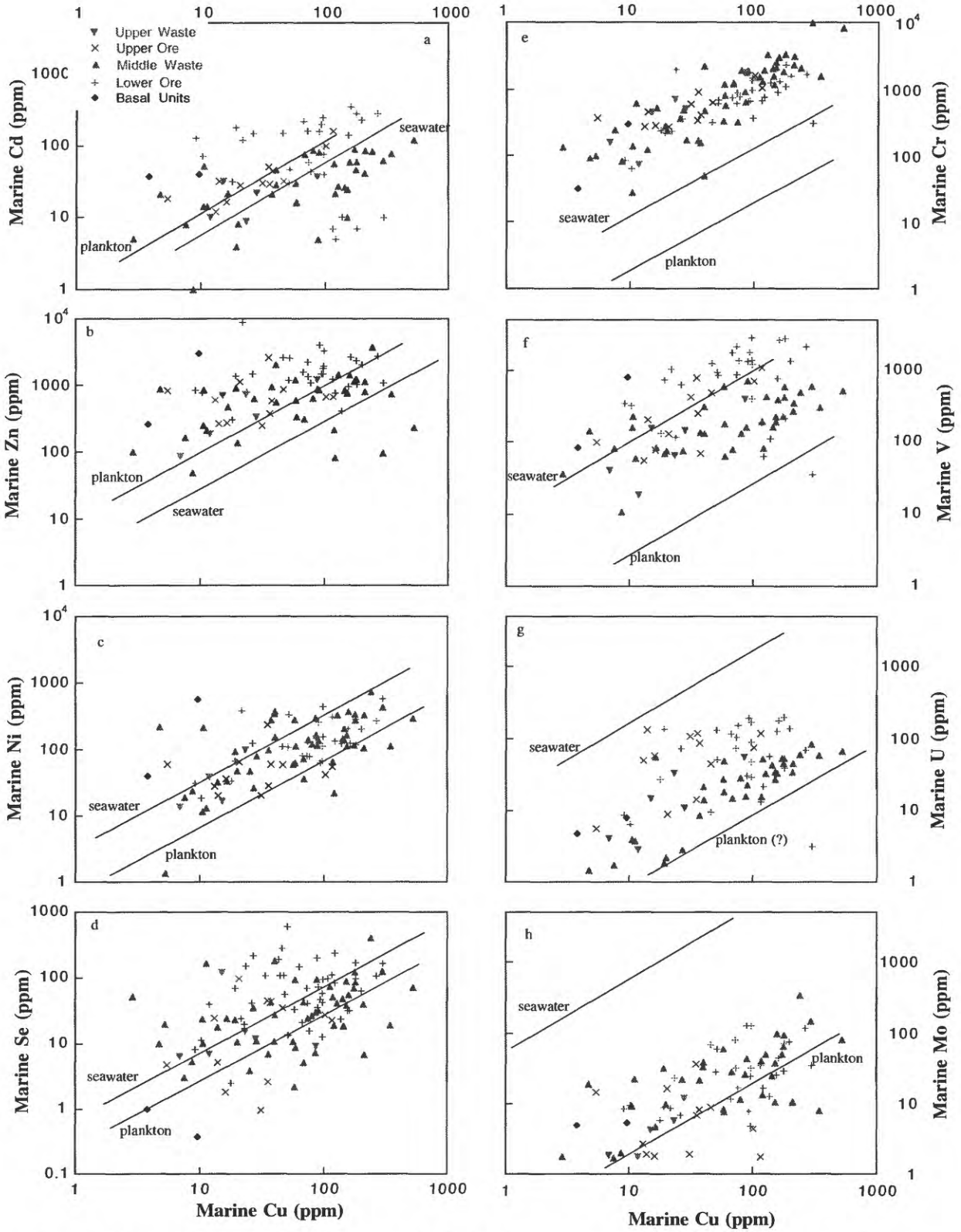

Figure 23. Relation between concentrations of Cu and of other trace elements. Note different y-axes scales. Plankton ratios of Cu:Cd and Cu:Zn are larger than their seawater ratios; the reverse is the case of all other trace elements. Ratios for seawater and plankton are given in table 9 and here projected into the sediment field.

grazing zooplankton, relative to the loss of phytoplankton from the aphotic zone through mortality, might decrease with a decrease in the above ratio. We can only speculate how the loss of phytoplankton via mortality versus via grazing (Grimm and others, 1996) might influence the overall flux and composition of accumulating organic matter. Our assumption is that the two different loss terms will not change significantly the trace-element composition of the organic matter accumulating on the sea floor.

It seems likely that the high intensity of the current system along the Peru Shelf (Arthur and others, 1998) further contributes to the complex mineralogy (Piper and others, 1988) and texture (Glenn and Arthur, 1988) of this deposit, as noted above. By contrast the texture and composition of the deposit that accumulated in the central part of the Phosphoria Basin suggest a quieter environment, in support of the interpretation of a less intense current regime, lower upwelling, and lower primary productivity. The pellets contain no pyrite or glauconite, commonly have a uniform texture; and are not associated with large, massive nodules and pavements.

The trace-element contribution by organic matter (planktonic debris) raining onto the sea floor can be evaluated in the same way as for P_2O_5. If the average marine Cu content in the Phosphoria Formation is 82 ppm (table 4) and the stoichiometry of accumulating organic matter was the same as that of modern plankton (table 9), then the accumulation rate of organic matter required to deliver Cu to the sea floor was 12 mg/cm^2 per year. Calculations based on the marine Mo and Zn contents (fig. 16) give rates of 23 and 15 mg/cm^2 per year, respectively. Cd requires a slightly lower rate of 8 mg/cm^2 per year. All of these values seem close enough to the value calculated for P_2O_5 to suggest that organic matter was the sole source for these trace elements.

The accumulation rate of organic matter required to deliver Ni to the sea floor is approximately 30 mg/cm^2 per year, or 3.5 times higher than that based on the contents of P_2O_5 and Cd. A somewhat higher rate was also obtained for the Monterey Formation, a phosphatic formation of Miocene age (Piper and Isaacs, 1995). The δ–seawater[Ni] value suggests that the Ni content of organic matter is 5 times higher than our stoichiometric model allows (table 9), which could account for the higher accumulation rate observed. But it seems very unlikely that the mean Ni content of plankton could be even as high as 15

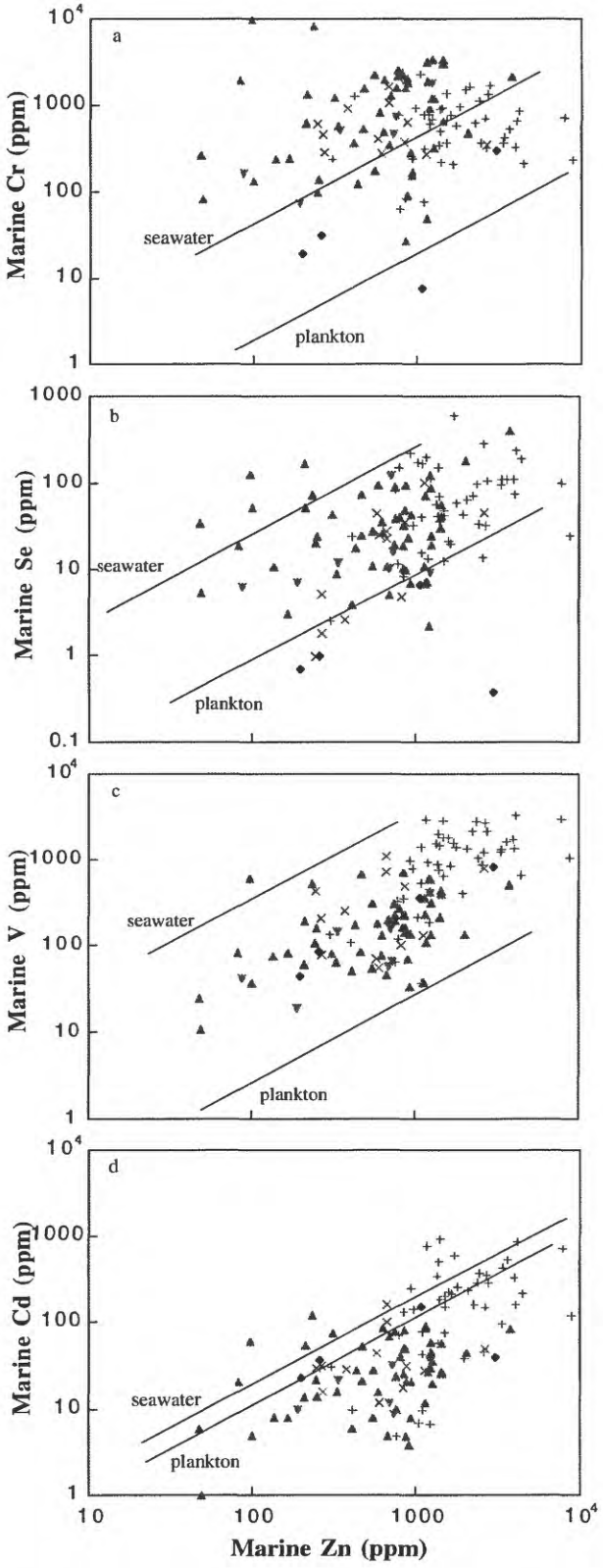

Figure 24. Relation between concentrations of Zn and selected trace elements. See Figure 23 for identification of symbols.

ppm without such high contents having been commonly observed (fig. 21) in plankton (Martin and Knauer, 1973, Collier and Edmond, 1984).

The alternative approach to examining the contribution of trace elements from organic matter is provided by ratios of the trace elements (fig. 23 and 24). The major reason for this approach is the similarity in the marine geochemistry of several of the trace elements. They should precipitate as sulfides (Jacobs and others, 1985, 1987; Landing and Lewis, 1991) and should be similarly retained in the sediment during and after early diagenesis as metal sulfides, or incorporated into organic matter. Phosphate, in contrast, is retained as carbonate fluorapatite (Burnett and others, 1988; Froelich and others, 1988). This difference could result in fractionation between PO_4^{3-} and the trace elements during diagenesis and weathering, and explain the absence of any correlation between apatite and the bioreactive trace elements (tables 7 and 8). The trace elements, however, should be less fractionated from each other, possibly allowing for a comparison between the interelement ratios in rocks, plankton, and seawater through simple x-y plots.

A second reason to consider trace-element ratios is that sediment-accumulation rates are seldom or poorly known. It might be argued that they are too poorly known even for the Phosphoria Formation to permit an evaluation of rates of primary productivity, as I did above. The agreement between the different calculations, however, suggests otherwise. The trace-element plots should permit a precise estimate of elemental contributions by the biogenic fraction and identify any possible hydrogenous fractions. This procedure is aided when the trace elements exhibit strong interelement correlations. Such plots will clearly show those elements that are enriched above a biogenic contribution.

This procedure points up the desirability of a single master element that defines the marine organic source, as Al_2O_3 defines the detrital source. In this discussion, we consider Cu and Zn as master elements for the marine biogenic (planktonic) fraction. Several aspects of their chemistry recommend them.

1. The contents of Cu and Zn in plankton (table 9) exceed those of most other trace elements (Martin and Knauer, 1973; Broecker and Peng, 1982; Bruland, 1983; Collier and Edmond, 1984; Brumsack, 1986), and so their biogenic signals might be strongly imprinted in rocks that initially had a high content of organic matter.

2. Although both accumulate in oxic sediment in strong association with Mn (Piper, 1988), they precipitate virtually completely from seawater under seawater sulfate-reducing conditions as a sulfide (Jacobs and others, 1985). However, their absolute concentrations in seawater should make the biogenic input greater than or, at worst, approximately equal to the hydrogenous input of many sedimentary deposits. If we assume redox and advection conditions similar to those in the Cariaco Trench (Jacobs and others, 1987) and a Cu concentration in seawater advecting into the basin equal to that in seawater at 2,000-m depth (table 9), then the accumulation rate for Cu that could precipitate as a sulfide is approximately 0.1 $\mu g/cm^2$ per year. Its accumulation rate in the biogenic fraction, estimated from the flux of organic matter to the seafloor of the Cariaco Basin (Thunell and others, 1997) is slightly greater, or approximately 0.22 $\mu g/cm^2$ per year. For Zn, the difference is even greater.

3. Cu and Zn should be retained in organic-matter-enriched sediment. The current organic-matter content of the Phosphoria Formation (Medrano and Piper, 1992) is high in terms of sedimentary rocks, even though it represents a small percent of the original rain rate of approximately 8 to 15 mg/cm^2 per year, or about 95 percent of the bulk sediment. It is considerably less than the organic-matter content of surface and near-surface sediment accumulating currently on the Peru Shelf, but it likely exceeded Peru Shelf concentration values at the time of deposition, owing to the vastly different rates of accumulation of terrigenous debris between these two environments, as considered above. A high accumulation rate for organic-matter allows sulfate reduction in the pore water to extend to or near the surface, as on the Peru Shelf (Froelich and others, 1988). A result of its degredation is a strongly negative $\delta^{13}C$ gradient in the uppermost few centimeters of sediment (Glenn and Arthur, 1988) as measured in the CO_3^{2-} of carbonate fluorapatite samples from the Phosphoria Formation (Piper and Kolodny, 1988). Cu and Zn should be retained under sulfate-reducing conditions, owing to the low solubility of Cu_2S, or CuS, and ZnS and reflected by their precipitation under natural seawater sulfate-reducing

conditions (Jacobs and others, 1985). They are quickly recycled into the overlying water under oxic pore-water conditions (Boyle and others, 1977; Fischer and others, 1986).

4. The marine fractions of Cu and Zn correlate with the marine fractions of several other trace elements in the Phosphoria Formation (table 8; fig. 23), allowing a rather precise comparison of trace-element ratios in the Phosphoria Formation with those in different modern marine phases through the use of x-y plots. The absence of such correlations does not preclude the use of this approach, inasmuch as the strength of present correlations should depend, perhaps, more on the composition of host, authigenic phases than on the composition of original source phases. In conclusion, plots of the trace elements with Zn give the same result as the plots with Cu (for example Cr). Thus, the interpretation presented here is not dependent on the distribution of a single element.

If the sole source of these trace elements was organic matter, then a projection of the interelement ratio of any pair of trace elements in plankton should extend into the field of trace-element concentrations in the Phosphoria Formation. Plots of Mo and Zn versus Cu (fig. 23) reinforce the calculations of their accumulation rates. The samples plot along the Cu versus trace-element curve of plankton. In the cases of Cd, Ni, and Se, the data scatter such as to preclude any firm conclusion, but the relation between Zn and Cd (fig. 24) supports the interpretation of a planktonic source. Thus, the conclusion from this exercise is that primary productivity in the photic zone provided the dominant marine fractions of Cd, Cu, Mo, and Zn to the floor of the Phosphoria Sea. The relation between Cu and Ni is more complex; Ni simply needs to be examined more closely than is possible with mere bulk chemical analyses, as presented in this study.

Accumulation within biogenic silica and $CaCO_3$, in addition to organic matter, might account for some of the displacement of these trace-element ratios away from the plankton value. The enrichment of Zn in biogenic silica (table 9) is supported by the similarity of the distribution of Zn in seawater (fig. 22) to that of $Si(OH)_4$ (Sclater and others, 1976). Analyses of biogenic silica (Martin and Knauer, 1973), however, show that Cu is equally enriched in this phase to that of Zn; it has a Zn:Cu ratio of about 1.0 (table 9). Accumulation of this phase on the sea floor, then, followed by its dissolution and the retention of Cu and Zn could not explain the shift in the Zn:Cu ratio away from the ratio in plankton (figure 23). The Zn:Cu ratios in the Monterey Formation of California suggested that biogenic silica could have supplied a major part of trace elements to the sediment (Piper and Isaacs, 1995). This mechanism might, however, contribute to the low Cd:Cu ratios. A Ni content in biogenic silica needed to explain the shift in the Ni:Cu ratio (figure 23) would seem to be much higher than we might expect. The behavior of Ni during early diagenesis seems only to add to its problem. It is apparently remobilized under O_2-depleted pore-water conditions (Shaw and others, 1990). The strong enrichment of Ni in these rocks, thus must remain enigmatic until its distribution in the terrigenous fraction and biogenic phases is more fully evaluated.

Invoking biogenic silica to explain the accumulation of trace elements in the Phosphoria Formation, unfortunately, has a major draw back. Certainly, biogenic silica constitutes an important part of the Phosphoria Formation and is the dominant fraction of the Rex Chert Member (table 5). However, the origin of the silica is spicules of siliceous sponges, i.e., consumers. In Tertiary rocks, such as the Monterey Formation, the origin of the silica is the siliceous tests of algae (diatoms), i.e., primary producers of organic matter. Even though the composition of the two forms of silica might be similar, which is certainly debatable, the accumulation rate of any consumer, or part therefrom, must be no more than perhaps one tenth that of a primary producer. Thus, the importance of silica as a source of trace elements in the Phosphoria Formation is greatly diminished over its possible importance in sedimentary deposits such as the Monterey Formation.

In the case of Cr:Cu and V:Cu ratios and possibly U:Cu and Se:Cu ratios, the offset away from the values for plankton are too great to be attributed solely to biogenic phases. The strong enrichments of Cr and V, particularly, require them to have had a hydrogenous source, in addition to a biogenic source and, of course, a minor detrital source.

Hydrogenous Source

Three mechanisms have been invoked by geochemists to account for the accumulation of trace elements in marine sediment directly from seawater. One mechanism involves equilibrium thermodynamics, first treated in depth by Krauskopf (1956) and

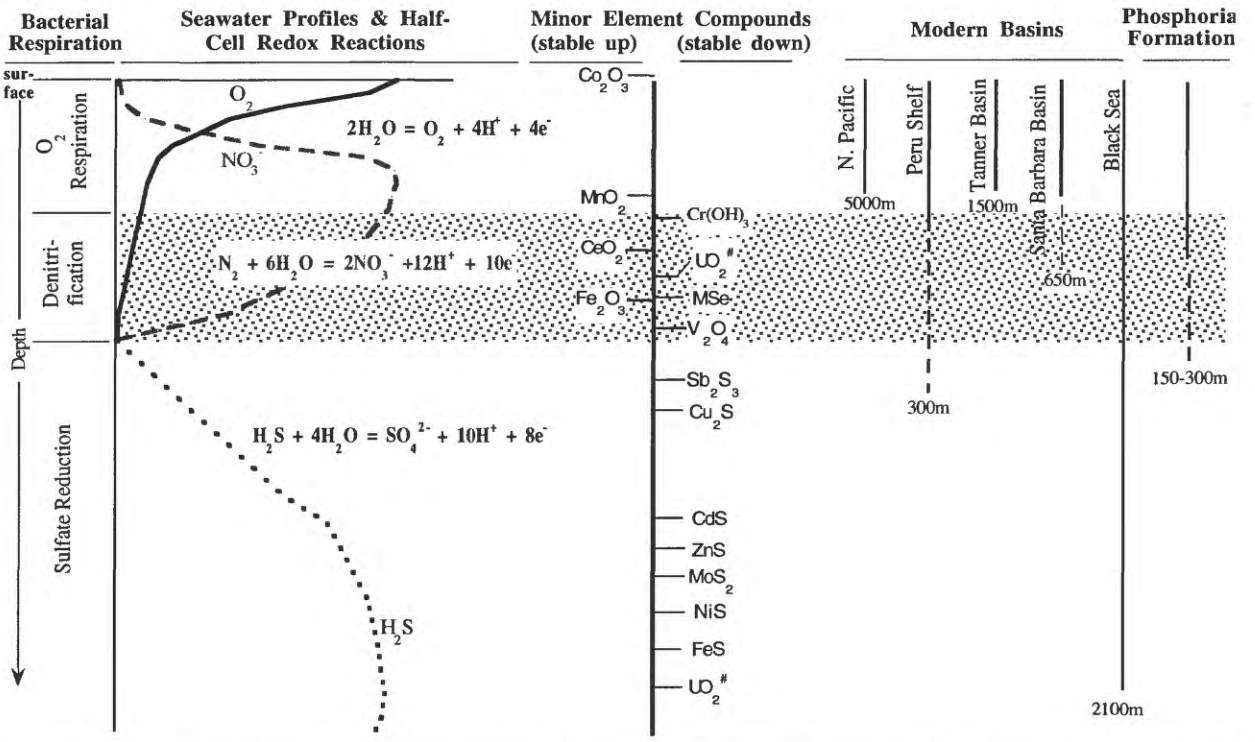

Figure 25. Schematic representation of bacterial respiration versus depth in water column of modern and ancient marine basins. Changes in O_2, NO_3^-, and H_2S concentration with depth are representative of Saanich Inlet, British Columbia (Emerson and others, 1979), along with half-cell reduction reactions for the three electron acceptors. Stabilities of trace-element compounds are also shown, calculated from thermodynamic constants (table 10). In the case of Cr, it precipitates or is adsorbed onto settling particles under conditions of mild denitrification, possibly as $Cr(OH)_3$, which is then stable under more reducing conditions. That is, it is stable throughout O_2-depleted regions. Under oxic conditions, Cr is in a more oxidized and soluble CrO_4^{2-} valence state (Murray and others, 1983). MnO_2 responds oppositely; it is reduced to a soluble valence state (probably Mn^{2+}) under increasingly reducing conditions. Approximate range of the three major types of bacterial respiration in modern basins is shown at far right, along with my interpretation of the Phosphoria Formation; solid lines show permanent and broken lines transient water-column conditions. Depth of each basin is listed below the column that gives the range of these conditions.

Garrels and Christ (1965). The second mechanism, proposed by Goldberg (1954) to explain incorporation of seawater-undersaturated trace elements into the inorganic phases of pelagic sediment, promotes seawater scavenging throughout the water column by both organic and inorganic particulate matter. The third mechanism proposed is diffusion of trace elements across the benthic boundary layer (Brumsack 1986; Francois, 1988; Klinkhammer and Palmer, 1991; Crusius and others, 1996).

The actual mechanism for removal of minor elements from the bottom water (precipitation from bottom water, adsorption onto settling particles, diffusion across the benthic boundary) is likely different for the different minor elements. Adsorption-diffusion reactions within the benthic boundary layer have been advocated as the most important mechanism for the accumulation of Mo, Cr, and V in modern, O_2-depleted marine environments (Brumsack, 1986; Francois, 1988; Pedersen and others, 1989; Emerson and Huested, 1991) and the distribution of H_2S in the water column (Broenkow, 1972; Fanning and Pilson, 1972). Whatever the mechanisms are for the removal of trace elements from bottom water, however, the important point is that their accumulation reflects the chemistry of the bottom water (Piper, 1994; Piper and Isaacs, 1995 and 1996; Helz and others, 1995; Dean and others, 1999), specifically the level of O_2 or its depletion, more so, or rather than the chemistry of sediment pore water.

The low REE, Cr, and V contents in organic matter (table 9) and their relatively high contents in

Enoch Valley rocks (figs. 19, 23, and 24) require that these elements had a hydrogenous marine source, in addition to their detrital and biogenic sources. Before accounting for these high values, I examine the geochemical properties of seawater under which trace elements in the modern ocean accumulate through inorganic processes. Their transfer from seawater to sediment under varying redox conditions is driven by the bacterial oxidation of organic matter, for which the three major electron acceptors are O_2, NO_3^-, and SO_4^{2-}. The major seawater redox reactions can be written as follows:

(3) O_2 respiration: $10CH_2O + 10O_2 + 10CaCO_3 = 20HCO_3^- + 10Ca^{2+}$

(4) Denitrification: $10CH_2O + 8NO_3^- + 2CaCO_3 = 4N_2 + 12HCO_3^- + 4H_2O + 2Ca^{2+}$

[5] SO_4^{2-} reduction: $10CH_2O + 5SO_4^{2-} + 5CaCO_3 = 5HS^- + 15HCO_3^- + 5Ca^{2+}$.

The formula for organic matter is better represented by the following formula:

$$(CH_2O)_{106}(NH_3)_{15}H_3PO_4(\text{trace elements})_{0.0x}.$$

The hierarchy of these three reactions is determined by the reaction yielding the greatest free energy (Froelich and others, 1979). Thus, reaction one proceeds until O_2 decreases to a concentration such that denitrification yields equal free energy, and so on.

Within several ocean-margin basins, advection is weak enough and the flux of settling organic matter great enough to allow depletion of successive electron acceptors with depth in the water column (Richards, 1975; Emerson and others, 1979). These basins include the Gulfo Dulce (Costa Rica), Baltic Sea, Black Sea, Cariaco Trench (Venezuela Shelf), and several fjords at high latitudes. Concentration profiles of O_2, NO_3^-, and H_2S (fig. 25) show that O_2 is abundant in the surface mixed layer, owing to mixing with atmospheric O_2 and to photosynthesis, but it decreases in the water column below the mixed layer, in response to oxygen respiration, predominantly by bacteria. The O_2 concentration is low at intermediate depth (Emerson and others, 1979), the depth interval over which NO_3^- concentrations decreases in response to denitrification. O_2 and NO_3^- are virtually absent in bottom water, that is, in the presence of H_2S under conditions of sulfate reduction (equation 5). Sulfate reduction continues into the sediment until SO_4^{2-} is depleted in the pore water, at which depth the residual labile organic matter is broken down through methanogenesis and fermentation reactions (equations not shown). In the Santa Barbara Basin (California Continental Borderland) and Darwin Bay (Galápagos Islands), bacterial respiration in the bottom water does not proceed beyond denitrification (Richards and Broenkow, 1971; Sholkovitz and Gieskes, 1971).

By contrast, the deep ocean exhibits oxygen respiration throughout. Denitrification occurs at intermediate depth in the oxygen-minimum zone (OMZ), but only along the Peru and Mexico Shelves in the eastern Pacific Ocean (Codispoti, 1980) and at a few other localities of limited areal extent in the Atlantic Ocean (Calvert and Price, 1971) and the Indian Ocean. Although the OMZ is present at intermediate depth throughout most of the oceans, only in these relatively small areas is the balance between advection in the OMZ and organic-matter productivity in the photic zone such that bacterial oxidation of settling organic matter drives down the O_2 content within the OMZ of the water column to a value that promotes and maintains denitrification.

On a cruise to the Peru Shelf in 1976, low H_2S concentrations were measured in the OMZ (Dugdale and others, 1977), indicating that sulfate-reducing conditions may occur in the OMZ of the open ocean, at least briefly. The existence of such conditions is easily understood. The maximum O_2, NO_3^-, and SO_4^{2-} concentrations in seawater are approximately 0.36, 0.04, and 28 mM, respectively. From equations 3 through 5, NO_3^- has only about 15 percent the oxidizing potential of O_2 and only 0.1 percent that of SO_4^{2-}. NO_3^- should be relatively quickly utilized once O_2 is depleted, pushing bacterial respiration into the field of sulfate reduction. It is perhaps surprising that H_2S has not been detected in the OMZ of the open ocean more often.

Trace species that act as electron acceptors include Cu^{2+}, CrO_4^{2-}, $Fe(OH)_3$, MnO_2, MoO_4^{2-}, SeO_4^{2-}, SeO_3^{2-}, $UO_2(CO_3)_2^{2-}$ (and, probably, $UO_2(CO_3)_3^{4-}$), and VO_4^{2-}. Their reduction can be calculated from Nernst equations and ordered according to Eh (table 10), where the half-cell reaction representing the oxidation of organic matter

(6) $CH_2O + H_2O = CO_2 + 4H^+ + 4e^-$

has been omitted. If this half-cell is included, as was done in equations 3 through 5, Fe(III) reduction, as an example, can be written in the following form:

Table 10. Half-cell reactions assuming standard-state conditions, as discussed in Piper and Isaacs [1995a] and Piper and Medrano [1994]. Selenium, as a selenide, might precipitate as a metal (MSe), although it is listed here as a soluble phase. The master half-cell reactions for drainage ground water are likely those three written in bold print.

Eh	Half-cell reactions	å#	Seawater concentration in moles/kg, or partial pressure	Ref.*
1.099	$3Co^{2+}(aq) + 4H_2O(l) \rightarrow Co_3O_4(s) + 2e^- + 8H^+(aq)$	6	$Co^{2+} = 2.04 \times 10^{-11}$	1, 2
0.805	$\mathbf{2H_2O(l) \rightarrow O_2(g) + 4e^- + 4H^+(aq)}$	--	$\mathbf{O_2 = 0.2\ atm}$	**3**
0.704	$Mn^{2+}(aq) + 2H_2O(l) \rightarrow MnO_2(s) + 2e^- + 4H^+(aq)$	6	$Mn^{2+} = 2.5 \times 10^{-10}$	3, 4
0.702	$I^-(aq) + 3H_2O(l) \rightarrow IO_3^-(aq) + 6e^- + 6H^+(aq)$	3 4	$I^- = 5.0 \times 10^{-9}$, $IO_3^- = 4.5 \times 10^{-7}$	1, 3
0.698	$\mathbf{N_2(g) + 6H_2O(l) \rightarrow 2NO_3^-(aq) + 10e^- + 12H^+(aq)}$	**3**	$\mathbf{N_2(g) = 0.8\ atm}$, $\mathbf{NO_3^- = 3.9 \times 10^{-5}}$	**3, 5**
0.545	$Cr(OH)_3(s) + H_2O(l) \rightarrow CrO_4^{2-}(aq) + 3e^- + 5H^+(aq)$	4	$CrO_4^{2-} = 4.04 \times 10^{-9}$	2, 6, 7
0.448	$SeO_3^{2-}(aq) + H_2O(l) \rightarrow SeO_4^{2-}(aq) + 2e^- + 2H^+(aq)$	4 4	$\Sigma Se = 2.22 \times 10^{-9}$, $SeO_3^{2-} = 0.92 \times 10^{-9}$	3, 8, 9
0.320	$Ce^{3+}(aq) + 2H_2O(l) \rightarrow CeO_2(s) + 1e^- + 4H^+(aq)$	9	$Ce^{3+} = 1.0 \times 10^{-11}$	3, 10
0.296	$Fe^{2+}(aq) + 3H_2O(l) \rightarrow Fe(OH)_3(s) + 1e^- + 3H^+(aq)$	6	$Fe^{2+} = 1.20 \times 10^{-9}$	3, 4
0.013	$UO_2(s) + 2HCO_3^-(aq) \rightarrow UO_2(CO_3)_2^{2-}(aq) + 2e^- + 2H^+(aq)$	4.5 4.5	$HCO_3^- = 2.47 \times 10^{-3}$, $UO_2(CO_3)_2^{2-} = 1.26 \times 10^{-8}$	3, 5, 11
0.025	$HSe^-(aq) + 3H_2O(l) \rightarrow SeO_3^{2-}(aq) + 6e^- + 7H^+(aq)$	3.5 4	$\Sigma Se = 2.22 \times 10^{-9}$, $SeO_3^{2-} = 1.11 \times 10^{-9}$	8
-0.018	$2Fe^{2+}(aq) + 3H_2O(l) \rightarrow Fe_2O_3(s) + 2e^- + 6H^+(aq)$	6	See above	3, 4
-0.040	$V_2O_4(s) + 4H_2O(l) \rightarrow 2H_2VO_4^-(aq) + 2e^- + 4H^+(aq)$	5.6	$H_2VO_4^- = 4.0 \times 10^{-8}$	2, 12
-0.055	$\mathbf{HS^-(aq) + 4H_2O(l) \rightarrow SO_4^{2-}(aq) + 8e^- + 9H^+(aq)}$	**3.5** **4**	$\mathbf{HS^- = 7.75 \times 10^{-25}}$, $\mathbf{SO_4^{2-} = 2.8 \times 10^{-2}}$	**3, 5**
-0.055	$Cu_2S(s) + 4H_2O(l) \rightarrow SO_4^{2-}(aq) + 2Cu^+(aq) + 8e^- + 8H^+(aq)$	4 2.5	$SO_4^{2-} = 2.8 \times 10^{-2}$, $Cu^+ = 3.59 \times 10^{-9}$	1, 3, 13
-0.137	$CdS(s) + 4H_2O(l) \rightarrow SO_4^{2-}(aq) + Cd^{2+}(aq) + 8e^- + 8H^+(aq)$	4 6	$SO_4^{2-} = 2.8 \times 10^{-2}$, $Cd^{2+} = 6.94 \times 10^{-10}$	1, 3, 5, 14
-0.162	$ZnS(s) + 4H_2O(l) \rightarrow SO_4^{2-}(aq) + Zn^{2+}(aq) + 8e^- + 8H^+(aq)$	4 6	$SO_4^{2-} = 2.8 \times 10^{-2}$, $Zn^{2+} = 5.97 \times 10^{-9}$	1, 3, 5
-0.175	$MoS2(s) + 12H_2O(l) \rightarrow MoO_4^{2-}(aq) + 18e^- + 2SO_4^{2-}(aq) + 24H^+(aq)$	4.5 4	$MoO_4^{2-} = 1.1 \times 10^{-7}$, $SO_4^{2-} = 2.8 \times 10^{-2}$	3, 15, 16
-0.188	$NiS(s) + 4H_2O(l) \rightarrow SO_4^{2-}(aq) + Ni^{2+}(aq) + 8e^- + 8H^+(aq)$	4 6	$SO_4^{2-} = 2.8 \times 10^{-2}$, $Ni^{2+} = 8.01 \times 10^{-9}$	1, 3, 5, 13
-0.209	$FeS(s) + 4H_2O(l) \rightarrow SO_4^{2-}(aq) + Fe^{2+}(aq) + 8e^- + 8H^+(aq)$	4 6	$SO_4^{2-} = 2.8 \times 10^{-2}$, $Fe^{2+} = 1.20 \times 10^{-9}$	1, 3, 5, 13
-0.210	$UO_2(s) + 3HCO_3^-(aq) \rightarrow UO_2(CO_3)_3^{4-}(aq) + 2e^- + 3H^+$	4.5 5.5	$HCO_3^- = 2.47 \times 10^{-3}$, $UO_2(CO_3)_3^{4-} = 1.26 \times 10^{-8}$	1, 3, 4

Values of å, the effective ionic diameter used in the Debye-Hückel equation, are listed in the order of their appearance in the chemical equation.

* References: 1-Bruland (1983); 2-Latimer (1953); 3-Wagman and others (1982); 4-Landing and Bruland (1987); 5-Broecker and Peng (1982); 6-Murray and others (1983); 7-Elderfield (1970); 8- Measures and others (1983); 9-Cutter and Bruland (1984); 10-DeBaar and others (1985); 11-Langmuir (1978); 12-Collier (1984); 13-Jacobs and others (1985); 14-Boyle and others (1976); 15-Collier (1985); 16-Emerson and Huested (1991).

(7) $10CH_2O + 40Fe(OH)_3 + 60HCO_3^- + 70Ca^{2+} = 70CaCO_3 + 40Fe^{2+}\ 100H_2O$

Its reduction occurs before sulfate reduction (table 10, fig. 25) and toward the end of denitrification (Berner, 1980; Bender and others, 1989); CrO_4^{2-} and SeO_3^{2-} /SeO_4^{2-} also are reduced under conditions of denitrification (table 10; Measures and others, 1980; Murray and others, 1983), and particulate Ce^{4+} is reduced to a soluble +3 valence state (de Baar and others, 1985, 1988).

The trace-element contents of inorganic particulate phases in seawater reflect these redox conditions. Under conditions of oxygen respiration, inorganic precipitates consist mostly of Fe and Mn oxyhydroxides (Landing and Bruland, 1987). Other trace elements are undersaturated in oxic seawater, except for Ce, but high concentrations of several trace elements in deep-ocean ferromanganese nodules indicate that a small fraction coprecipitates with the Fe and Mn oxide phases (Goldberg, 1963a; Piper, 1988) or is scavenged by these oxides (Goldberg, 1954; Balistrieri and others, 1981; Li, 1981; Clegg and Sarmiento, 1989). Pelagic sediment, however, remains a minor sink for most metals, except Mn (Lyle and others, 1984). Their high metal contents in this environment merely reflect low bulk-sediment accumulation rates rather than high metal accumulation rates, somewhat analogous to the importance of a low bulk-sediment accumulation rate to the composition of the Phosphoria Formation.

Within basins that exhibit sulfate reduction in bottom water (fig. 24), Fe^{2+}, Cu^{+}, Cd^{2+}, and Zn^{2+} precipitate as sulfides, CrO_4^{2-} is reduced and precipitates as $Cr(OH)_3$ (Brewer and Spencer, 1974; Emerson and others, 1979; Jacobs and others, 1985, 1987), and VO_4^{2-} may be reduced to V_2O_3 or, possibly, some form of $V(OH)_3$ (Wanty and Goldhaber, 1992). Mo and U also are removed from the bottom water (Bruland, 1983; Anderson and others, 1989; Emerson and Huested, 1991). Although this environment is limited in areal extent, it represents an important sink for several elements in the ocean today (Kolodny and Kaplan, 1970; Bertine and Turekian, 1973; Cutter, 1982; Jacobs and others, 1987; Haraldsson and Westerlund, 1988; Emerson and Huested, 1991; Klinkhammer and Palmer, 1991).

The much higher concentration of Mo in open-ocean seawater relative to the other trace elements (table 9) and its low content in detrital phases and organic matter (tables 6 and 9) make it *the* diagnostic trace element for identifying rocks that accumulated in a sulfate-reducing environment (table 10; fig. 25). Its distribution in modern sediment of the Cariaco Trench (Jacobs and others, 1987; Dean and others, 1999) and the Black Sea (Calvert, 1990) supports this conclusion. Its modest enrichment in the Phosphoria Formation, above a biogenic source (fig. 23), would seem to preclude accumulation of this deposit under sulfate-reducing conditions.

Of the elements that accumulate under the intermediate redox conditions of denitrification, U, V, Cr, and possibly Se should have the highest concentrations in sediment, although there are possible problems with V and U. The absence of a clear signal of U reduction and precipitation in the water column under denitrifying conditions (Anderson and others, 1989a and b) makes its distribution in sedimentary deposits possibly less diagnostic of bottom-water conditions than that of other trace elements. Its pos-

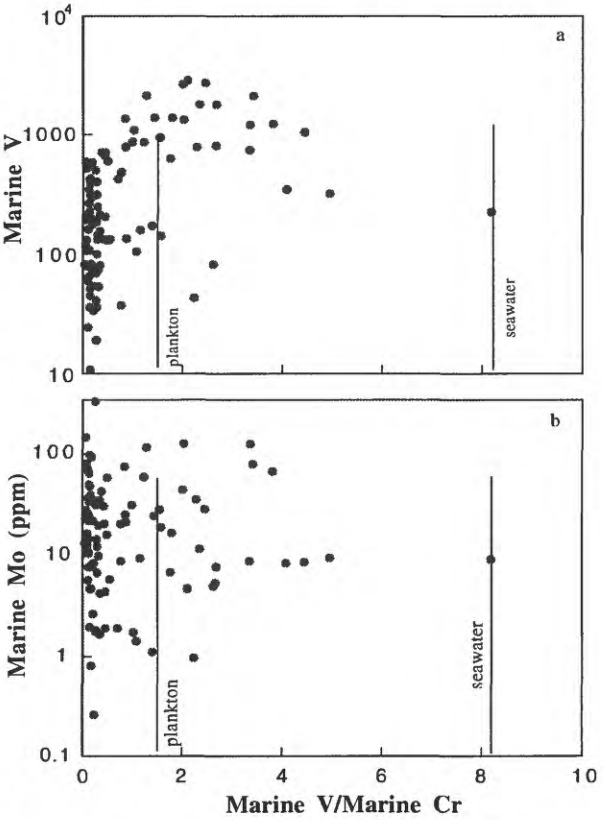

Figure 26. Relation between marine V:Cr ratio and (a) V and between the marine V:Cr ratio and (b) Mo. V:Cr ratios for seawater and plankton are also shown. Units below the "false cap" contribute all but two of the V:Cr ratios greater than the ratio of plankton. Sample P-195 is not plotted.

possible occurrence as $UO_2(CO_3)_3^{4-}$ (Goldberg, 1963b; Anderson and others, 1989a), instead of, or as well as, $UO_2(CO_3)_2^{2-}$ (Langmuir, 1978), may account for this; $UO_2(CO_3)_3^{4-}$ should be reduced well into the zone of sulfate reduction (Eh = -0.21v), rather than in the zone of denitrification.

The accumulation of V should occur near the NO_3^-/SO_4^{2-}-reduction boundary, which is defined by the precipitation of the least soluble trace-element sulfide (Cu_2S) under consideration. A slight error in either the V or Cu half-cell reactions could push the precipitation of V into the zone of sulfate reduction, although the close association of V with Cr in several phosphate deposits (Piper, 1991; Piper and Isaacs, 1995 , 1996) indicates initial precipitation in the less reducing environment. In this deposit, the V:Cr ratio increases with the increase in V concentration (fig. 26), just as one might expect given the order of their precipitation under increasingly negative Eh conditions. The ratio does not approach the seawater valued as it does in black shale deposits, which also have a strong hydrogenous Mo fraction (Piper, 1994). Indeed, the absence of a clear relation between V:Cr ratios and Mo concentrations (fig. 26) further suggests the absence of sulfate reduction in the water column.

The REEs have a still different distribution in O_2-depleted seawater environments that further defines bottom-water redox conditions. They maintain their 3+ valence state throughout the marine environment, except for Ce, which is oxidized to the 4+ valence state under denitrifying conditions (table 10, fig. 25). Within the zone of denitrification in the Cariaco Trench and the Black Sea, immediately above the zone of sulfate reduction (Hashimoto and others, 1983; Codispoti and others, 1991), the 3+ valence-state REE (La, Pr, Nd, and Sm) show concentration minima (de Baar and others, 1988; German and others, 1991; Schijf and others, 1991). In both basins, their concentrations increase sharply at greater depth, toward the NO_3^-/SO_4^{2-}-reduction interface and into the sulfate-reducing water. Within the zone of denitrification in the OMZ in the eastern Pacific Ocean, the concentrations of the 3+ valence-state REEs also show minima. They are apparently scavenged by particulate phases, most likely oxyhydroxides of Mn (German and others, 1993) or Fe (Sholkovitz, 1993), under mildly denitrifying conditions and released to solution under sulfate-reducing conditions. The carrier phase in the zone of denitrification in the OMZ of the eastern Pacific Ocean is unlikely a Mn phase. The concentration of dissolved Mn shows a maximum, whereas those of the REEs show minima (Klinkhammer and Bender, 1980; de Baar and others, 1985; German and others, 1991). Thus, the mechanism whereby the 3+ valence-state REEs are transferred to the sea floor within the hydrogenous fraction remains problematic, but the oxic-to-denitrifying redox conditions under which their removal to the sediment occurs are well established. The important point here is that sulfate-reducing conditions would have prevented their accumulation on the sea floor altogether.

Ce is somewhat more complex than the other REEs. Its occurrence as insoluble $Ce(OH)_4$ under oxic-to-denitrifying conditions (table 10) accounts for the negative Ce anomaly of seawater and positive anomaly of open-ocean hydrogenous particulate phases (Sholkovitz and others, 1994). Its reduction to the 3+ valence state under more reducing conditions has been proposed to account for the increase in Ce concentration and the more positive Ce anomaly in the OMZ of the eastern Pacific Ocean and the Cariaco Trench (de Baar and others, 1988).

In the Black Sea, however, the trend of the Ce anomaly is different (German and others, 1991; Schijf and others, 1991); the dissolved Ce concentration in the zone of denitrification decreases to a minimum, as does the anomaly. This trend parallels those of the 3+ valence-state REEs, which mirror the maximum concentration of particulate Mn. All the REEs are scavenged in the upper part of the zone of denitrification, Ce more so than the other REEs. The difference in the distribution of the Ce anomaly between the Black Sea and the Cariaco Trench places an unfortunate constraint on the uniqueness of the Ce anomaly in unraveling the geochemistry of ancient sediment (Wright and others, 1987). However, the apparent invariance of the Ce anomaly in the apatite component in this deposit (figs. 10 and 11), the dominant host phase for the REE, further suggests that the Ce anomaly may not be a sensitive indicator of redox conditions (German and others, 1991), beyond a negative value precluding accumulation under sulfate reduction within the water column.

Certainly, the other trace elements in the ocean also fail to behave in an easily predictable way, requiring caution in the acceptance of my interpretation of their distributions in ancient rocks. Reference was made above to U, for example, indicating that it may

be present in seawater as $UO_2(CO_3)_2^{2-}$ and $UO_2(CO_3)_3^{4-}$ (Langmuir, 1978). Its distribution in the Black Sea (Anderson and others, 1989a) supports its reduction only under conditions of sulfate reduction, indicating that the complex $UO_2(CO_3)_3^{4-}$ is the stable seawater species, and its reduction apparently occurs within the sediment pore water, not within the water column. Similarly, V should be reduced under strongly denitrifying conditions (figure 25), but its distribution in several basins that exhibit O_2-depletion in bottom water (Emerson and Huested, 1991) suggests it is reduced under sulfate reducing conditions. Several explanations might be advanced to account for the apparent non-ideal behavior of these and other trace elements. For example, the calculations of stable species (table 10) are limited to those for which equilibrium constants are available; these may not necessarily be the species that actually control trace-element solubilities. Second, the effects of complexation (Kremling, 1983; Jacobs and others, 1985; Landing and Lewis, 1991) have not been evaluated. And third, diffusion across the benthic boundary layer has not been evaluated and included. To better define trace-element behaviors, particularly under denitrifying conditions, this environment in the modern environment, in the absence of sulfate reduction in the water column, should be examined for the full suite of trace elements in both the bottom water, particulate phases, and surface sediment.

Trace-element scavenging by seawater particulate phases (Balistrieri and others, 1981; Li, 1981; Whitfield and Turner, 1987), although offering an alternative mechanism for removal of trace elements from seawater, likely is complicated by the geochemically complex water columns as those in basins which exhibit O_2 depletion in bottom water. Nonetheless, the results of research into metallic-ion adsorption under oxic conditions clearly identify the importance of scavenging for many trace elements. Of the trace elements I have examined here, Zn and Cu should have been strongly scavenged and Ni and Cd less so (Clegg and Sarmiento, 1989; Balistrieri and Murray, 1984). Thus, hydrolytic scavenging should enrich Zn over Ni and Cd, owing to the greater tendency for Zn to be adsorbed onto particulate matter. Unfortunately, the opposite seems to be the case for the Phosphoria Formation. Also, the distributions of Zn, Ni, and Cd in the marine fraction of sediment of the Gulf of California (Brumsack, 1986) seem to reflect a strong, possibly solely, biogenic input, suggesting that scavenging is a minor process under continental-shelf conditions of moderate to high primary productivity and O_2 depletion in the water column. Thus, my interpretation of the accumulation of the full suite of trace elements within organic matter and biogenic silica, both of which must have been in large part lost from the sediment during diagenesis, in contrast to the trace elements which were retained, still seems to best explain interelement relation between Cd, Cu, Mo, Ni, and Zn in the Phosphoria Formation.

Despite the complex behavior of trace elements in the marine environment, I have attempted to generalize their relative accumulation rates for a continental-shelf area of moderate-to-high primary productivity (figure 27), under the different seawater-redox conditions. Obviously, the figure should be considered with some caution, because the elemental contribution by any single source changes with primary productivity, water depth, bulk-sediment-accumulation rate, and residence time of the bottom water, to name but four factors. Also, scavenging and diffusion are not included as major mechanisms of trace-element enrichment, except for REEs. The flux of a hydrogenous fraction of trace elements to the sea floor (fig. 27), then is low under oxic conditions, except for Mn and Fe, with REE exhibiting a widely varying, but commonly positive, Ce anomaly; the hydrogenous flux is virtually zero for Mn and high for REEs (negative Ce anomaly), Cr, and V under denitrifying conditions; and it is zero for Mn and REEs and high for Cr, V, Mo, Se, Fe, Cu, Cd, and Zn under sulfate-reducing conditions. Although Fe precipitates as a sulfide under sulfate-reducing conditions, detection of a hydrogenous fraction is hampered by large detrital and organic supplies, even under conditions of the low bulk-sediment-accumulation rates of the Phosphoria Formation.

Thus, the oceanographic and (or) thermodynamic properties of trace elements require bottom-water conditions of denitrification to explain the much greater enrichments of Cr , V, and the REE, and possibly Se and U, in the Phosphoria Formation than that of other trace elements, particularly Mo, but also Cd, Cu, and Zn. The enrichments of Cr and V occur by precipitation as oxyhydroxides and (or) adsorption onto particulate phases within seawater, and perhaps less so by diffusion across the benthic boundary layer. Diffusion might explain the slight enrichments of Mo and U above a biogenic contribution, but we cannot dismiss the possibility of brief periods of

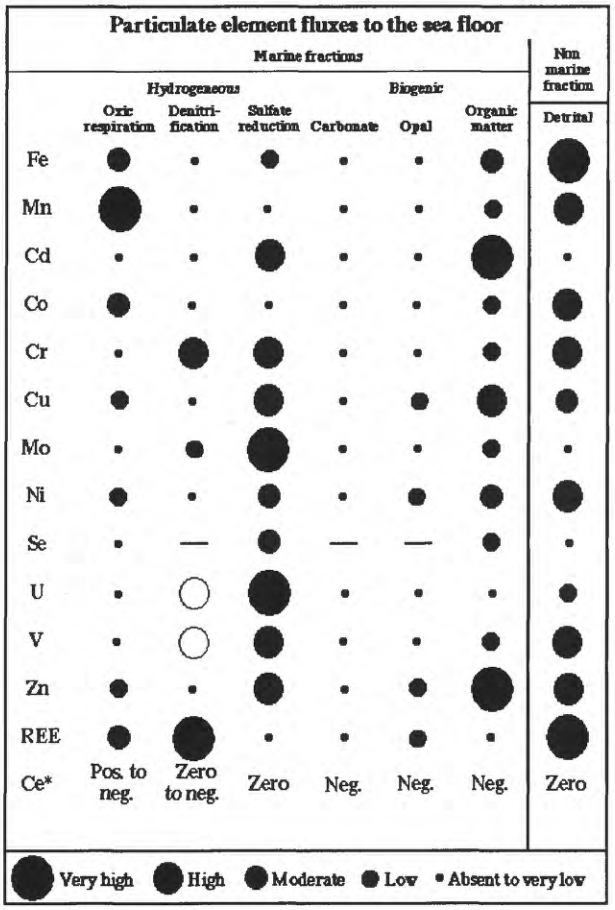

Figure 27. Generalized summary of elemental accumulations in marine sediment on a continental shelf, or basin (water depth 200 to 500 m), under conditions of moderate to high primary productivity in the photic zone, for which seawater sources (hydrogenous and biogenic) are not masked by detrital sources (terrigenous). Chart should be read across, rather than down; for example, the dominant sediment source of Cd under conditions of such primary productivity is organic matter. Under conditions of sulfate reduction in bottom water, as well as under conditions of moderate to high primary productivity in the photic zone, Cd also accumulates as an inorganic precipitate, possibly CdS; its accumulation inorganically under bottom-water conditions of denitrification or oxic respiration is minor, as is its accumulation with the detrital fraction of sediment under all condition. Sizes of circles in any one column are unrelated; open circles are used in those cases for which theoretical predictions do not seem to be supported by observations of modern environments. Ce*, the Ce anomaly, is defined in Figure 10. Dashes represent no available information.

sulfate reduction in the bottom water, as occurs on the Peru Shelf (Dugdale and others, 1977) to account for these enrichments. A simple calculation, similar to that made for Mo in early Quaternary sediment from the Sea of Japan (Piper and Isaacs, 1996), however, limits sulfate-reducing conditions in the bottom water considered here to have been less than 1 percent of the time.

Again, I should point out that each sample represents several thousand years of deposition. As a result, a sample may contain an association of trace elements that thermodynamics and geochemical signals of the modern marine environment do not allow, for example, the co-occurrence of Mo and the REEs, both in excess of biological and detrital inputs.

Establishment of denitrification in the bottom water constrains bottom-water advection. If we assume that the denitrifying part of the water column was 250 m thick and that approximately 25 percent of surface productivity was oxidized in the bottom water, conditions somewhat similar to those on the Peru Shelf today, a residence time for the bottom water of approximately 5 years would be required to establish denitrification. Although this value will change by adjusting the various parameters, the instability of the water column of the present-day Santa Barbara Basin (Sholkovitz and Gieskes, 1971) clearly suggests a residence time in this modern, open-ocean, denitrifying basin on the order of years. This calculation applies to "bottom" waters, whether a basin environment or an open shelf environment is being considered.

The Cr content of the Phosphoria Formation also limits the residence time of the bottom water at the time of deposition. Assuming that (1) the thickness of denitrifying water was 250 m, as above; (2) the initial Cr concentration in the water advecting into the basin was 0.21 ppb (table 10), 25 percent of which was removed to the sea floor, the approximate maximum amount of Cr (III) in the OMZ of the eastern Pacific Ocean (Murray and others, 1983); (3) the average Cr content in the marine fraction of the Phosphoria Formation is 1000 ppm, over 90 percent of which accumulated as a hydrogenous fraction (table 6); and (4) the sediment-accumulation rate was 1.6 mg cm^{-2} per year; then the maximum residence time for bottom water in the basin is calculated at 2 to 3 years. This residence time is the residence time only for the time that water is within the OMZ itself, that is, within the denitrifying part of the water column,

not the full length of time since the water left the surface photic zone.

The low concentrations of trace elements in seawater severely limit their contributions to the actual oxidation of organic matter but contribute significantly to the sensitivity with which their contents in the marine fraction of sediment might record geochemical conditions in the water column. Let us consider Mo. Its concentration in seawater is approximately 10^{-7} M, or 1/400 that of NO_3^-. Clearly, it will contribute insignificantly to the oxidation of organic matter and, yet, it is the most abundant trace element in seawater. In order to demonstrate the relation between its accumulation and seawater redox, let us assume that the bottom-water of the Phosphoria Sea was sulfate reducing, neglecting for the moment the conditions necessary to bring about the depletion of O_2 and NO_3^- and the unlikelihood that those conditions were met. The Phosphoria Formation had an average bulk-sediment-accumulation rate of about 1.6 mg/cm^2 per year, 39 percent of which was a terrigenous fraction (Table 5). The detrital Mo accumulation rate was approximately 0.0016 μg/cm^2 per year. If primary productivity was about one half that on the Peru Shelf, as shown above, the Mo-accumulation rate within organic matter (that is, as planktonic debris) was 0.02 μg/cm^2 per year. Its approximate total rate was .03 to .05 μg/cm^2 per year.

Assuming that the residence time of bottom water was 5 years and only 5 percent of the Mo was removed from the bottom 100 m of the water column in the Phosphoria Basin, the hydrogenous Mo-accumulation rate would have been 1 μg/cm^2 per year. Such an accumulation rate requires the Mo content of the Phosphoria Formation to be, on average 600 ppm. Although a few samples exceed 100 ppm, the average is 24 ppm (table 4). We could change several factors to possibly reduce the accumulation rate. The residence time of the bottom water could be increased, but this would likely increase the percentage of Mo removed from bottom water (Piper and Isaacs, 1996) and the thickness of the sulfate-reducing water. Indeed, there seem to be feedback mechanisms that tend to counter most possible changes, other than increasing the mixing rate to preclude sulfate reduction altogether. Even though this calculation is simplistic, it again suggests that the bottom water of the Phosphoria Sea could not have been sulfate reducing for any significant period of time. The samples with highest Mo contents (fig. 26) suggest that bottom-water Eh might have slipped into the field of sulfate reduction, but only very briefly. Otherwise, a few samples would have shown an enrichment that pushed them close to the Cu-Mo relation of seawater, rather than all scattering about the value for plankton (fig. 23h), and the V:Cr ratios (fig. 26) would have shown a maximum at maximum Mo concentration (Piper, 1994), rather than scattering over the full range of Mo concentrations (fig. 26). Also, the REEs in samples most enriched in Mo would have been hosted in total by the detrital fraction. In actual fact, La and Mo exhibit a weak positive correlation (table 7).

These calculations of the accumulation of marine components on the sea floor demonstrate the dominance of primary productivity in the photic zone of the ocean and advection of the bottom water to trace-element accumulation on the sea floor. Examination of other sections of the formation, such as the Vanadiferous Zone (a discrete section within the Meade Peak Phosphatic Shale Member with an unusually high V content (Love, 1961; McKelvey and others, 1986), might show higher Mo contents and, thus evidence of sulfate reduction. In such sediment, the V:Cr ratio should increase toward its seawater value of 8.6 (table 9), as it does in some black shale deposits (Piper, 1994). There is no reason to expect the seawater properties that controlled the composition of sediment to have been constant throughout the basin and to have remained constant throughout the time of deposition.

Summary

The stoichiometric approach, clearly, is a simplified representation of a complex system. Froelich and others (1979, 1988), Bender and others (1989), Jahnke (1990), and Ingall and van Cappellen (1990) have examined the complex geochemistry of major nutrients during diagenesis, from oxygen respiration, through manganese reduction, denitrification, Fe(III) reduction, sulfate reduction, to methanogenesis. The behavior of trace elements during early diagenesis is equally complex (Shaw and others, 1990). As future research better defines the geochemistry of trace elements in the modern marine environment, this interpretation of trace-element distributions in sedimentary rocks strongly enriched in organic matter will surely require adjustment.

Even so, elemental concentrations at any one horizon should reflect the level of primary productivity, bottom-water residence time, and, of course, ac-

cumulation rate of the detrital fraction. Detailed information about the bulk sediment accumulation might permit the different parameters of the environment to be ascertained for separate intervals of the deposit. For example, V and Mo are high in the lower ore zone (fig. 20), suggesting that bottom water might have been more reducing during this period of time. Did an increase in bottom-water residence time allow for an increase in the intensity of reducing conditions; was primary productivity at a maximum, thus resulting in a maximum flux of organic matter into the bottom water and a maximum in the rate of bacterial respiration; or was dilution by the detrital fraction merely at a minimum? Distributions of the other trace elements fail to limit the explanation to a single scenario. In the future, improved dating and more detailed sampling of this formation might better allow one to isolate the influence of each factor.

Still, the interpretation of a dynamic environment of varying geochemistry is required by the distributions of the carbonate minerals—calcite and dolomite—with apatite (fig. 13a). The same exclusion of components was seen between the carbonate minerals and organic matter (fig. 15). These relations and the strong partitioning of trace elements into either apatite or organic matter (table 8) restrict the enrichment of most of the trace elements to sedimentary units with low carbonate contents. Virtually all of the trace elements have their lowest concentrations in the carbonate units (tables 2 and 4). There are several possible explanations but the most plausible seems to be a reduction in primary productivity during deposition of the carbonate-enriched units, possibly accompanied by an increase in bulk sediment accumulation rate. The former might allow for oxygen respiration throughout the water column and the latter for dilution within the sediment of other marine phases. Again detailed dating of the rocks could help to resolve the conditions of deposition for the different sediment facies.

CONCLUSIONS

The precision of the elemental-oxide and trace-element analyses of this study allows identification of (1) the current major host components of trace elements (detrital material, organic matter, apatite, biogenic silica, dolomite, calcite, and possibly trace-metal sulfides) and (2) the source phases of trace elements (detrital debris, marine biogenic matter, and marine hydrogenous phases) at the time of deposition. The interelement relations between the major oxides and several trace elements (for example, Al_2O_3 versus Th) approach those of the standard, WSA. These relations indicate that the detrital fraction is the sole host for several elements and that the fraction had a terrigenous source. The strength of these relations allows us to determine the detrital contribution of other trace elements (Cd, Cr, Cu, Mo, Ni, Se, U, Zn, and REEs) from the content of the detrital fraction in each sample alone, even though this latter group does not correlate with the detrital fraction.

The difference between the bulk content of trace elements and the detrital contribution to each sample represents the marine fraction of trace elements, that is, the contribution of seawater. The interelement relations between Cd, Cu, Mo, and Zn in this marine fraction of the rocks approximate those in modern plankton, suggesting that these trace elements and, possibly, Ni, had a predominantly biogenic source. During Phosphoria time, the rate of accumulation of organic matter on the sea floor at Enoch Valley necessary to provide these elements to the sediment was significantly less than the rate of accumulation of organic matter on the present-day Peru Continental Shelf, which has exceptionally intense coastal upwelling and high primary productivity in the photic zone, perhaps the highest in the ocean today. Perhaps a better modern analog for the level of primary productivity is the Gulf of California, in which the flux of organic matter at 500-m depth is only slightly greater than that necessary to supply metals to the sea floor as measured in the Phosphoria Formation. Thus, primary productivity in the Phosphoria Sea was probably only moderate to high, although it surely varied over a large range within the Phosphoria Basin and throughout the time of deposition. Such variation is strongly evidenced by essentially an exclusion of carbonate components with apatite- and organic-matter-enriched components.

The enrichments of Cr, V, REEs, and possibly Se and U, required accumulation directly from seawater, a hydrogenous input. On the basis of their chemical properties and distributions in O_2-depleted environments of the ocean today, the accumulation of this group of elements from seawater would have been enhanced by conditions of denitrification in the bottom water. The mean rate of accumulation of Cr and La in this fraction gives a residence time for bottom water in the basin of approximately 1 to 3 years. The relation between these two elements and V fur-

thermore suggests that the bottom water was more strongly denitrifying during deposition of the ore zones. By contrast, during much of the time of deposition of the carbonate-enriched units, the water column was very possibly oxic from the surface to the bottom.

Sulfate reduction was not established in the bottom water for any significant period of time. This interpretation is based on the preservation of a seawater-derived REE enrichment throughout the Phosphoria Formation and the absence of an enrichment of Cu, Cd, Zn, and, particularly, Mo above a biogenic input. Otherwise, this group would have accumulated from bottom water, in addition to accumulating in an organic fraction derived from the photic zone of the water column. A slight enrichment of Mo, particularly in the lower part of the section, suggests that sulfate reduction was possibly more important during deposition of this section of the formation, but again only for brief periods of time. Otherwise, the REEs would not have accumulated from seawater at all but would have had solely a terrigenous source. Sulfate reduction was probably restricted to the sediment pore water; it likely closely approached the benthic boundary layer, but did not extend into the water column.

The near absence of glauconite and pyrite in association with this pelletal deposit at Enoch Valley, and only a very weakly developed oolitic texture, contrasts with the texture of phosphatic pellets in the modern deposit on the Peru Shelf (Piper and others, 1988). Also, the pelletal deposit on the Peru Shelf is associated with phosphatic nodular crusts, nodules exceeding 10 cm in diameter, and pavements (Glenn and Arthur, 1988). One possible explanation for the contrasting textures between the modern and ancient deposit is the intensity of bottom currents, strong on the Peru Shelf (Arthur and others, 1998) and weak in the Phosphoria Basin (my interpretation). The result is a highly variable bottom-water and pore-water chemistry on the Peru Shelf, both temporally (Codispoti, 1980) and arealy (Froelich and others, 1988), and a proposed highly stable bottom-water and pore-water chemistry for the Phosphoria Basin.

No single environment in the ocean today represents a perfect analog of the Phosphoria Formation. Biologic processes were somewhat similar to those in the Gulf of California, as regards upwelling and primary productivity in the photic zone. They were significantly less than on the Peru Shelf, but denitrification, as established on the Peru Shelf, was the dominant form of bacterial respiration in the bottom water. Other differences between the Phosphoria Sea and the Peru Shelf environment include sea floor bathymetry, tectonism, and proximity to major ocean currents. The overall bathymetry and isolation from major ocean currents might be represented by the East China Sea, although the differences here too are noteworthy. The Phosphoria Shelf was situated on an eastern ocean boundary, not a western boundary. It was at much lower latitude (Sheldon, 1964), within the belt of the easterly trade winds. Low rainfall limited the influx of terrigenous debris. The low elevation of the landmass to the east and the vastness of the shelf further reduced the flux of otherwise diluting terrigenous debris, allowing accumulation of a marine-dominated deposit throughout the basin—evaporites along the coast and biogenic sediment within the basin. The Antler Uplift or a more westerly island arc, analogous to the Ryukyu Islands in the East China Sea, shielded the shelf from strong coastal currents, such as the Kuroshio Current, thus providing a relatively undisturbed depositional regime for the dominantly marine debris that settled out of the water column. The basin floor, itself, was probably rather featureless and, as Yochelson (1968) concluded from faunal evidence, likely had a maximum depth of only a few hundred meters. A trough oceanward of the shelf, analogous to the Okinawa Trough in the East China Sea, limited the flux of detritus from the west into the shallower phosphogenic area of the basin. Weak tectonic activity and strong easterlies further limited the input of volcanic debris. Because few formations compositionally equivalent to the Phosphoria Formation are present in the geologic record, these conditions of sea-floor morphology, seawater chemistry and biology, climate, provenance, and tectonism likely have seldom coexisted in the past and certainly do not today.

Under oxic conditions of surface and ground water, the current hosts of trace elements, rather than sources, will contribute to the behavior of the trace elements during subaerial weathering. Th is hosted by the detrital fraction. Ba, Ni, and As are hosted in large part by the detrital fraction, but significant portions of As and Ni are also present in the organic phases. The rare-earth elements and U are hosted mostly by the apatite phase. Ag, Cu, Cr, Mo, and Se are largely hosted by organic matter. Cd, V, and

Zn occur in an as yet undefined phase, which may also contain significant fractions of Ag, As, Cu, Mo, Ni, and U. It is tempting to attribute this phase to a sulfide, but we have no evidence of the presence of a sulfide, other than the presence of minor pyrite, and no evidence of partitioning of these elements in that phase.

The order of decomposition for the dominant host phases is probably

metal sulfides > organic matter > carbonates > apatite > chert > detrital debris.

Thus, we can expect elements hosted predominantly by metal sulfides and organic matter to be more readily released to ground water than those hosted by apatite. Those hosted by detritus, for example, Th, should be the least labile, or slowest released to ground water.

Profiles of the trace elements through the stratigraphic section show that many trace elements have highest concentrations in samples from the lower ore zone (As, Cd, Cu, Mo, Se, U, V, and Zn). Se and As also have high concentrations in the main waste zone as well; Cr has its highest concentrations in the waste zone. Trace elements that show little or no stratigraphic control include Ni and Pb. These distributions and the order of weathering will contribute to the availability of trace elements into ground and surface water. In the case of Se, both its distribution and partitioning enhance its introduction into ground and surface waters, and into the food web (Presser, 1994), owing to its strongly bioaccumulative properties.

ACKNOWLEDGMENTS

I am deeply grateful to the members of the staff at the Solutia mine for the help they gave me during the collection of samples and description of the section, and particularly R. Bolton. M. Medrano provided tremendous help in the field. G. Orris generously agreed to review the manuscript and offered many helpful and constructive suggestions.

REFERENCES CITED

Altschuler, Z.S., Berman, S., and Cuttitta, F., 1967, Rare earths in phosphorites--geochemistry and potential recovery: U.S. Geological Survey Professional Paper 575B, p. 1-9.

Anderson, R.F., Fleisher, M.Q., and LeHuray, A.P., 1989a, Concentration, oxidation state, and particle flux of uranium in the Black Sea: Geochimica et Cosmochimica Acta, v. 53, p. 2215-2224.

Anderson, R.F., LeHuray, A.P., Fleisher, M.Q., and Murray, J.W., 1989b, Uranium deposition in Saanich Inlet sediments, Vancouver Island: Geochimica et Cosmochimica, v. 53, p. 2205-2213.

Arbogast, B.F. (Ed.), 1990, Quality assurance manual for the Branch of Geochemistry, U.S. Geological Survey: U.S. Geological Survey Open-File Report 90-668, 184p.

Arthur, M.A., Dean, W.E., and Laarkamp, K., 1998, Organic carbon accumulation and preservation in surface sediments on the Peru margin: Chemical Geology, v. 152, p. 273-286.

Baedecker, P.A. (ed.), 1987, Methods for geochemical analysis: U.S. Geological Survey Bulletin 1770.

Baines, S.B., Pace, M.L., and Karl, D.M., 1994, Why does the relationship between sinking flux and planktonic primary productivity differ between lakes and oceans?: Limnology and Oceanography, v. 39, p. 213-226.

Baldwin, R.J., Glatts, R.C., Smith, K.L., Jr., 1998, Particulate matter fluxes to the benthic boundary layer at a long time-series station in the abyssal NE Pacific--composition and fluxes: Deep-Sea Research, v. 45, p. 643-665.

Balistrieri, L.S., Brewer, P.G., and Murray, J.W., 1981, Scavenging residence times of trace metals and surface chemistry of sinking particles in the deep ocean: Deep-Sea Research, v. 28, p. 101-121.

Balistrieri, L.S., and Murray, J.W., 1984, Marine scavenging: trace metal adsorption by interfacial sediment from MANOP Site H: Geochimica et Cosmochimica Acta, v. 48, p. 921-929.

Bender, Michael, Jahnke, Richard, Weiss, Ray, Martin, William, Heggie, D.T., Orchardo, Joseph, and Sowers, Todd, 1989, Organic carbon oxidation and benthic nitrogen and silica dynamics in San Clemente Basin--a continental borderland site: Geochimica et Cosmochimica Acta, v. 53, p. 685-697.

Berger, W.H., Fischer, K., Lai, C., and Wu, G., 1988, Ocean carbon flux: global maps of primary production and export production, *in* Agegian, C.R., ed., Biogeochemical cycling and fluxes

between the deep euphotic zone and other cceanic realms: NOAA Under Sea Research Program, Report 88-1, p. 131-176.

Bertine, K.K. and Turekian, K.K., 1973, Molybdenum in marine deposits: Geochimica et Cosmochimica Acta, v. 37, p. 1415-1434.

Bodkin, J.B., 1977, Determination of fluorine in silicates by use of an ion-selective electrode following fusion with lithium metaborate: The Analyst, v. 102, p.409-413.

Boyle, E.A., Sclater, F.R., and Edmond, J.M., 1976, On the marine geochemistry of cadmium: Nature, v. 263, p. 42-44.

Boyle, E.A., Sclater, F.R., and Edmond, J.M., 1977, The distribution of dissolved copper in the Pacific: Earth and Planetary Science Letters, v. 37, no. 1, p. 38-54.

Brewer, P.G., and Spencer, D.W., 1974, Distribution of some trace elements in Black Sea and their flux between dissolved and particulate phases, *in* Ross, D.A., and Degens, E.T., eds., The Black Sea--geology, chemistry, and biology: American Association of Petroleum Geologists Memoir 20, p. 137-143

Broecker, W.S., and Peng, T-H., 1982, Tracers in the sea: Palisades, N.Y., Eldigio Press, 690 p.

Bruland, K.W., 1983, Trace elements in sea-water: *in* Riley, J.P., and Chester, R. eds., Chemical oceanography, v. 8, p. 158-220.

Bruland, K.W., Donat, J.R., and Hutchins, D.A., 1991, Interactive influences of bioactive trace metals on biological production in oceanic waters: Limnology and Oceanography, v. 36, no. 8, p. 1555-1577.

Brumsack, H.J., 1983, A note on black shales and recent sediments from oxygen deficient environments, paleoceanographic implications, *in* Suess, Erwin, and Thiede, Jörn, eds., Coastal upwelling--its sediment record: New York, Plenum Press, p. 471-483.

Brumsack, H.J., 1986, The inorganic geochemistry of Cretaceous black shales (DSDP Leg 41) in comparison to modern upwelling sediments from the Gulf of California, *in* Summerhayes, C.P., and Shackleton, N.J., eds., North Atlantic paleoceanography: Geological Society of London Special Publication 21, p. 447-462.

Burnett, W.C., Baker, K.B., Chin, P.A., McCabe, William, and Ditchburn, Robert, 1988, Uranium-series and AMS ^{14}C studies of modern phosphate pellets from Peru shelf muds: Marine Geology, v. 80, p. 215-230.

Burnett, W.C., and Froelich, P.N., 1988, The origin of marine phosphorite--the results of the R/V Robert D. Conrad Cruise 23-06 to the Peru shelf: Marine Geology, v. 80, p. 181-343.

Calvert, S.E., 1990, Geochemistry and origin of the Holocene sapropel in the Black Sea, *in* Ittekkot, Venugopalan, Kempe, Stephan, Michaelis, Walter, and Spitzy, Alejandro, eds., Facets of modern biogeochemistry: Berlin, Springer-Verlag, p. 326-352.

Calvert, S.E., and Price, N.B., 1971, Upwelling and nutrient regeneration in the Benguela Current, October, 1968: Deep-Sea Research, v. 18, p. 505-523.

Calvert, S.E., and Price, N.B., 1983, Geochemistry of Namibian shelf sediments, *in* Suess, Erwin, and Thiede, Jörn, eds., Coastal upwelling, its sediment records: New York, Plenum, p. 337-375.

Chavez, F.P., and Barber, R.T., 1987, An estimate of new production in the equatorial Pacific: Deep-Sea Research, v. 34, p. 1229-1244.

Clayton, J.L., and Swetland, P.J., 1978, Subaerial weathering of sedimentary organic matter: Geochimica et Cosmochimica Acta, v. 42, p. 305-312.

Clayton, J.L., King, J.D., 1987, Effects of weathering on biological marker and aromatic hydrocarbon composition of organic matter in Phosphoria shale outcrop: Geochimica et Cosmochimica Acta, v. 51, p. 2153-2157.

Clegg, S.L., and Sarmiento, J.L., 1989, The hydrolytic scavenging of metal ions by marine particulate matter: Progress in Oceanography, v. 23, p. 1-21.

Coale, K.H., Johnson, K.S., Fitzwater, S.E., Blain, S.P.G., Stanton, T.P., and Coley, T.L., 1998, Iron ex-1, an in situ iron-enrichment experiment--experimental design, implementation and results: Deep-Sea Research, v. 45, p. 919-945.

Codispoti, L.A., 1980, Temporal nutrient variability in three different upwelling regimes, *in* Richards, F.A., ed., Coastal upwelling, v. 1 of Coastal and estuarine science: Washington, D.C., American Geophysical Union, p. 209-220.

Codispoti, L.A., 1989, Phosphorus vs. nitrogen limitation of new and export production, *in* Berger, W.H., Smetacek, V.S., and Wefer, Gerold, eds., Productivity of the oceans--present and past:

Chichester, U.K., John Wiley and Sons, p. 377-394.

Codispoti, L.A., Friederich, G.E., Murray, J.W., and Sakamoto, C.M., 1991, Chemical variability in the Black Sea--implications of continuous vertical profiles that penetrated the oxic/anoxic interface: Deep-Sea Research, v. 38, supp. 2, p. S691-S710.

Collier, R.W., 1984, Particulate and dissolved vanadium in the North Pacific Ocean: Nature, v. 309, p. 441-444.

Collier, R.W., 1985, Molybdenum in the northeast Pacific Ocean: Limnology and Oceanography, v. 30, p. 1351-1354.

Collier, R.W., and Edmond, J.M., 1984, The trace element chemistry of marine biogenic particulate matter: Progress in Oceanography, v. 13, p. 113-119.

Condit, D.D., 1924, Phosphate deposits in the Wind River Mountains near Lander, Wyoming: U.S. Geological Survey Bulletin 764.

Copin-Montegut, C., and, Copin-Montegut, G., 1983, Stoichiometry of carbon, nitrogen, and phosphorus in marine particulate matter, Deep-Sea Ressearch, Part A, v. 30, p. 31-46.

Coveney, R.M., Jr., and Glascock, M.D., 1989, A review of the origins of metal-rich Pennsylvanian black shales, central U.S.A., with an inferred role for basinal brines: Applied Geochemistry, v. 4, p. 347-367.

Cremer, M.J., Klock, P.R., Neil, S.T., and Riviello, J.M., 1984, Chemical methods for analysis of rocks and minerals: U.S. Geological Survey Open-File Report 84-565, 148p.

Crusius, J., Calvert, S., Pedersen, T., and Sage, D., 1996, Rhenium and molybdenum enrichments in sediments as indicators of oxic, suboxic, and sulfidic conditions of deposition: Earth Planetary Science Letters, v. 145, 65-78, 1996.

Cutter, G.A., 1982, Selenium in reducing waters: Science: v. 217, no. 4562, p. 829-831.

Cutter, G.A., and Bruland, K.W., 1984, The marine biogeochemistry of selenium--a re-evaluation: Limnology and Oceanography, v. 29, p. 1179-1192.

Dean, W.E., Jr., Gardner, J.V., and Piper, D.Z., 1995, Inorganic geochemical indicators of glacial-interglacial changes in productivity and anoxia on the California continental margin: Geochimica et Cosmochimica Acta, v. 61, p. 4507-4518.

Dean, W.E., Jr., Piper, D. Z., and Peterson, L. C., 1998, Distribution of Mo in Cariaco basin sediment--a record of climate change 0 to 20,000 years: Geology (In Press).

de Baar, H.J.W., Bacon, M.P., Brewer, P.G., and Bruland, K.W., 1985, Rare earth elements in the Pacific and Atlantic Oceans: Geochimica et Cosmochimica Acta, v. 4, p. 1943-1959.

de Baar, H.J.W., German, C.R., Elderfield, Henry, and van Gaans, Pauline, 1988, Rare earth element distributions in anoxic waters of the Cariaco Trench: Geochimica et Cosmochimica Acta, v. 52, p. 1203-1219.

Desborough, G., DeWitt, E., Jones, J., Meier, A., and Meeker, G., 1999, Preliminary mineralogical and chemical studies related to the potential mobility of selenium and associated elements in Phosphoria Formation strata, southeastern Idaho: U.S. Geological Survey Open-File Report 99-129, 20p.

Douglas, G.S., Mills, G.L., and Quinn, J.G., 1986, Organic copper and chromium complexes in the interstitial waters of Narragansett Bay sediments: Marine Chemistry, v. 19, p. 161-174.

Dugdale, R.C., and Goering, J.J., 1970, Nutrient limitation and the path of nitrogen in Peru Current production: Anton Bruun Reports, v. 5, p. 3-8.

Dugdale, R.C., Goering, J.J., Barber, R.T., Smith, R.L., and Packard, T.T, 1977, Denitrification and hydrogen sulfide in the Peru upwelling region during 1976: Deep-Sea Research, v. 24, p. 601-608.

Eisler, Ronald, 1981, Trace metal concentrations in marine organisms: New York, Pergamon, 687p.

Elderfield, H., 1970, Chromium speciation in sea water: Earth and Planetary Science Letters, v. 9, p. 10-16.

Elderfield, Henry, Hawkesworth, C.J., Greaves, M.J. and Calvert, S.E., 1981, Rare earth element geochemistry of oceanic ferromanganese nodules and associated sediments: Geochimica et Cosmochimica Acta, v. 45, p. 513-528.

Emerson, S.R., Cranston, R.E., and Liss, P.S., 1979, Redox species in a reducing fjord--equilibrium and kinetic observations: Deep-Sea Research, v. 26, p. 859-878.

Emerson, S.R. and Huested, S.S., 1991, Ocean anoxia and the concentrations of molybdenum and

vanadium in seawater: Marine Chemistry, v. 34, p. 177-196.

Eppley, R.W., and Holm-Hansen, O. 1986, Primary production in the Southern California Bight, *in* Eppley, R.W., ed., Plankton dynamics of the southern California Bight: New York, Springer-Verlag, p. 176-215.

Fischer, Kathleen, Dymond, Jack, Lyle, Mitchell, Soutar, Andrew, and Rau, Susan, 1986, The benthic cycle of copper--evidence from sediment trap experiments in the eastern tropical North Pacific Ocean: Geochimica et Cosmochimica Acta, v. 50, p. 1535-1543.

Fisher, N.S., and Wente, M., 1993, The release of trace elements by dying marine phytoplankton: Deep-Sea Research, v. 40, p. 671-694.

Francois, Roger, 1988, A study on the regulation of the concentrations of some trace metals (Rb, Sr, Zn, Pb, Cu, V, Cr, Ni, Mn and Mo) in Saanich Inlet sediments, British Columbia, Canada: Marine Geology, v. 83, p. 285-308.

Froelich, P.N., Arthur, M.A., Burnett, W.C., Deakin, M., Hensley, V., Jahnke, Richard, Kaul, L., Kim, Kee Hyun, Roe, K., Soutar, Andrew, and Vathakanon, C., 1988, Early diagenesis of organic matter Peru continental margin sediments--phosphorite precipitation: Marine Geology, v. 80, p. 309-343.

Froelich, P.N., Klinkhammer, G.P., Bender, M.L., Luedtke, N.A., Heath, G.R., Cullen, Doug, and Dauphin, Paul, Hammond, Doug, Hartman, Blayne, and Maynard, Val, 1979, Early oxidation of organic matter in pelagic sediments of the eastern equatorial Atlantic--suboxic diagenesis: Geochimica et Cosmochimica Acta, v. 43, no. 7, p. 1075-1090.

Garrels, R.M., and Christ, C.L., 1965, Solution, minerals, and equilibia: New York, Harper and Row, 450 p.

German, C.R., Holliday, B.P., and Elderfield, Henry, 1991, Redox cycling of rare earth elements in the suboxic zone of the Black Sea: Geochimica et Cosmochimica Acta, v. 55, p. 3553-3558.

German, C.R., Holliday, B.P., and Elderfield, Henry, 1993, Reply to the comment by E.R. Sholkovitz on "recycling of rare earth elements in the suboxic zone of the Black Sea": Geochimica et Cosmochimica Acta, v. 56, p. 4309-4313.

Glenn, C.R., and Arthur, M.A., 1988, Petrology and major element geochemistry of Peru margin phosphorites and associated diagenetic minerals--authigenesis in modern organic-rich sediments: Marine Geology, v. 80, p. 231-267.

Goldberg, E.D., 1954, Chemical scavengers of the sea: Journal of Geology, v. 62, p. 249-265.

Goldberg, E.D., 1963a, Mineralogy and chemistry of marine sedimentation, *in* Shepard, F.P., Submarine geology: New York, Harper and Row, p. 436-466.

Goldberg, E.D., 1963b, The oceans as a chemical system, *in* Hill, M.N., ed., The composition of seawater; comparative and descriptive oceanography, v. 2 of The sea--ideas and observations on progress in the study of the sea: New York, Wiley-Interscience, p. 3-25.

Goldhaber, M.B., and Kaplan, I.R., 1974, The sulfur cycle, *in* Goldberg, E.D., ed., Marine chemistry, v. 5 of The Sea--ideas and observations on progress in the study of the seas: New York, Wiley-Interscience, p. 569-655.

Grimm, K.A., Lange, C,B., and Gill, A.S., 1996, Biological forcing of hemipelagic sedimentary laminae-evidence from ODP site 893, Santa Barbara Basin, California: Journal of Sedimentary Research, v. 66, p. 613-624.

Gromet, P.L., Dymek, R.F., Haskin, L.A., and Korotev, R.L., 1984, The "North American shale composite"--its compilation, major and trace element characteristics: Geochimica et Cosmochimica Acta, v. 48, p 2469-2482.

Gulbrandsen, R.A., 1960, Petrology of the Meade Peak phosphatic shale member of the Phosphoria Formation at Coal Canyon, Wyoming: U.S. Geological Survey Bulletin 1111-C, p 71-146.

Gulbrandsen, R.A., 1966, Composition of phosphorites of the Phosphoria Formation: Geochimica et Cosmochimica Acta, v. 30, p. 769-778.

Gulbrandsen, R.A., 1970, Relation of carbon dioxide content of apatite of the Phosphoria Formation to regional facies: U.S. Geological Survey Professional Paper 700-B, p. B9-B13.

Haraldsson, Conny, and Westerlund, Stig, 1988, Trace metals in the water column of the Black Sea and Framvaren Fjord: Marine Chemistry, v. 23, p. 417-424.

Harland, W.B., Armstrong, R.L., Cox, A.V., Craig, L.E., Smith, A.G., and Smith D.G., 1990, A geologic time scale: Cambridge, U.K., Cambridge University Press, 266p.

Hashimoto, L.K., Kaplan, W.A., Wofsy, S.C., and McElroy, M.B., 1983, Transformation of fixed nitrogen and N_2O in the Cariaco Trench: Deep-Sea Research, v. 30, no. 6, p. 575-590.

Haskin, M.A., and Haskin, L.A., 1966, Rare earths in European shales--a redetermination: Science, v. 154, p. 507-509.

Helz, G.R., Miller, C.V., Charnock, J.M., Mosselmans, J.F.W., Patrick, R.A.D., Garner, C.D., and Vaughan, D.J., 1996, Mechanism of molybdenum removal from the sea and its concentration in black shales: EXAFS evidence, Geochimica et Cosmochimica Acta, v. 60, p. 3631-3642.

Ingall, E.D., and Van Cappellen, Philippe, 1990, Relation between sedimentation rate and burial of organic phosphorus and organic carbon in marine sediments: Geochimica et Cosmochimica Acta, v. 54, p. 373-386.

Isaacs, C.M., 1980, Diagenesis in the Monterey Formation examined laterally along the coast near Santa Barbara, California: Stanford University, California, Ph.D. thesis, 329 p. [U.S. Geological Survey Open-File Report 80-606].

Jackson, L.L, Brown, F.W., and Neil, S.T., 1987, Major and minor elements requiring individual determination, classical whole rock analysis, and rapid rock analysis, *in* Baedecker, P.A., ed., Methods of geochemical analysis: U.S. Geological Survey Bulletin 1770, p. G1-G23.

Jacobs, Lucinda, Emerson, S.R., and Skei, Jens, 1985, Partitioning and transport of metals across the O_2/H_2S interface in a permanently anoxic basin, Framvaren Fjord, Norway: Geochimica et Cosmochimica Acta, v. 49, p. 1433-1444.

Jacobs, Lucinda, Emerson, S.R., and Huested, S.S., 1987, Trace metal chemistry in the Cariaco Trench: Deep-Sea Research, v. 34, no. 5-6A, p. 965-981.

Jahnke, R.A., 1990, Early diagenesis and recycling of biogenic debris at the sea floor--Santa Monica Basin, California: Journal of Marine Research, v. 48, p. 413-436.

Klinkhammer, G.P., and Bender, M.L., 1980, The distribution of manganese in the Pacific Ocean: Earth and Planetary Science Letters, v. 46, p. 361-384.

Klinkhammer, G.P., and Palmer, M.R., 1991, Uranium in the oceans--where it goes and why: Geochimica et Cosmochimica Acta, v. 55, no. 7, p. 1799-1806.

Kolodny, Yehoshua. 1981, Phosphorites, *in* Emiliani, Chesare, ed., The oceanic lithosphere, v.7 of The Sea--ideas and observations on progress in the study of the seas: New York, Wiley-Inerscience, p. 981-1023.

Kolodny, Yehoshua, and Kaplan, I.R., 1970, Carbon and oxygen isotopes in apatite CO_2 and coexisting calcite from sedimentary phosphorite: Journal of Sedimentary Petrology, v. 40, p. 954-959.

Krauskopf, K.B., 1956, Factors controlling the concentrations of thirteen rare metals in seawater: Geochimica et Cosmochimica Acta, v. 9, p. 1-32.

Kremling, Klaus, 1983, The behavior of Zn, Cd, Cu, Ni, Co, Fe, and Mn in anoxic Baltic waters: Marine Chemistry, v. 13, no. 1-4, p. 87-108.

Landing, W.M., and Bruland, K.W., 1987, The contrasting biochemistry of iron and manganese in the Pacific Ocean: Geochimica et Cosmochimica Acta, v. 51, p. 29-43.

Landing, W.M., and Lewis, B.L., 1991, Thermodynamic modelling of trace metal speciation in the Black Sea, *in* Izdar, Erol, and Murray, J.W., eds., Black Sea oceanography: Dordrecht, Kluwer, p. 125-160.

Langmuir, Donald, 1978, Uranium solution-mineral equilibria at low temperatures with applications to sedimentary ore deposits: Geochimica et Cosmochimica Acta, v. 42, no. 6, p. 547-569.

Latimer, W.M., 1953, Oxidation potentials: New York, Prentice Hall, 392 p.

Leventhal, J.S., 1989, Geochemistry of minor and trace elements of 22 core samples from the Monterey Formation and related rocks in the Santa Maria Basin, California: U.S. Geological Survey Bulletin 1581-B, p. B1-B11.

Lewan, M.D., 1984, Factors controlling the proportionality of vanadium to nickel in crude oils: Geochimica et Cosmochimica Acta, v. 48, no. 11, p. 2231-2238.

Li, Y.-H., 1981, Ultimate removal mechanisms of elements from the oceans: Geochimica et Cosmochimica Acta, v. 45, no. 10, p. 1659-1664.

Lichte, F.E., Golightly, D., and Lamothe, P.J., 1987a, Inductively coupled plasma-atomic emission spectrometry, *in* Baedecker, P.A., ed., Methods of geochemical analysis: U.S. Geological Survey Bulletin 1770, p. B1-B10.

Lichte, F.E., Meier, A.L., and Crock, J.G., 1987b, Determination of the rare-earth elements in geological materials by inductively coupled plasma mass spectrometry: Analytical Chemistry, v. 59, p. 1150-1157.

Littke, R., Klussmann, U., Krooss, B., and Leythaeuser, D., 1991, Quatification of loss of calcite, pyrite, and organic matter due to weathering of Toarcian black shales and effects on kerogen and bitumen characteristics: Geochimica et Cosmochimica Acta, v. 55, p. 3369-3378.

Love, J.D., 1961, Vanadium and associated elements in the Phosphoria Formation in the Afton area--western Wyoming--article 250 of Short papers in the geologic and hydrologic sciences: U.S. Geological Survey Professional Paper 424–C, p. C279-C282.

Lyle, Mitchell, Heath, G.R., and Robbins, J.M., 1984, Transport and release of transition elements during early diagenesis--sequential leaching of sediments from MANOP Sites M and H. Part I. pH 5 acetic acid leach: Geochimica et Cosmochimica Acta, v. 48, no. 9, p. 1705-1715.

Mansfield, G.R.,1916, A reconnaissance for phosphate in the Salt River Range, Wyoming: U.S. Geological Survey Bulletin, v. 620, p. 331-350.

Martin, J.H., and Knauer, G.A., 1973, The elemental composition of plankton: Geochimica et Cosmochimica Acta, v. 37, no. 7, p. 1639-1653.

Martin, J.H., and Gordon, R.M., 1988, Northeast Pacific iron distribution in relation of phytoplankton productivity: Deep-Sea Research, v. 35, p. 177-196.

Maughan, E.K., 1976, Organic carbon and selected element distributions in the phosphatic shale members of the Permian Phosphoria Formation, eastern Idaho and parts of adjacent States: U.S. Geological Survey Open-File Report, 76-577, 92p.

McClellan, G.H., and Lehr, J.R., 1969, Crystal-chemical investigation of natural apatites: The American Mineralogist, v. 54, p 1374-1391.

McKelvey, V.E., Williams, J.S., Sheldon, R.P., Cressman, E.R., Cheney, T.M., and Swanson, R.W., 1959, The Phosphoria, Park City, and Shedhorn Formations in the western phosphate field: U.S. Geological Survey Professional Paper 313-A, 47p.

McKelvey, V.E., Strobell, J.D., Jr., and Slaughterz, A.L., 1986, The vanadiferous zone of the Phosphoria Formation in western Wyoming and southeastern Idaho: U.S. Geological Survey Professional Paper 1465, 27p.

Measures, C.I., McDuff, R.E., and Edmond, J.M., 1980, Selenium redox chemistry at GEOSECS I re-occupation: Earth and Planetary Science Letters, v. 49, no. 1, p. 102-108.

Measures, C.I., Grant, B.C., Mangum, B.J., and Edmond, J.M., 1983, The relation of the distribution of selenium IV and VI in three oceans to physical and biological processes, *in* Wong, C.S., Boyle, Edward, Bruland, K.W., Burton, J.D., and Goldberg, E.D., eds., Trace metals in seawater: New York, Plenum Press, p. 73-83.

Medrano, M.D., and Piper, D.Z., 1992, A normative calculation procedure used to determine mineral abundances in rocks from the Montpelier Canyon section of the Phosphoria Formation, Idaho–a tool in deciphering the minor-element geochemistry of sedimentary rocks: U.S. Geological Survey Bulletin 2023-A, p. A1-A23.

Medrano, M.D., and Piper, D.Z., 1995, Partition of minor elements and major-element oxides between rock components and calculation of the marine-derived fraction of the minor elements in rocks of the Phosphoria Formation, Idaho and Wyoming, U.S. Geological Survey Open-File Report 95-270, 79pp.

Moldowan, J.M., Sundararaman, Padmanabhan, and Schoell, Martin, 1986, Sensitivity of biomarker properties to depositional environments and/or source input in the lower Toarcian of SW Germany: Organic Geochemistry, v. 10, no. 4-6, p. 915-926.

Mossmann, J.-R., Aplin, A.C., Curtis, C.D., and Coleman, M.L., 1991, Geochemistry of inorganic and organic sulfur in organic-rich sediments from the Peru Margin: Geochimica et Cosmochimica Acta, v. 55, no. 12, p. 3581-3595.

Murata, K.J., Friedman, I., and Gulbrandsen, R.A., 1972, Geochemistry of carbonate rocks in the Phosphoria and related formations of the western phosphate field: U.S. Geological Survey Professional Paper 800D, p. D103-D110.

Murchey, B.L., and Jones, D.L., 1992, A mid-Permian chert event–widespread deposition of biogenic siliceous sediments in coastal, island arc, and oceanic basins: Palaeogeography, Palaeoclimatology, Palaeoecology, v. 96, p. 161-174.

Murray, J.W., Spell, Berry, and Paul, Barbara, 1983, The contrasting geochemistry of manganese and chromium in the eastern tropical Pacific Ocean, *in* Wong, C.S., Boyle, Edward, Bruland, K.W., Burton, J.D., and Goldberg, E.D., eds., Trace metals in seawater: New York, Plenum, p. 643-669.

Murray, J.W., Top, Zafer, and Özsoy, Emin, 1991, Hydrographic properties and ventilation of the Black Sea: Deep-Sea Research, v. 38, Supplement 2A, p. S663-S689.

Nelson, D.M., Goering, J.J., and Boisseau, D.W., 1981, Consumption and regeneration of silicic acid in three coastal upwelling systems, *in* Richards, F.A., ed., Coastal upwelling, v. 1 of Coastal and estuarine science: Washington, D.C., American Geophysical Union, p. 242-256.

Nissenbaum, A., and Swaine, D.J., 1976, Organic matter-metal interactions in recent sediments--the role of humic substances: Geochimica et Cosmochimica Acta, v. 40, p. 809-816.

Nordstrom, D.K., and Munoz, J.L., 1985, Geochemical thermodynamics: Menlo Park, N.J., Benjamin-Cummings, 477 p.

Odermatt, J.R., and Curiale, J.A., 1991, Organically bound metals and biomarkers in the Monterey Formation of the Santa Maria Basin, California: Chemical Geology, v. 91, no. 2, p. 99-113.

Östlund, H.G., 1974, Expedition "Odysseus 65"--radiocarbon age of Black Sea bottom water, *in* Degens, E.T., and Ross, D.A., eds., The Black Sea--geology, chemistry, and biology: American Association of Petroleum Geologists Memoir 20, p. 127-132.

Palmer, M.A., 1985, Rare earth elements in foraminifera tests: Earth and Planetary Science Letters, v. 73, no. 2-4, p. 285-298.

Pederson, T.F., and Calvert, S.E., 1990, Anoxia vs productivity--what controls the formation of organic-carbon rich sediments and sedimentary rocks?: American Association of Petroleum Geologists Bulletin, v. 74, no. 4, p. 454-466.

Pedersen, T.F., Waters, R.D., and MacDonald, R.W., 1989, On the natural enrichment of cadmium and molybdenum in the sediments of Ucluelet Inlet, British Columbia: Science of the Total Environment, v. 79, no. 2, p. 125-139.

Peterson, J.A., 1980, Depositional history and petroleum geology of the Permian Phosphoria, Park City, and Shedhorn Formations, Wyoming and Southeastern Idaho: U.S. Geological Survey Open-File Report 80-667, p. 18-20.

Piper, D.Z., 1974, Rare earth elements in the sedimentary cycle--a summary: Chemical Geology, v. 14, p. 285-304.

Piper, D.Z., Baedecker, P.A., Crock, J.G., Burnett, W.C., and Loebner, B.J., 1988, Rare Earth Elements in the phosphatic-enriched sediment of the Peru Shelf: Marine Geology, v. 80, p. 269-285.

Piper, D.Z., 1988, The metal oxide fraction of pelagic sediment in the equatorial North Pacific Ocean--a source of metals in ferromanganese nodules: Geochimica et Cosmochimica Acta, v. 52, p 2127-2145.

Piper, D.Z., 1991, Geochemistry of a Tertiary sedimentary phosphate deposit, Baja California Sur, Mexico: Chemical Geology, v. 92, p. 283-316.

Piper, D.Z., 1994, Seawater as a source of minor elements in black shales, phosphorites, and other sedimentary deposits: Chemical Geology, v. 114, p. 95-114.

Piper, D.Z., and Isaacs, C.M., 1995, Geochemistry of minor elements in the Monterey Formation, California--seawater chemistry of deposition: U.S. Geological Survey Professional Paper 1566, 41p.

Piper, D.Z., and Isaacs, C.M., 1996, Instability of bottom-water redox conditions during deposition of Quaternary sediment, Sea of Japan: Paleoceanography, v. 11, p. 171-190.

Piper, D.Z., and Medrano, M.D., 1994, Geochemistry of the Phosphoria Formation at Montpelier Canyon, Idaho--environment of deposition: U.S. Geological Survey Bulletin 2023-B, p. B1-B28.

Powell, T.G., Cook, P.J., and McKirdy, D.M., 1975, Organic geochemistry of phosphorites--relevance to petroleum genesis: AAPG Bulletin 59, no. 4, p 618-632.

Presser, T.S., 1994, The Kesterson effect: Environmental Management, v. 18, p. 437-454.

Presser, T.S. and Ohlendorf, H.M., 1987, Biogeochemical cycling of selenium in the San Joaquin Valley, California: Environmental Management, v. 11, pp. 805-821.

Presser, T.S., Sylvester, M.A., and Low, W.H., 1994, Bioaccumulation of selenium from natural geologic sources in the Western States and its potential consequences: Environmental Management, v. 18, no. 3, pp.423-436

Presser, T.S., and Piper, D.Z., 1998, Mass balance approach to selenium cycling through the San

Joaquin Valley from source to river to bay, *in* Frankenberger, W.T., Jr., and Engberg, R.A., eds., Environmental chemistry of selenium: New York, Marcel Decker, Inc., p. 153-182.

Redfield, A.C., Ketchum, B.H., and Richards, F.A., 1963, The influence of organisms on the composition of seawater, *in* Hill, M.N., ed., The composition of seawater--comparative and descriptive oceanography, v. 2 of The sea--ideas and observations on progress in the study of the sea: New York, Wiley-Interscience, p. 26-77.

Reimers, C.E., and Suess, Erwin, 1983, Late Quaternary fluctuations in the cycling of organic matter off central Peru, *in* Suess, Erwin, and Theide, Jörn, eds., Coastal upwelling--its sediment records--part A, responses of the sedimentary regime to present coastal upwelling: London, Plenum, p. 497-526.

Richards, F.A., 1975, The Cariaco Basin (Trench): Oceanography and Marine Biology Annual Review, v. 13, p. 11-67.

Richards, F.A., and Broenkow, W.W., 1971, Chemical changes including nitrate reduction in Darwin Bay, Galapagos Archipelago, over a two month period, 1969: Limnology and Oceanography, v. 126. p. 758-765.

Sarnthein, M., Winn, K., Duplessy, J-C., and Fontugne, M.R., 1988, Global variations of surface ocean productivity in low and mid latitudes--influence on CO_2 reservoirs on the deep ocean and atmosphere during the last 21,000 years: Paleoceanography, v. 3, p. 361-399.

Schijf, Johan, de Baar, H.J.W., Wijbrans, J.R., and Landing, W.M., 1991, Dissolved rare earth elements in the Black Sea: Deep-Sea Research, v. 38, supp. 2A, p. S805-S823.

Sclater, R.F., Boyle, Edward, and Edmond, J.M., 1976, On the marine geochemistry of nickel: Earth and Planetary Science Letters, v. 31, no. 7, p. 119-128.

Shaw, T.J., Gieskes, J.M., and Jahnke, R.A., 1990, Early diagenesis in differing depositional environments--the response of transition metals in pore water: Geochimica et Cosmochimica Acta, v. 54, no. 5, p. 1233-1246.

Sheldon, R.P., Waring, R.G., Warner, M.A., and Smart, R.A., 1953, Stratigraphic sections of the Phosphoria Formation in Wyoming, 1949-1950: U.S. Geological Survey Circular 307, 57p.

Sheldon, R.P., 1963, Physical stratigraphy and mineral resources of Permian rocks in western Wyoming: U.S. Geological Survey Professional Paper 313-B, 267p.

Sheldon, R.P., 1964, Paleolatitudinal and paleogeographic distribution of phosphorite: U.S. Geological Survey Professional Paper 501-C, p. C106-C113.

Sheldon, R.P., Cressman, E.R., Carswell, L.D., and Smart, R.A., 1954, Stratigraphic sections of the Phosphoria Formation in Wyoming: U.S. Geological Survey Circular 325, 24p.

Sherrell, R.M., 1989, The trace-element geochemistry of suspended oceanic particulate matter: PhD Dissertation, Massachusetts Institute of Technology, Woods Hole Oceanographic Institute, Woods Hole, Mass, 211p.

Sholkovitz, E.R., 1993, Comment on "redox cycling of rare earth elements in the suboxic zone of the Black Sea" by C.R. German, B.P. Holliday, and H. Elderfield: Geochimica et Cosmochimica Acta, v. 56, no. 12, p. 4305-4307.

Sholkovitz, E.R., and Gieskes, J.M., 1991, A physical-chemical study of the flushing of the Santa Barbara Basin: Limnology and Oceanography, v. 16, p. 479-489.

Sholkovitz, E.R., Landing, W.M., and Lewis, B.L., 1994, Ocean particle chemistry--the fraction of rare earth elements between suspended particles and seawater: Geochimica et Cosmochimica Acta, v. 58, p. 1567-1579.

Skorupa, J.P., 1998, Selenium poisoning of fish and wildlife in nature-lessons from twelve real-world examples, *in* Frankenberger, W.T., Jr., and Engberg, R.A., eds., Environmental chemistry of selenium: New York, Marcel Decker, Inc., p. 315-354.

Suess, E., 1980, Particulate organic carbon flux in the oceans--surface productivity and oxygen utilization: Nature, v. 288, p. 260-263.

Smart, R.A., Waring, R.G., Cheney, T.M., and Sheldon, R.P., 1954, Stratigraphic sections of the Phosphoria Formation in Idaho, 1950-51: U.S. Geological Survey Circular 327, 21p.

Sverdrup, H.U., Johnson, M.W., and Fleming, R.H., 1942, The oceans--their physics, chemistry, and general biology: New Jersey, Prentice-Hall, 1,087 p.

Swanson, V.E., 1961, Geology and geochemistry of uranium in marine black shales--a review: U.S.

Geological Survey Professional Paper 356-C, p. 67-112.

Taggart, J.E., Jr., Lindsey, J.R., Scott, B.A., Vivit, D.V., Bartel, A.J., Stewart, K.C., 1987, Analysis of geologic materials by wavelength-dispersive X-ray fluorescence spectrometry: *in* Baedecker, P.A., ed., Methods for geochemical analyses, U. S. Geological Survey Bulletin 1770, p. E1-E19.

Thunell, R.C., 1998, Seasonal and annual variability in particle fluxes in the Gulf of California—a response to climate forcing: Deep-Sea Research, v. 45, p. 2059-2083.

Thunell, R.C., Varela, R., Coolister, J., Sigman, D., Muller-Karger, F., and Bohrer, R., 1997, Sediment fluxes in Cariaco Basin--preliminary results of a time series study, EOS Transactions of the American Geophysical Union, v. 78, p. F338.

Turekian, K.K., and Wedepohl, K.H., 1961, Distribution of the elements in some major units of the Earth's crust: Geological Society of America Bulletin, v. 72, no. 2, p. 175-191.

U.S. Department of Interior, 1998, Guidelines for interpretation of the biological effects of selected constituents in biota, water, and sediment: National Irrigation Water Quality Program, Information Report no. 3, U.S. Bureau of Reclamation, U.S. Fish and Wildlife Service, U.S. Geological Survey, and U.S. Bureau of Indian Affairs, in the U.S. Department of the Interior, Washington, D.C., 198 p.

Varela, R, Capelo, J.C., Gutierrez, J., Muller-Karger, F., and Diaz-Ramos, J.R., 1997, Primary productivity in Cariaco Basin waters: EOS Transactions, American Geophysical Union, v. 78, p. F342.

Von Bockel, Klaus, 1981, A note on short-term production and sedimentation in the upwelling region off Peru, *in* Richards, F.A., ed., Coastal upwelling, v. 1 of Coastal and estuarine sciences: Washington, D.C., American Geophysical Union, p. 291-297.

Wagman, D.D., Evans, W.H., Parker, V.B., Schumm, R.H., Halow, I., Bailey, S.M., Churney, K.L., and Nutall, R.L., 1982, The NBS tables of chemical thermodynamic properties: Journal of Physical Chemistry, reference data., Supp. 2., 392 p.

Wanty, R.B., and Goldhaber, M.B., 1992, Thermodynamics and kinetics of reactions involving vanadium in natural systems--accumulation of vanadium in sedimentary rocks: Geochimica et Cosmochimica Acta, v. 56, no. 4, p. 1471-1483.

Wardlaw, B.R. and Collinson, J.W., 1984, Conodont paleoecology of Permian Phosphoria Formation and related rocks of Wyoming and adjacent areas, *in* Clark, D.L., ed., Conodont biofacies and provincialism: Geological Society of America, Special Paper 196, p. 263-281.

Wardlaw, B.R. and Collinson, J.W., 1986, Paleontology and deposition of the Phosphoria Formation: *in* Boyd, D.W., and Lillegraven, J.A., eds., Contributions to geology: Phosphoria Issue, v. 24, no. 2., p 107-142.

Wedepohl, K.H. (editor), 1969-1978, Handbook of geochemistry: Berlin, Springer-Verlag, 4 volumes.

Whitfield, Michael, and Turner, D.R., 1987, The role of particles in regulating the composition of seawater, *in* Stumm, Werner, ed., Aquatic surface chemistry: New York, John Wiley and Sons, p. 457-493.

Wright, Judith, Schrader, Hans, and Holser, W.T., 1987, Paleoredox variations in ancient oceans recorded by rare earth elements in fossil apatite: Geochimica et Cosmochimica Acta, v. 51, no. 3, p. 631-644.

Yochelson, E.L., 1968, Biostratigraphy of the Phosphoria, Park City, and Shedhorn Formations. U.S. Geological Survey Professional Paper 313-D, p. 571-660